Abstract

We present a search for anomalous production of the signature ℓ+γ+b-quark+$\not\!E_{\rm T}$ produced in $p\bar{p}$ collisions at $\sqrt{s} = 1.96$ TeV using 5.7 fb^{-1} of data taken with the CDF detector in Run II at the Tevatron. In addition to this signature-based search, we present a search for top pair production with an additional radiated photon, $t\bar{t} + \gamma$. We find 84 $\ell\gamma\not\!E_{\rm T}b$ events versus an expectation of $86.4^{+7.6}_{-xxx}$ events. High-statistics control samples, $\ell\ell\gamma$ and $\ell\gamma\not\!E_{\rm T}$ were used to evaluate a low-energy photon χ^2 cut. Additionally requiring the events to contain at least 3 jets and to have a total transverse energy of 200 GeV, and the photon to pass the new χ^2 cut we observe 30 $t\bar{t}\gamma$ candidate events versus an expectation from non-top standard model (SM) sources of $13.9^{+2.4}_{-xxx}$. Assuming the difference between the observed number and the predicted non-top SM total is due to top production, we measure the $t\bar{t}\gamma$ cross section to be $0.10 \pm 0.04 \pm 0.02 \pm 0.01$ pb. We also measure a ratio of the $t\bar{t}\gamma$ cross section to the $t\bar{t}$ cross section to be 0.013 ± 0.005, which compares well with a theoretical ratio of $0.010\ ^{+0.005}_{-0.006}$.

A Signature-Based Search for Anomalous Lepton, Photon, Missing Transverse Energy and b-jet Production and Standard Model Radiative Top-AntiTop Production in 5.7 fb^{-1} with the CDF-II Detector

Benjamin Auerbach

2011

A Signature-Based Search for Anomalous Lepton, Photon, Missing Transverse Energy and b-jet Production and Standard Model Radiative Top-AntiTop Production in 5.7 fb^{-1} with the CDF-II Detector

A Dissertation
Presented to the Faculty of the Graduate School
of
Yale University
in Candidacy for the Degree of
Doctor of Philosophy

by
Benjamin Auerbach

Dissertation Director: Paul Tipton

May 2011

Contents

List of Figures

List of Tables

1 Introduction and Theoretical Motivation

To describe nearly every object around us, it is usually only neccessary to consider three basic building blocks: the proton, the neutron, and the electron. However, looking closer, there is the photon, which is required for us to see the objects around us, and to carry the forces of electromagnetism; and for weak interactions involved in nuclear reactions, there are the $W^{\pm}$ bosons, and the Z boson.

At higher energies, the forces of electromagnetism, and the weak interactions are indistinguishable, and this is the elctroweak unification. Experiments have shown, and Nobel Prizes have been awarded, for explaining the composition of protons, and neutrons, as quarks and gluons. The gluons are a force-carrier for the strong force and these objects tie up and down quarks up in the nucleus of protons and neutrons. Through careful experimentation, we have found that the universe we reside in has many different particles that can be made, and that the up and down quarks have additional members in their family. In addition to electrons, our universe has two more massive leptons, the muon and the tau. One of the ways that a massive lepton interacts with a $W^{\pm}$ boson, is the production of a neutrino; each massive lepton has a corresponding neutrino. The neutrino is also a lepton. And to, nearly, complete the picture, each of the quarks, and leptons, has a corresponding anti-particle. This sums up all the fundamental objects in particle physics that have been observed so far.

1.1 The Standard Model

The ways in which each of these particles interacts with each other is described to extraordinary precision by the Standard Model (SM) of Particle Physics, but the SM has known problems at very high energies. As we ever increase the energies of collisions we observe, we hope to see a break down of the SM, in the hopes of seeing a new particle, gaining a better understanding of the SM, or possible extensions to it. Many corresponding discoveries of a fundamental particle has occurred through a larger and larger amount of energy. A heuristic for this comes from Einstein's famous E = mc^2 equation. Many of the objects discovered later are more massive, and thus require more thereshold energy to be created.

The SM descibes interactions of fermions (spin-$\frac{1}{2}$) objects with the force carrying bosons. These fermions are further subdivided into two classes, leptons, and quarks. The lepton generations are grouped with a charged lepton and an uncharged neutrino. Quark generations group together pairs of quarks together, up with down, charm with strange, and top with bottom. These quark generations have corresponding charges of $\frac{-1}{3}e$ and $\frac{2}{3}e$, where e is the charge of the electron. Both the quarks and the leptons interact with the electroweak bosons, W$^{\pm}$, Z, and γ. However to interact with the photon, the fermion must be charged, so the neutrino has no interaction with the photon. The quarks have an additional structure, called color, and their interactions are dictated by quantum-chromodynamics (QCD).

The SM is built on top of a $SU(3)_c \otimes SU(2)_L \otimes U(1)_Y$ group structure. The subscripts in the group structure refer to quantum numbers of the fields, "c" is color, "L" is left-handed, and "Y" is the field's hypercharge.

One of the principles of the SM is local gauge invariance, which means an infinitessimal phase rotation with one of those group's operators should result in no change to the predictions. Unfortunately, this leads to a modification for the SM.

The symmetry of $SU(2)_L$, the group responsible for the weak-force bosons $W^{\pm}$, and Z, requires these bosons to be massless, otherwise it violates gauge invariance. This is referred to in particle physics, as a broken symmetry, and because of this there should be a massive particle responsible.

The explanation for these particles' mass, and description of its properties have taken many shapes and sizes; perhaps the most well-known of which is the Higgs boson.

1.2 The Higgs Boson

Suppose that at some energy regime that the symmetry of $SU(2) \oplus U(1)$, the electroweak group structure, is not broken. That is to say we are going to think of this model in a way where the symmetry still holds, and the W, Z, and photon are all inter-related massless bosons. If we introduce additional terms to the Lagrangian of this theory that interact with these bosons, it is possible to generate mass in such a way that local gauge invariance is preserved.

The Higgs field is a scalar doublet that interacts with the massless gauge bosons of the electroweak force. The theory of the massless gauge bosons has the SM group structure we mentioned above, however this is before the symmetry is broken, and the W, and Z bosons do not have any mass. We assume that in addition to this SM we add a complex scalar doublet field, ϕ. We then have an addition to the SM that looks like

$$\mathcal{L} = (D^{\mu}\phi)^{\dagger}(D_{\mu}\phi) + \mu^2\phi^*\phi - \lambda(\phi^*\phi)^2 \tag{1.1}$$

In this equation we have the covariant derivative, D^{μ}, and the constants μ, and λ are not known, but $\mu^2 > 0$, and $\lambda > 0$. Furthermore, $D^{\mu} = \partial^{\mu} + igA^{a\mu}\tau^a + \frac{ig'}{2}B^{\mu}$. In these definitions, g is a coupling of the SU(2) gauge fields ($A^{a\mu}$) and g' is the coupling of the U(1) gauge fields (B^{μ}), and τ^a is an infinitessimal generator of the SU(2) group.

We can see, with a little bit of work, that the minimum of the Eq. 1.1 does not occur at zero, but at $\phi = \sqrt{\mu^2/2\lambda} = v/\sqrt{2}$. This says that mathematically the ground state of the vacuum does not occur where ϕ =0, but instead is at a point $\phi = v/\sqrt{2}$. If we attempt to write out the terms around a perturbation about this minimum, with

$\phi(x) = \begin{pmatrix} 0 \\ \frac{v}{\sqrt{2}} \end{pmatrix}$ then there is a change in the Lagrangian in the derivative terms that looks like:

$$\Delta\mathcal{L} = \frac{1}{2}\frac{v^2}{4}\left(g^2(A^1_{\mu})^2 + g^2(A^2_{\mu})^2 + (g'B_{\mu} - gA^3_{\mu})^2\right). \tag{1.2}$$

We then make the substitution that $W^{\pm}_{\mu} = \frac{1}{\sqrt{2}}(A^1_{\mu} \mp iA^2_{\mu})$, and $Z^0_{\mu} = \frac{1}{\sqrt{g^2+g'^2}}\left(-gA^3_{\mu} + g'B_{\mu}\right)$, and the photon field, $\tilde{A}_{\mu} = \frac{1}{\sqrt{g^2+g'^2}}\left(g'A^3_{\mu} + gB_{\mu}\right)$, in Eq. 1.2. We know from Field Theory that when we have a term proportional to the square of the field, that this is the mass of the field. Substituting

$$M_W = g\frac{v}{2},\ M_Z = \sqrt{g^2 + g'^2}\frac{v}{2}$$

into the equation above we find terms that look like $M_W^2(W^+)^2$, $M_W^2(W^-)2$, and $M_Z^2(Z^0)^2$. This shows that assuming there is a Higgs mechanism, we are able to break the $SU(2) \otimes U(1)$ symmetry, and produce the correct masses for the photon, and the W and Z bosons, all while maintaining gauge invariance.

The values of g, g′, and v, have all been measured to spectacular precision through measurements on the muon decay lifetimes, and the measurements of the mass of the W and Z bosons. This does imply that v = 246 GeV.

Accepting this as the explanation requires the existence of an uncharged, spin-0 boson, the Higgs boson, whose existence has not yet been confirmed. The Higgs field is a complex scalar doublet, which has four degrees of freedom; two of these degrees of freedoms are required to give mass to the W bosons, and one is required to give mass to the Z boson, which leaves one degree of freedom, this is the elusive Higgs boson.

It would be nice if this were the end of the story, however all is not well with this theory. If one exapnds about the minimum of the Higgs field, so that v→ v+ h(x), there are terms that arise in Eq. 1.1, that are proportional to h^2, h^3, and h^4. This implies that at very high energies, the Higgs boson will interact with itself, and at high energies these terms diverge, and some other sort of mechanism must exist to cancel these divergences. Candidate theories have emerged to eliminate these divergences such as Super Symmetry (SUSY). SUSY is an attractive theory as it encompasses the Higgs mechanism, eliminates the divergences at high energies, and as a bonus has objects which could explain dark matter in the universe.

There are additional connections that can be added to the Standard Model to explain the degeneracy of masses of all the quarks and leptons. Through machinations similar to those above, the Higgs field couples to the fields of the quarks, and leptons. The coulping strength of the Higgs field to these fields would then be proportional to the observed masses of the leptons and the quarks. This would then explain the large difference between the masses of each of the quarks. Moreover the coupling strengths of the Higgs boson to all objects in the SM are proportional to the mass of the objects, the heavier an object is, is due to a stronger coupling strength. Thus the top quark should couple very strongly to the Higgs mass.

1.3 Top Quark Phenomenology

To date, the top quark is the most massive of all the fundamental particles, and is nearly as massive as a gold atom. Although it was discovered more than 10 years ago, many of its properties are not very well known, such as its cross section, its mass, and its coupling to the photon.

This quark is the only quark that decays before hadronization. Nature has provided us with the only bare quark we can study. Top quarks at the Tevatron are primarily pair produced via quark-antiquark annihilation, with a small fraction coming from gluon fusion. At the Tevatron's energy regime quark-antiquark annihilation production dominates, which is why we use proton antiproton collisions.

In events with top quarks pairs, and each top quark decays almost exclusively to a W boson and a b quark. The W boson is capable of decaying to electrons, muons and taus, or to quark pairs. The easiest events to identify are those where at least one of the W bosons decays to an electron or muon, and corresponding neutrino. When this occurs we are able to identify the lepton, and the neutrino escapes the detector undetected. The neutrino presence is made known by a significant imbalance in transverse energy. From conservation of momentum, the total momentum moving perpendicular to the incoming proton-antiproton beams should be zero. If after summing up all of the transverse momentum there appears to be a large amount missing we are confident in saying this is due to a neutrino.

In the production of top quark pairs many charged objects are involved such as the incoming quarks, the top quarks themselves, the W bosons, the leptons from the W decay, and also final state quarks. Each of these objects can produce a photon that can be identified by the detector and these events are called radiative top decays, or $t\bar{t}\gamma$ events. Events from $t\bar{t}\gamma$ decays, are remarkably similar to the non-radiative pair production, the exception is of course the photon. A photon in a $t\bar{t}\gamma$ event is most likely to occur from one of the initial state quarks radiating off a photon.

Although this quark is exceptionally interesting in its own right, it is now in the transition stages of being a standard candle for ATLAS and CMS detectors at the LHC. Namely the detectors at the LHC will be able to use it to better calibrate their measurements. However the connection between $t\bar{t}$ and the photon is not very well known.

The $t\bar{t}\gamma$ production could be used as a tool to measure the $tt\gamma$ coupling [3]. The $t\bar{t}\gamma$ will also serve as a control sample for $t\bar{t}$+Higgs production at the LHC and a probe of the charge of the top quark [4]. The ratio between the $t\bar{t}\gamma$ production cross section, and the $t\bar{t}$ cross section will serve as precision measurement for the LHC and their search for Higgs $\rightarrow t\bar{t}$. Furthermore the $t\bar{t}\gamma$ signature should be the first associated electroweak boson with top pair production to be observed at the LHC.

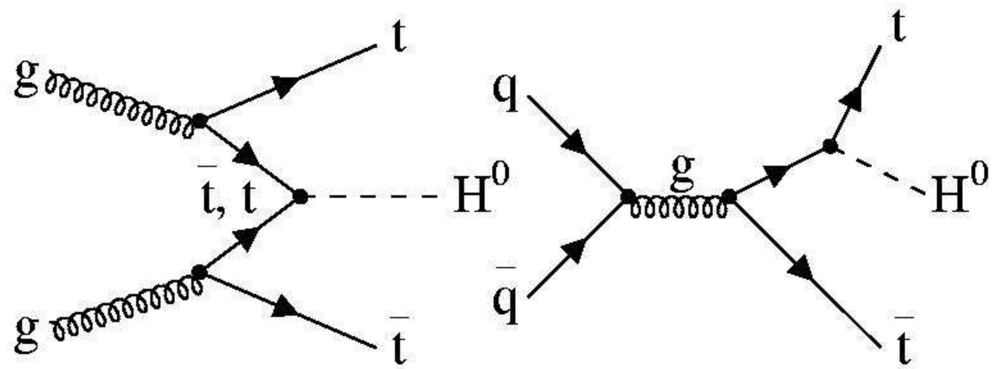

Figure 1.1: $t\bar{t}$ + Higgs Production

1.4 Signature-Based Searches

At this point, all we know is that there is some sort of physics that has not yet been observed. Unfortunately this also means that we do not know in what direction we should be looking. There are many candidate theories out there and we cannot currently test all of them so we constrain ourselves to a particular signature.

For our search for new physics we are using a signature-based search. Given the unknown nature of potential new physics, it is good to expect the unexpected, and look for significant deviations from the SM. We will be looking for events that should dominantly involve the top quark, and a photon.

This signature is appealing because if there is something else outside the SM, accessible at the Tevatron, it is likely that it will be heavier than the top quark, and might prefer to decay to this quark. Also if this object is charged or if there is some connection to our currently understood quantum numbers, there is a possibility of a radiated photon. The top quark decays almost exclusively to a b quark and a W boson. The b quark is very interesting to particle physics searches as it will hadronize, and travel for small distances before decaying. In CDF this appears as a secondary vertex, the primary vertex is due to the proton anti-proton collision, where we see additional decay products occurring from this point. We rely on one of the W bosons to decay to leptons which will produce either an electron or muon that we can detect, and a corresponding neutrino which we detect as energy missing in the transverse direction.

The W bosons are also quite capable of decaying to taus as well as the previously mentioned electrons and neutrinos, however it is very difficult to identify tau leptons at the Tevatron. As such for the remainder of this thesis when we mention identifying leptons, we are only talking about electrons and muons.

In this thesis we present a search for anomalous production of events with a high-$\mathrm{P_T}$ lepton (electron, e or muon, μ), photon (γ), jet tagged as containing b-meson (b-jet), and missing transverse energy ($\not\!\!E_{\mathrm{T}}$), ($\ell\gamma\not\!\!E_{\mathrm{T}}b$ events) This search is an improvement of a previous analysis, described in detail in Ref. [5].

The $\ell\gamma\not\!\!E_{\mathrm{T}}b$ signature is possible [3] in different models beyond the SM, such as gauge-mediated Supersymmetry (SUSY) models [6]. The signature has known SM backgrounds, and could be produced in decays of heavy particles. This type of signature contains fundamental particles, such as two third-generation quarks, t-quark and b-quark, and two gauge bosons, W ($W \rightarrow \ell\nu$) and γ. This search is related to the $\ell\gamma + X$ search [7], but with b-tag requirement in addition to lower photon E_T, lepton P_T and $\not{E}_T$ requirements. There is expected to be small SM backgrounds in this signature which should give us a chance to see statistically anomalous events outside of the SM expectations.

1.5 Outline of the Thesis

The $\ell\gamma\not{E}_T b$ signature involves many different objects, and the possibility of each of them to be misidentified (Sec. 5), it is then necessary to have a solid understanding of the detector we will be using and we discuss that in Section 2.

The largest SM background event in the $\ell\gamma\not{E}_T b$ signature is the production of top pairs with an additional photon, $t\bar{t}\gamma$. It is a natural extension of the $\ell\gamma\not{E}_T b$ signature-based search, as the $t\bar{t}\gamma$ signature is characterized by the same components as the $\ell\gamma\not{E}_T b$ signature. Additional cuts are then applied so that radiative top-pair events dominate the SM predictions: we require large H_T (the sum of the transverse energies of the lepton, photon, jets and $\not{E}_T$) and 3-or-more jets.

There have been previous experiments to measure the cross section of the $t\bar{t}\gamma$ process [5], but there has note yet been evidence of it. We have attempted in this thesis to be the first to claim to have seen evidence of this process by using a novel method to identify photons.

To make a precision measurement of the ratio of the production cross sections of $t\bar{t}\gamma$ and $t\bar{t}$ we will use nearly the same event selection for $t\bar{t}$ candidate events as we used in $t\bar{t}\gamma$ events, but we will not require the photon. The selection criteria for all of our signatures can be found in Section 3.

Sections B.1, B.2, B.3, and B.4 explain our selection criteria for muons, electrons, photons, and jets identified as having heavy flavor, respectively. In Sections B.5.1, and B.5.2 we define and describe the calculation of $\not{E}_T$ and H_T.

In Section 5 we describe "fakes", backgrounds from SM processes which can mimic one of our signatures via one or more objects being misidentified.

To verify our object identification as well as to check our data-driven background measurements we examine the control samples $\ell\gamma\not{E}_T$, $\ell\ell\gamma$, and a $t\bar{t}$ sample without the b-hadron identification these are all described in Section 7. While these samples are not independent of the events we will reconstruct, namely the $\ell\gamma\not\!\!E_{\mathrm{T}}b$, $t\bar{t}\gamma$, and $t\bar{t}$ samples, the overlap of these samples with their control groups is minimal. These povide a high-statistics sample on which to examine potential modifications to our object identification, as well as to corroborate the ways we estimate our object misidentification.

Using the $\ell\gamma\not\!\!E_{\mathrm{T}}$ and $\ell\ell\gamma$ control samples we use and explain a new tighter cut on photon's χ^2 of the CES position. One of the largest backgrounds in our sample is due to hadrons decaying to photons. For many of these events, the hadrons decay to multiple photons. These groups of photons tend to be collimated, especially for low-energy photons. Taking advantage of the resolution of the CES, and were able to find a difference in the χ^2 values between real low-energy photons, and fake low-energy photons. We examined true photons from $Z\gamma$ decays where the 3-body mass of a dileptonic and photon decay is nearly equal to the Z mass, and fake photons contained in the $W\gamma$ distribution. The method and results are explained in Section 8.

We show in Section 11 the comparison between predicted and observed event yields in 5.7fb^{-1}. Using these results we show the calculation of the measured $t\bar{t}\gamma$ cross section in Section 12.

2 Detector Description

One of the most important parts in the study of particle physics is to have a working understanding of the tools of the experiment. This includes, the accelerators, the beams, and perhaps most important of all, the detector.

2.1 The Tevatron

Fermilab uses a series of accelerators to create its 980 GeV particle beams. The beams begin as H^- ions created from the ionization of hydrogen gas, and are accelerated to 750 KeV in the Cockcroft-Walton pre-accelerator. The ions then enter a linear accelerator (LINAC), where they are accelerated up to 400 MeV. The acceleration in the LINAC occurs in a series of "kicks" from Radio Frequency (RF) cavities. The RF cavities also separate the ions into bunches. At the end of the LINAC the hydrogen ions pass through a carbon foil which strips the hydrogen ions of their electrons, leaving bare protons. The protons are then injected into the circular synchrotron ("Booster"). The protons travel around the Booster to a final energy of 8 GeV.

Protons are then emptied from the Booster into the Main Injector, where they are further accelerated from 8 GeV to 150 GeV before the injection into the Tevatron. The Main Injector also produces 120 GeV protons which are extracted, and then sent down a transfer line until they collide with a Nickel target. These collisions produce many secondary particles including antiprotons ($\bar{p}$). Studies have shown that 120 GeV is the optimal energy for antiproton production. In these collisions about 20 $\bar{p}$ are created per one million protons.

The $\bar{p}$ are then sent to the Accumulator. The Accumulator is a long term $\bar{p}$ storage ring, which is capable of storing $\bar{p}$ with minimal losses for days. When the Accumulator reaches optimum capacity, they are sent to the Main Injector and accelerated to 150 GeV.

In the final step, the p and $\bar{p}$ are injected into the Tevatron. The Tevatron is a 1 km in radius synchrotron that accelerates both protons and antiprotons from 150 GeV to 980 GeV. Both protons and antiprotons are kept in the same beam pipe revolving in opposite directions; there is a large electro-static field which keeps the two beams from touching except at the collision points. The beam is steered by 774 super-conducting dipole magnets and 240 quadrupole magnets.

The Tevatron holds 36 bunches each of protons and antiprotons. The protons are added one bunch at a time, and the antiprotons are loaded 4 bunches at a time. Each bunch is moving at 150 GeV from the Main Injector. RF cavities then accelerate the bunches to 980 GeV. The bunches are now beams of protons and antiprotons, and then some electrostatic fields are reversed causing the protons and antiprotons to collide at two points. Each interaction point lies at the heart of the two particle detectors, D0 (named for the position in the Tevatron ring) and the

Collider Detector Facility (CDF).

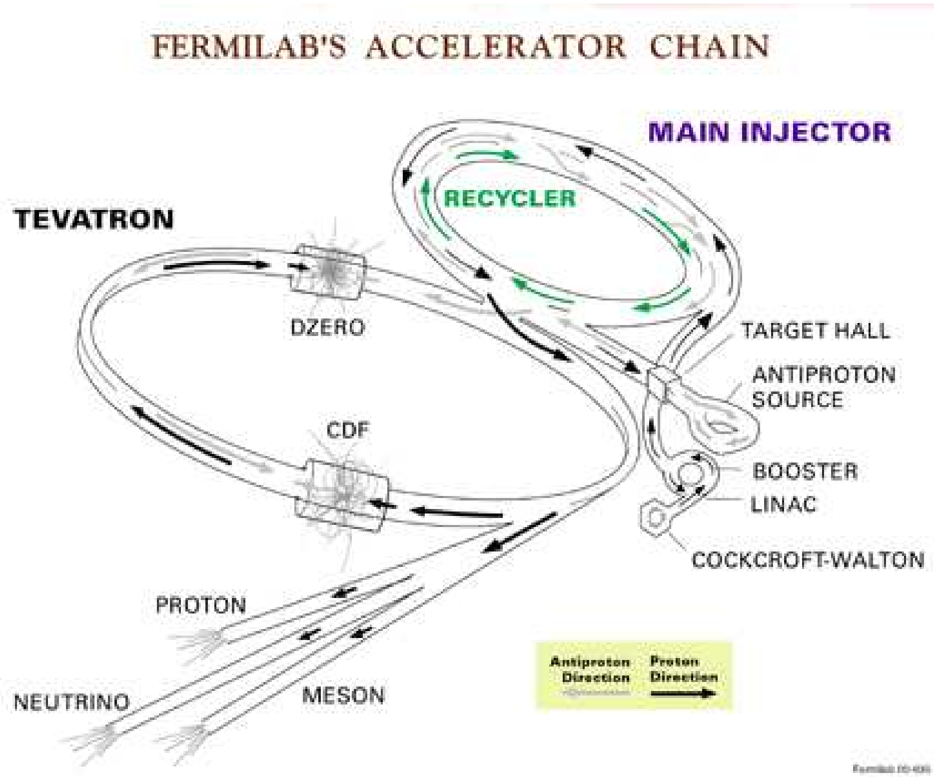

Figure 2.1: Cartoon of Fermilab's Proton and AntiProton Accelerators

2.2 The Collider Detector Facility and its Geometry

The Collider Detector Facility (CDF) is a cylindrically symmetric detector designed to study a wide range of physics at the Tevatron. The detector is made up of layers of sub-detectors, with silicon layers near the collision point, and additional detector subsystems layered on top of one another with increasing radial distances. CDF uses a right handed coordinate system, with the z-axis pointing in a tangent to the ring of the Tevatron, and aligned with the direction of the proton beam trajectory. The x-axis points out along a radius of the Tevatron; it is parallel to the ground and it is perpendicular to the z-axis. The y-axis is the final component in the right handed coordinate system, and points up. The polar angle, θ = arccos(z/r). The azimuthal angle, ϕ = arctan(y/ x), and the pseudo-rapidity, η, is defined as, η = -log tan $(\frac{\theta}{2})$.

Two aspects for our detector are critical: the identification of particles, and the resolution of the detector. The objects, of which we understand both their efficiencies and fake-rates, are those for which tracking is essential: electrons, muons, and photons (i.e. a high confidence of the absence of a track) all in the central region. Also, the energy scale, and resolution is well understood in the calorimeters. The following sections describe the subsystems used to identify objects. A good resolution is important in the identification of secondary vertices which tend to occur in the decays of B hadrons, and resolving the different tracks from many different objects in the detector.

2.3 Tracking System

The tracking system of CDF is used to reconstruct the trajectory of charged particles. The trajectory of charged objects moving through the detector gives valuable information about the decay products from a collision. The tracking system is very close to the interaction point to help distinguish many different particles. Good resolution is especially useful for detecting a secondary vertex a feature common to B hadrons. A secondary vertex comes from B hadrons, which while not stable, can travel on average several millimeters before decaying, and the tracking system is able to see this decay. The tracking system of CDF can be broken down into two components: an open cell wire drift chamber, and the silicon systems.

Both systems are located in a 1.4 Tesla uniform magnetic field pointing along the z-axis, created by a superconducting solenoid 5 m in length, and a radius of 1.5 m. Charged particles in a magnetic field will follow a helical trajectory; the curvature of these tracks are used for charge identification, and for transverse momenta measurements.

The silicon system, is made of 3 subcomponents; from smallest radius to largest: Layer 00 (L00), the Silicon Vertex Detector (SVX), and the Intermediate Silicon Layer (ISL). L00 is a single layer of radiation hard silicon mounted directly on the beam pipe (r = 1.6 cm), and provides only axial tracking information only. The second subsystem, SVX, contains 5 layers of double-sided silicon, it reaches from r

= 2.44 cm to r =10.6 cm away from the beam line. One side of each wafer of silicon in the SVX is able to make measurements in the r-ϕ plane. The other side of wafers in the 1st, 3rd, and 5th layer, make stereo measurements in the z-phi plane, and the 2nd and 4th layers contain small stereo angle strips pitched 1.2° away from the strips to make axial measurements. The SVX is divided into 12 identical wedges equally spaced in ϕ and is divided into three barrel shaped segments in z. The strip pitch is 55-65 μm for axial strips, 60-75 μm for small stereo angle strips, and 125-145 μm for 90° stereo angle strips. Fig. 2.2 is an artist's rendition of the SVX system.

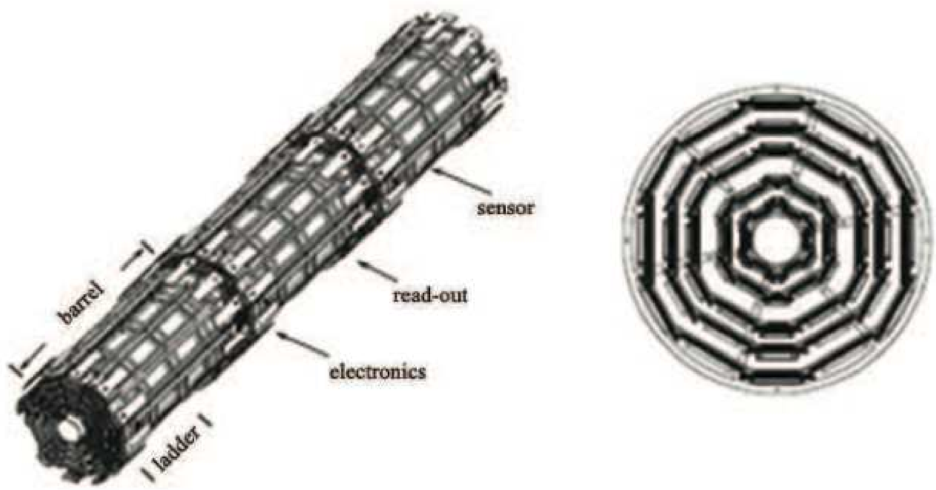

Figure 2.2: An artist's rendition of SVX, left side view, right end on view.

The ISL has two layers and is located at radii 20-29 cm. One side of the ISL contains strips with a pitch of 55 μm making axial measurements, while the opposite sides make small angle stereo measurements with a pitch of 73 μm.

The Central Outer Tracker (COT) [8] is an open-cell drift chamber with 2520 cells organized into eight superlayers, lying outside of the silicon systems and with a radius extending to 137 cm. A super layer is a group of cells all at the same radius in the COT. Each cell has a total of 12 sense wires and 13 potential wires; the even layered superlayers have wires oriented axially, and the odd layers' wires are oriented with an angle offset ± 2° for stereo measurements.

The COT is filled with a mixture of equal parts of ethane and argon; and

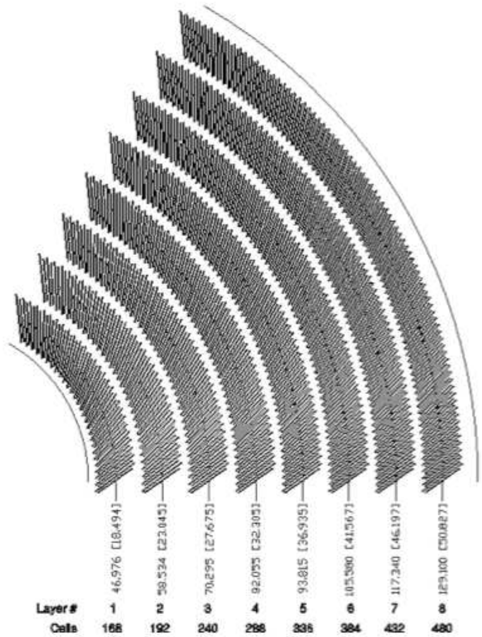

Figure 2.3: A section (1/6 of the total) of the Central Outer Tracker

the drift time for electrons produced from passing particles is designed to be less than 100 ns. As a charged particle travels through the COT, it produces ionization electrons. These electrons drift toward the sense wires in the electric field produced by the potential wires, and the cathode field panels. The drift electrons will move in a direction perpendicular to the magnetic field, at an angle α with respect to the electric field lines. In the COT $\alpha \sim 35°$.

The optimal resolution for a track occurs when the drift angle α is perpendicular to that of the track. Most high p_T tracks will be nearly radial, thus each of the COT cells are tilted by 35° with respect to the radial. A schematic diagram of a portion of the COT can be seen in Fig. 2.3; the 35° tilt can be seen as well. The transverse momentum resolution is $\sigma_{PT}\ /\ p_T = 0.15\ \% \times p_T$.

When an electron gets near a sense wire the wire's local 1/r field accelerates the electron, which in turn causes more ionization. The resulting ionization forms an "avalanche" and we measure this as a signal (hit) on the sense wire. The location of the hit can be found by finding the time of the hit, and the time of the collision;

this determines the distance.

2.4 Calorimetry

The measurement of energy is done by sampling calorimeters. The calorimeter is located outside of the solenoid and consist of alternate layers of scintillator and absorbing material. It is designed to absorb and measure the energy of the photons, electrons and hadrons. The calorimeter is split into two layers, the electromagnetic calorimeter, and the hadronic calorimeter. The innermost layer is the electromagnetic calorimeter, is designed to stop electrons and photons and uses lead as its absorbing material. The hadronic calorimeter is designed to measure charged and neutral hadrons and uses steel as its absorbing material. The calorimeter is split into two regions, one covering the positive η region, the other the negative η region.

A high energy electron or photon passing through the EM calorimeter will undergo pair production ($\gamma \rightarrow e^+e^-$) or bremsstrahlung ($e^\pm \rightarrow \gamma e^\pm$). This particle multiplication is called a shower. In each transition the energy per particle will drop, until there is not enough energy to allow farther travel or create more particles. The point where the largest number of particle occur is called the shower maximum. Beyond the shower maximum, the particles slowly lose their energy through either Compton scattering for photons or ionization losses for electrons and positrons. The EM calorimeter measures the energy from each of the particles in the shower, and the calorimeter is designed to fully contain showers from electrons and photons.

Both the central ($|\eta| < 1.1$) and plug ($1.1 < |\eta| < 3.6$) electromagnetic (EM) calorimeters have fine grained shower profile detectors at electron shower maximum, and preshower pulse height detectors at approximately $1X_0$ depth. Electrons are identified by E/p measurements in the EM calorimeter, HAD/EM (Hadronic energy divided by EM energy) ~ 0, and using shower shape and position matching in the shower max detectors.

Hadrons lose their energy through nuclear interaction cascades which have pions, protons, kaons, muons, photons, etc. These reactions are much more complicated than those in the EM calorimeter, and as a result there is a larger fluctuation in the energy resolution.

2.4.1 Central Calorimeters

The central calorimeters consist of the central electromagnetic calorimeter (CEM) and the central hadronic calorimeter (CHA), and the end wall hadronic calorimeter (WHA).

The CEM and CHA are constructed in wedges of about 15° in azimuth, and extend 250 cm in the positive and negative z direction. There are 24 such wedges in each of the positive and negative z sides. Each wedge contains 10 towers each covering a range 0.11 in pseudorapidity.

There are five separate subsystems in the calorimeter. The CEM covers $|\eta| < 1.1$ and contains 31 layers made up of lead layers and polystyrene scintillator layers. The calorimetry is segmented in "towers" in a projective geometry in η and ϕ pointing towards the center of the detector, with 10 groups in η, and 24 wedges in ϕ. Two photo multipliers are used to read out the light from the scintillators for each tower. There is an energy resolution of $13.5\%/\sqrt{(}\mathrm{E_T}))\oplus$ 2%. [1]

The Central Electromagnetic Shower (CES) detector is embedded inside the CEM at the shower maximum. at a depth of about 6 radiation lengths. The CES detector is made up of a strip and wire chamber located at a radius of 184 cm from the beamline. Cathode strips measure the z-position, and the anode wires measure the ϕ position. The CES is capable of distinguishing a single shower from a prompt photon and two showers from a decay of a neutral meson to two photons (i.e. $\pi^0 \rightarrow \gamma\gamma$), with a resolution of 2 mm at 50 GeV.

The central preradiator detector (CPR) is located at the front of each calorimeter wedge, and it uses the solenoid and tracking detectors as a radiator. It uses proportional chambers to sample the early development of the shower to measure conversions in the coil. A prompt photon has a 60% chance of converting, while the chance of at least one photon from a π^0 decay is about 80% [9].

Outside of the CEM, is the central hadronic calorimeter, CHA, and WHA. The

[1] where the symbol $\oplus$ means added in quadrature.

CHA covers the region $|\eta| < 0.6$ and the WHA covers the region $0.7 < |\eta| < 1.2$. They use steel as the absorbing material for the hadrons to interact with. When the hadrons interact with the steel they create showers of lighter hadrons, such as pions, kaons, and protons. In each of these showers the hadronic particles lose energy to the calorimeter which can be measured in towers just like in the CEM. The scintilator material in the CHA and WHA is acrylic. Their energy resolution is $75\%/\sqrt{\mathrm{E_T}} \oplus 3\%$, as measured on the test beam for single pions.

2.4.2 Plug Calorimeters

The plug calorimeters consist of the plug electromagnetic calorimeter (PEM) and the plug hadronic calorimeter (PHA). The plug calorimeters are so named because in order to fit into the end of the central region of CDF it is shaped like a giant plug. The plug calorimeters' layers are oriented perpendicular to the beam, and allow measurement of the energy of particles with a pseudorapidity of $1.1 < |\eta| < 3.6$. The plug shower max (PES) detector is located at about 6 X_0 in depth in the PEM.

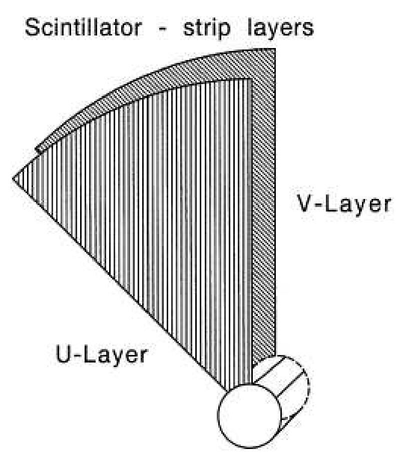

Figure 2.4: View of U and V layers of Plug Shower Max Detectors

Wedges in the plug calorimeter span 15° in azimuth for $2.1 < |\eta| < 3.6$, and 7.5° in azimuth for $1.1 < |\eta| < 2.1$. The PEM is a series of 22 alternating layers of lead and scintillator, and has the same structure as CEM. The transverse energy resolution of the PEM is $16\%/\sqrt{E} \oplus 1\%$.

The PEM is segmented into U and V layers which are offset from the radial direction by +22.5° and -22.5° respectively, leading to a resolution of about 1 mm. PHA is located behind the PEM, and has the same tower segmentation. As in the CHA, there is a 23 layer steel scintillator sampling calorimeter and the resolution is about $80\%\sqrt{E}\oplus5\%$ [10].

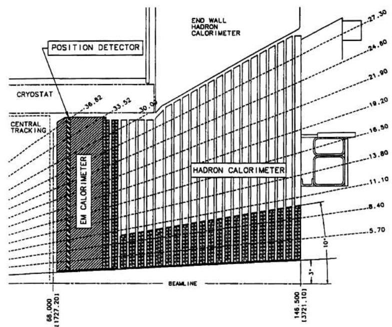

Figure 2.5: Longitudinal View of the CDF Plug Calorimeter

2.5 Muon Detectors

The previously described calorimeter is unable to reliably detect muons because nearly all muons make it through the calorimeter without being stopped, leaving behind only ionization energy.

In order to detect muons, the muon detectors are located behind the calorimeters, and are covered with large amounts of steel shielding to stop remnant hadronic particles escaping the calorimeter. The shielding does not stop the muons, which pass through leaving behind hits in the muon detectors, which are four layers of single-wire drift cells four layers deep. Behind the CHA and the steel shielding is the central muon detector (CMU), which covers $|\eta| < 0.6$. After the CMU there is the central muon upgrade (CMP). The return yoke of the solenoid magnet provides shielding from hadrons punching through the calorimeter. CMP covers the same η range as the CMU. Muons that are detected in this region are required to have at least three hits in both the CMU and CMP subsystems, and are called CMUP muons, and the group of three such hits is called a "stub". The central muon extension, CMX covers $0.6 < |\eta| < 1.0$, and like the CMU and CMP subsystems has four layers of drift tubes. However due to the floor, in the bottom quadrant the drift tubes take a fan shape referred to as the “miniskirt” [11]. Similar to the CMUP muons, CMX muons require the presence of a stub in the CMX detector.

The maximum drift time of the CMU is greater than the bunch crossing time; this can cause discrepancies in the Level 1 trigger in Sec. 2.8. There are scintillation counters to resolve this discrepancy.

2.6 Time of Flight System

The Time of Flight (TOF) [12] system is meant to precisely measure the time between a collision and when objects reach the TOF. The design resolution of the TOF is 100 ps and this provides differentiation between decays of Kaons and Pions. The TOF is also used to differentiate muons from the collisions from those to cosmic rays, and while the TOF is not explicitly used in this analysis, the rejection of muons from cosmic rays is.

The TOF has a radius of 140 cm, which corresponds to a flight time of about 5 ns for the fastest particles. It is located between the COT and the solenoid.

The TOF is constructed of 216 scintillator bars each with dimensions 4x4X279 cm; each bar covers 1.7° in phi. Each scintillator has a photon multiplier tube (PMT) attached at each end. The sigal from the PMTs provide information on integrated charge as well as timing.

2.7 Luminosity Counters

Any measurement of a cross section will require good knowledge of the integrated luminosity for normalization, and to estimate the magnitude of Monte Carlo driven backgrounds. Luminosity is a measure of particle interactions; in our case the chance that a proton will collide with an antiproton. The rate of inelastic scattering of in $p\bar{p}$ can be used to determine the luminosity.

The luminosity of CDF is calculated using Cerenkov Luminosity Counters (CLC) [13]. The CLC are located in the very forward regions of the detector, 3.7

$< |\eta| < 4.7$. The luminosity is measured based on the numbers of proton antiproton interactions, and this is converted to a luminosity amount.

The luminosity of a $p\bar{p}$ collider can be estimated using the following equation:

$$\mathcal{L} = \frac{f \times \mu}{\sigma}. \tag{2.1}$$

where f is the frequency of beam crossing, μ is the average number of interactions per beam crossing, and σ is the inelastic cross section of $p\bar{p}$ scattering.

The integrated luminosity amount is assigned a systematic uncertainty of 6% due to uncertainties in the proton antiproton total elastic cross section.

2.8 Trigger and Data Acquisition

Physical processes of interest to us occur at rates many orders of magnitude below the total $p\bar{p}$ inelastic cross section. Furthermore, the rate of collisions at the Tevatron is much too rapid to possibly save all events. It is necessary, then, to have a system which saves events which could be interesting to physicists at CDF, and to reject events which are not interesting.

The CDF trigger system does exactly this. It uses a three level architecture to accept or reject events, Level 1 (L1), Level 2 (L2), and Level 3 (L3). At each increase in level, the data volume is further reduced.

At L1 the trigger must make its decisions within 5 μs of each collision. Collisions occur at a rate of 1.7 MHz; and the L1 triggers system lowers the acceptance rate to about 40 kHz. L1 can make its decision based on axial layers of the COT which are used by the eXtreme Fast Tracker (XFT) to reconstruct ϕ and p_T of tracks left by charged objects. L1 can look at the ratio of Hadronic to Electromagnetic Energy in calorimeter towers and identify electrons and photons, and differentiate them from jets. Muons can be reconstructed using XFT and hits made in the muon subsytems. $\not\!\!E_T$ and $\sum E_T$ (a scalar sum of the transverse energy of all of the calorimeter towers) are also reconstructed at L1. Events which pass L1 acceptance are then passed to the L2 hardware.

At L2 the event selection is further refined, and decisions are made within 30 μs. L2 uses information from layers 0-3 of SVX, and combines this information with the XFT tracks. At L2 there is a more careful clustering in the calorimeter including information from the CES. The SVX data is processed by the Silicon Vertex Tracker (SVT), and this system looks for displaced vertex. An event at the L2 trigger sytem is asynchronous (i.e. an event does not need to be finished by a fixed time after the collision occurred.) The acceptance rate of L2 is about 400 Hz.

All accepted L2 events are sent to the highest level trigger which is implemented in software on a farm of several hundred computers. At L3 each event is sent to the event builder, which fully reconstructs and analyzes the event using the latest calibrations of the detector. Events which pass L3 are now ready to be saved; the L3 accept rate is about 100 Hz. [14]. We show a block diagram of the trigger decision of the CDF in Fig. 2.6.

There are a variety of triggers available to CDF users, and these triggers correspond to various phyiscs processes. It is important to be cognizant of the choice of trigger one makes.

For our purposes we are using triggers corresponding to high-p_T leptons; these are standard triggers used by the CDF top-quark research group. This is a useful choice for a couple of reasons. First, we want to measure the ratio of production cross sections of $t\bar{t}\gamma$ and $t\bar{t}$, and therefore using a photon trigger would include a systematic error that would not cancel out in the ratio. Second, these tiggers allow us to make a good comparison between our measurement of $t\bar{t}$ and a combination of many different measurements, made by CDF, of the $t\bar{t}$ cross section.

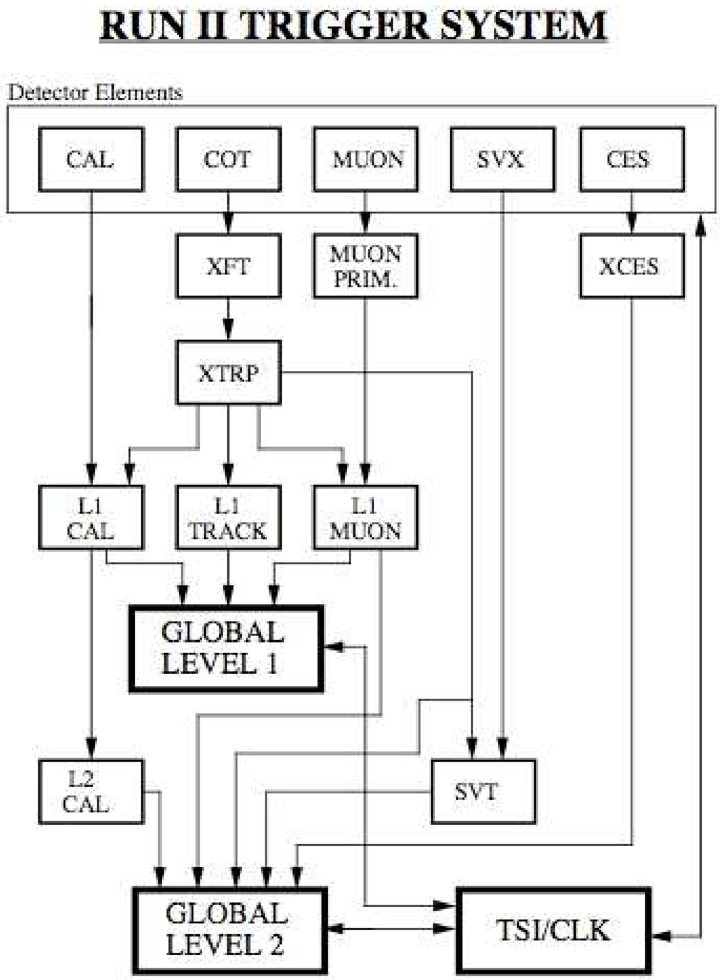

Figure 2.6: Block Diagram of CDF's Trigger System. Flow of data through the L1 and L2 of trigger system. The SVT information, based on the track impact parameter of displaced tracks is used by L2. At each progressive level the volume of data is reduced. The L3 trigger is completely software based, and is run on a computer farm.

3 Defining the Event Categories by Topology

We are primarily concerned with three signatures: $t\bar{t}\gamma$, $\ell\gamma\not\!\!E_{\mathrm{T}}b$, and $t\bar{t}$. Each of these signatures begins with the event selection enumerated in Tab. 3.1. A large $\not\!\!E_{\mathrm{T}}$ cut of 20 GeV is applied to reduce the amount of QCD contamination that will enter these selections.

The distribution of data events in the $t\bar{t}$ sample with no $\not\!\!E_{\mathrm{T}}$ cut is shown in Fig

6.1; it can be seen that most of the QCD contribution is in the low $\not\!\!E_T$ range.

Selection Criteria for lepton, jets, and $\not\!\!E_T$ channel	
Variable	**Selection Critera**
Jet E_T	$\geq$ 20 GeV
Jet η	$\leq$ 2.0
Lepton E_T	$\geq$ 20 GeV
Lepton type	1 CEM Electron or CMUP muon or CMX muon
$\not\!\!E_T$	$>$ 20 GeV

Table 3.1: Basic selection criteria of lepton, jets, and $\not\!\!E_T$ events. The full requirements of muons, electrons, and $\not\!\!E_T$ can be found in Secs. B.1, B.2 and B.5.1 respectively.

Each of our samples requires identification of a b-tagged jet. From previous analyses in this channel we expect a very small signal from this channel [5]. For identification of b-tagged jets we will be using SecVtx "loose"-tagged jets. This category, as its name implies, has a lower selection criteria for b-tagging than the "tight" tagging that CDF's top-quark group uses. This means we will have more misidentified b-tagged jets than CDF's top-quark group, but this is a necessary selection for both $\ell\gamma\not\!\!E_T b$ and $t\bar{t}\gamma$ signals.

The full list of additional cuts is shown in Tab. 3.2.

Selection Criteria for $\ell\gamma\not\!\!E_T b$ channel	
Variable	**Selection Critera**
Jet E_T	$\geq$ 20 GeV
Jet η	$\leq$ 2.0
Lepton E_T	$\geq$ 20 GeV
Lepton type	1 CEM electron or CMUP muon or CMX muon
$\not\!\!E_T$	$>$ 20 GeV
N_{b-tag}	$\geq$ 1
Photon type	1 Central Photon
Photon E_T	$\geq$ 10 GeV

Table 3.2: This is the full list of requirements for the $\ell\gamma\not\!\!E_T b$ event selection.

The $\ell\gamma\not\!\!E_T b$ and $t\bar{t}\gamma$ event selection will require the identification of a tigt photon. All photon cuts are enumerated in Tab. B.3. In order to better identify signal processes from background processes in the $t\bar{t}\gamma$ sample we added an additional re-

Selection Criteria for $t\bar{t}$ Signal	
Variable	**Selection Critera**
N_{b-tag}	≥ 1
Jet E_T	≥ 20 GeV
Jet η	≤ 2.0
N_{Jets}	≥ 3
Lepton E_T	≥ 20 GeV
Lepton type	1 CEM Electron or CMUP muon or CMX muon
$\not{E}_T$	> 20 GeV
H_T	> 200 GeV
M_T	< 20 GeV (electrons) < 10 GeV (muons)

Table 3.3: This is the full list of requirements for the $t\bar{t}$ event selection.

quirement on a photon's χ^2 value of the reconstructed energy deposits in the CES (this is explained in Sec. 8).

Additionally to differentiate $t\bar{t}$ and $t\bar{t}\gamma$ signals from their backgrounds an additional requirement of $H_T > 200$ GeV was required for both of these event selections.

It was also found that to better model the QCD contamination of the $t\bar{t}$ sample, it was necessary to require the transverse mass of the lepton, $\not{E}_T$ object to be > 20 GeV for electrons and > 10 GeV for muons. Removing these regions allows for a much better kinematic fit of the data. This was not required for $\ell\gamma\not{E}_T b$ or $t\bar{t}\gamma$ due to very low statistics when modelling the QCD contribution.

For all of our samples we require that the event be triggered with a high-p_T lepton trigger in order to be selected, and we discuss this further in Sec 3.2.

3.1 Datasets

The data presented in the analysis represent 5.7fb^{-1} for which the silicon detector and all three central muon systems CMP, CMU and CMX were operational. Previous results for these analyses with $929pb^{-1}$ and 1.9fb^{-1} of data are described in [15] and [5] respectively.

Our data involving muons comes from the inclusive high-P_T muon samples: *bhmu0d*, *bhmu0h*, *bhmu0i* , *bhmu0j*, *bhmu0k*, and *bhmu0m*. The data involving

Selection Criteria for $t\bar{t}\gamma$ Signal	
Variable	**Selection Critera**
N_{b-tag}	≥ 1
Jet E_T	≥ 20 GeV
Jet η	≤ 2.0
N_{Jets}	≥ 3
Lepton E_T	≥ 20 GeV
Lepton type	1 CEM Electron or CMUP muon or CMX muon
$\not{E}_T$	> 20 GeV
H_T	> 200 GeV
Photon type	1 Central Photon
Photon E_T	> 10 GeV

Table 3.4: This is the full list of requirements for the $t\bar{t}\gamma$ event selection.

electrons comes from the inclusive high-P_T electron samples: *bhel0d*, *bhel0h*, *bhel0i* and *bhel0j*, *bhel0k*, and *bhel0m*.

Each of these samples was ntupled using the TTGNtupler package (Appendix A.3). In both previous analyses the ntupling was done using the UC flat ntuple details of which can be found in [16, 17].

In the following section we describe the event selection for each of our three analysis categories, $\ell\gamma\not{E}_T b$, $t\bar{t}\gamma$, and $t\bar{t}$.

3.2 Triggers Used in this Analysis

There are a variety of triggers available to CDF users, and these triggers correspond to various phyiscs processes. It is important to be cognizant of the choice of trigger one makes.

For our purposes we are using triggers corresponding to high-p_T leptons; these are standard triggers used by the CDF top-quark research group. This is a useful choice for a couple of reasons. First, we want to measure the ratio of production cross sections of $t\bar{t}\gamma$ and $t\bar{t}$, and therefore using a photon trigger would include a systematic error that would not cancel out in the ratio. Second, these tiggers allow us to make a good comparison between our measurement of the $t\bar{t}$ cross section and a measurement of the $t\bar{t}$ cross section made by CDF through a combination of several measurements.

The trigger paths used in this analysis can be found in Table 3.6, which is the same triggers that CDF's top group uses. The previous analysis of $t\bar{t}\gamma$, [18], used the trigger paths found in Table 3.5. The MUON_CMX18_JET10 trigger requires an additional jet in order to fire; this was done to lower the rate at which the CMX18 triggers were firing.

Trigger Path Used	Run Range
MUON_CMX18	ALL
MUON_CMX18_LUMI_250	ALL
MUON_CMX18_L2_PT15	ALL
MUON_CMX18_L2_PT15_LUMI_200	ALL
MUON_CMX18_&_JET10	ALL
MUON_CMX18_&_JET10_LUMI_270	ALL
MUON_CMX18_&_JET10_DPS	ALL
MUON_CMUP18	ALL
MUON_CMUP18_L2_PT15	ALL
ELECTRON_CENTRAL_18	ALL

Table 3.5: List of Triggers used in the previous $t\bar{t}\gamma$ analysis, but there have been updates in the current analysis.

Trigger Path Used	Run Range (inclusive)
MUON_CMX18	138425 - 200272
MUON_CMX18_L2_PT15	138425 - 226194
MUON_CMX18_L2_PT15_LUMI_200	200273 - 226194
MUON_CMX18_&_JET10	226195 - 257201
MUON_CMX18_&_JET10_LUMI_270	226195 - 257201
MUON_CMX18_&_JET10_DPS	226195 - 257201
MUON_CMX18	257201 - and up
MUON_CMUP18	ALL
MUON_CMUP18_L2_PT15	138425 - 229763
ELECTRON_CENTRAL_18	ALL

Table 3.6: List of Triggers used by the CDF Top Group, and this analysis

We ran over the first 4.8 fb^{-1} of data and looked for W, Z, $Z\gamma$ and $W\gamma$ candidate events. We normalized the yields by the amount of luminosity in the data set. We used the triggers shown in Table 3.5, and found the results shown in Table 3.7.

It was noted that the rate of W$\rightarrow$ $\mu\nu$ production seemed quite low in the bhmu0j

Object	0d	0h	0i	0j	0k	0m	0mn
W	488.66 ± 1.25	537.91 ± 1.23	502.86 ± 0.93	362.03 ± 0.62	363.36 ± 0.87	454.81 ± 0.62	461.41 ± 0.71
Z	30.57 ± 0.31	34.41 ± 0.31	33.31 ± 0.24	26.76 ± 0.17	27.03 ± 0.24	26.88 ± 0.15	27.52 ± 0.17
$\ell\gamma\not{E}_T$	0.68 ± 0.047	0.79 ± 0.047	0.77 ± 0.037	0.66 ± 0.027	0.71 ± 0.039	0.57 ± 0.022	0.55 ± 0.024
$\ell\ell\gamma$	0.23 ± 0.027	0.17 ± 0.022	0.18 ± 0.018	0.19 ± 0.014	0.12 ± 0.016	0.14 ± 0.011	0.15 ± 0.013

Table 3.7: Results using top triggers as shown in Table 3.5, which are independent of run number. This table only shows results for Muon samples. Each category has been normalized by the total integrated luminosity in the sample.

Object	0d	0h	0i	0j	0k	0m	0mn
W	742.24 ± 1.54	754.89 ± 1.46	716.47 ± 1.12	674.73 ± 0.85	676.81 ± 1.19	636.22 ± 0.74	645.79 ± 0.84
Z	33.91 ± 0.33	33.46 ± 0.31	32.84 ± 0.24	31.21 ± 0.18	31.59 ± 0.26	29.12 ± 0.16	29.43 ± 0.18
$\ell\gamma\not{E}_T$	0.87 ± 0.053	0.88 ± 0.050	0.86 ± 0.039	0.79 ± 0.029	0.69 ± 0.038	0.67 ± 0.024	0.68 ± 0.027
$\ell\ell\gamma$	0.37 ± 0.034	0.30 ± 0.029	0.27 ± 0.022	0.22 ± 0.015	0.21 ± 0.021	0.21 ± 0.013	0.20 ± 0.015

Table 3.8: Results using top triggers, as shown in Table 3.5. which is independent of run number. This table only shows results for Electrons. Each categroy has been normalized by the integrated luminosity in the sample.

and bhmu0k datasets. To investigate this we reran the bhmu0j and bhmu0k datasets using the additional trigger MUON_CMX18_L2_LOOSE_DPS.

The CMX trigger path was changed during runs contained in the bhmu0j and bhmu0k datasets; the CMX trigger required a central jet with E_T greater than 10 GeV. We see better agreement, but we have not corrected the luminosity in the sample, and this latest trigger is pre-scaled so that is necessary. Our latest results with this trigger can be seen in Table 3.9.

While the additional trigger does indeed increase the event yield for W $\rightarrow \mu\nu$ events we do not use this trigger to be consistent with CDF's top quark group . In order to make the best measurement of the $t\bar{t}$ cross section we use only the triggers shown in Table 3.6.

Object	0j	0k
W	447.14 ± 0.69	433.65 ± 0.96
Z	30.64 ± 0.18	30.16 ± 0.25
$\ell\gamma\not{E}_T$	0.67 ± 0.027	0.72 ± 0.039
$\ell\ell\gamma$	0.19 ± 0.014	0.12 ± 0.016

Table 3.9: Results allowing additional MUON_CMX18_L2_LOOSE_DPS trigger. We can see that in this case there were considerable gains made (compared to Table 3.8) in the event selection for each of these four samples, however the choice was made to be consistent to the CDF top-quark group's trigger selection as shown in Table 3.6

3.3 Selecting Candidate Events from Data

To reduce processing time, we took a few steps to select events. At the first step (STNtuple $\rightarrow$ TTGNtuple) we required an event to contain at least one loose electron (Table B.2, we required $\mathrm{E_T^e} > 12$ GeV cut), or at least one loose muon (Table B.1, we required $\mathrm{P_T^\mu} > 12$ GeV cut), or an anti-electron (Table A.7). We performed this step on CDF CAFs (a large network of computers), and output TTGNtuples were saved on the University of Chicago (UC) disk space (Appendix A.3).

At the second step we have selected events needed for signal and background studies, and also for cross-checks of W, Z, $\ell\gamma\not{E}_{\mathrm{T}}$ and $\ell\ell\gamma$ event yields for different data-taking periods. We performed this step on the University of Chicago batch system and output TTGNtuples were saved on the Yale disk space (Appendix A.3) for further analysis. In Table A.5 we list the raw number of events in the datasets, the run ranges for the datasets as well as the number of events selected the datasets.

4 Standard Model Predictions

The dominant sources of $\ell\gamma\not{E}_{\mathrm{T}}b$ events at the Tevatron come from leptonic W decays with associated heavy flavor production from gluon-splitting, or $t\bar{t}$ events, with a photon radiated from an initial state quark, a W boson, or a final state lepton. The number of events from these types of decays are calculated using Monte Carlo (MC) event generator programs. For the $\ell\gamma\not{E}_{\mathrm{T}}b$ events we exclusively use the MadGraph event generation software.

4.1 New MadGraph Samples

4.1.1 Introduction: The Matrix Element Generators

The number of $\ell\gamma\not{E}_{\mathrm{T}}b$ and $t\bar{t}\gamma$ events from $t\bar{t}\gamma$ production is estimated using leading-order (LO) Monte Carlo event generator program MadGraph [19] (kinematic cuts are listed in Table 4.1).

This program outputs 4-vectors and helicities of particles emanating from a diboson production event in an ASCII format. In addition the information on how the particles are produced ("mother" and "daughter") is recorded, including the energy scale and other parameters used for the matrix element calculation.

These files are then fed into the LesHouchesModule [20], which runs Pythia to add parton fragmentation and final-state radiation and initial-state radiation (both QED and QCD) , and then writes out the events in CDF HEPG format. The CDF HEPG format is a code that is used to identify all of the event parameters, including kinematics and identification of objects.

These files are then used as input to the CDF detector simulation program. This program outputs simulated data in a format identical to that of an actual CDF Run II event. Each of the objects from the event interacts in a computer simulation of the detector. Simulated $\ell\gamma \not\!\!E_{\mathrm{T}} b$ event rates can then be estimated in a manner identical to that of CDF data.

We performed an additional check of MadGraph $t\bar{t}$ MC. We generated $t\bar{t}$ MC with MadGraph and compared cross-sections of the processes with standard CDF Top group MC.

4.1.2 $t\bar{t}\gamma$ MC Samples

The information about new MadGraph samples including all cuts and settings etc is listed in this section.

To generate $t\bar{t}\gamma$ and $\ell\gamma \not\!\!E_{\mathrm{T}} b$ MC we employed MadGraph and requested the dileptonic contribution be split into three pieces shown below.

The processes above show the t quark or tbar quark decaying to a b quark, charged lepton, and corresponding neutrino. The top (anti top) quark decay to a W boson and b (anti-b) quark. The W boson then decays to a charged lepton. In the first process, either the initial quarks of the proton, the top quark, or the anti-top quark radiate a photon. In the other two process, a decay product of the top, or anti-top, quark radiates off a photon.

The process for semileptonic decay of ttbar plus a photon is broken down into six sub processes for ease of running on the MadGraph website as well as simulating locally. There have been 15 runs generated, and the following table shows the number of events contained per run.

As a comparison I am showing the results from the 1.9 fb^{-1} note for $t\bar{t}\gamma$ cross sections which can be seen in Table 4.1.

DataSet Name	Events	Crossection (pb)
Mad_$t\bar{t}\gamma$ semileptonic (e and μ)	43724	0.0726349
Mad_$t\bar{t}\gamma$ dileptonic (e and μ)	33801	0.0216773

Table 4.1: The $t\bar{t}\gamma$ MadGraph datasets.

DataSet Sample	Events per Run	Cross Section (pb)	Cross Section Uncertainty
(t$\rightarrow \bar{d}ub)(\bar{t} \rightarrow \bar{b}l^{-}\bar{\nu}$)a	17,304	0.009737	0.000024
(t$\rightarrow \bar{s}cb)(\bar{t} \rightarrow \bar{b}l^{-}\bar{\nu}$)a	9,134	0.009730	0.000016
(t$\rightarrow \bar{d}uba)(\bar{t} \rightarrow \bar{b}l^{-}\bar{\nu})$	1,236	0.003954	0.000040
(t$\rightarrow \bar{s}cba)(\bar{t} \rightarrow \bar{b}l^{-}\bar{\nu})$	1,248	0.003953	0.000030
(t$\rightarrow \bar{d}ub)(\bar{t} \rightarrow \bar{b}l^{-}\bar{\nu}$a)	1,284	0.006206	0.000237
(t$\rightarrow \bar{s}cb)(\bar{t} \rightarrow \bar{b}l^{-}\bar{\nu}a)$	1,284	0.006206	0.000237
ttg_Semileptonic	xxx	0.039720	0.000360
(t$\rightarrow bl+\nu)(\bar{t} \rightarrow \bar{b}l^{-}\bar{\nu}$)a	12,623	0.010349	0.000019
(t$\rightarrow bl+\nu)(\bar{t} \rightarrow \bar{b}l^{-}\bar{\nu}a)$	1,365	0.006685	0.000430
(t$\rightarrow bl+\nu$a)($\bar{t} \rightarrow \bar{b}l^{-}\bar{\nu})$	1,126	0.006444	0.001224
ttg_Dileptonic	xxx	0.023478	0.001297

Table 4.2: The $t\bar{t}\gamma$ Semileptonic and Dileptonic Decay MadGraph datasets. In each of these decays the lepton may be any of the three flavors.

DataSet Sample	Events per Run	Cross Section (pb)	Cross Section Uncertainty
W$\rightarrow l^{+}\bar{\nu}+\bar{b}b\gamma$ (e, μ, τ)	2,677	0.054738	0.000113
W$\rightarrow l^{+}\bar{\nu}+\bar{c}c\gamma$ (e, μ, τ)	17,244	0.10097	0.000410
W$\rightarrow l^{+}\bar{\nu}+c\gamma$ (e, μ, τ)	17,329	0.4386	0.0009

Table 4.3: The W plus heavy flavor decay MadGraph datasets. In each of these decays the lepton can take on any of three flavors of lepton.

We also simulated three W decays to heavy flavor quarks.

The full list of our requirements on the event kinematics is shown below:

```
#*********************************************************************
# Minimum pt's                                                       *
```

```
#*********************************************************************
  6  = ptj ! minimum pt for the jets
  6  = ptb ! minimum pt for the b
  6  = pta ! minimum pt for the photons
  6  = ptl ! minimum pt for the charged leptons
#*********************************************************************
# Maximum rapidity                                                   *
#*********************************************************************
 4.0  = etaj ! max rap for the jets
 4.0  = etab ! max rap for the b
 2.0  = etaa ! max rap for the photons
 4.0  = etal ! max rap for the charged leptons
#*********************************************************************
# Minimum DeltaR distance                                            *
#*********************************************************************
 0.4 = drjj ! distance between jets
 0.4   = drbb ! distance between b's
 0.4 = drll ! distance between leptons
 0.4 = draa ! distance between gammas
 0.4   = drbj ! distance between b and jet
 0.4 = draj ! distance between gamma and jet
 0.4 = drjl ! distance between jet and lepton
 0.4   = drab ! distance between gamma and b
 0.4   = drbl ! distance between b and lepton
 0.4 = dral ! distance between gamma and lepton
#*********************************************************************
# Minimum invariant mass for pairs                                   *
#*********************************************************************
 0  = mmjj ! min invariant mass of a jet pair
 10  = mmbb ! min invariant mass of a b pair
```

```
 0  = mmaa ! min invariant mass of gamma gamma pair
 10  = mmll ! min invariant mass of l+l- (same flavour) lepton pair
#*********************************************************************
```

4.2 The other SM Processes as Sources of $\ell\gamma\not{E}_{\rm T}b$ and $t\bar{t}\gamma$ Events

We consider WW, WZ, W$c\bar{c}\gamma$, W$\bar{b}\gamma$ and W$c\gamma$ as the other sources for $\ell\gamma\not{E}_{\rm T}b$ and $t\bar{t}\gamma$ events.

We use $t\bar{t}$ sample (ttopel) for estimating $\tau \to hadron \to \gamma$ fake rate.

We use the WW sample (ihhs1a) which is an inclusive WW decay sample used by both the Higgs group and Top group at CDF.

The generator-level monte carlo (MC) events were run through Pythia. They were then run through CdfSim and 5.3.3 Production, and then ntupled [16]; a tabulation of the datasets is given in Ref. [16].

The description of these MC Samples:

sample	x-sec,pb	events
WZ	3.65	409648
Wbbgamma	0.03737	12279
Wcgamma	0.29904	48261
Wccgamma	0.069102	14152
ttbar (topel)	6.1	1146088
WW (ihhs1a)	12.4	4880529

The samples above with parentheses are common names of MC samples used by working groups at CDF.

4.3 SM Processes as Sources of $t\bar{t}$ Events

The dominant source of events with a lepton, true $\not\!\!E_T$ and significant transverse energy, and 3 or more jets with at least one originating from a b-hadron is $t\bar{t}$, and W decays with associated heavy flavor decays. The MC Sets we used for this signature is listed in Table 4.4.

4.3.1 Discussion of K-factors for MC processes

There are numerous ways in which a MC cross section may not adequately scale for a SM process. Most often MC samples are generated solely at tree level. As a result, the higher order processes which will affect a sample's cross section in the detector is not adequately calculated in the MC. We adjust the cross section by using a multiplicative cross section. This is the case for the W plus heavy flavor (W+HF) samples, and for the Z decays. The W decays require an additional multiplicative factor of 1.36 to be used, whereas the Z decays require a factor of 2.

Unfortunately this is not the only k factor used. It has been found in low jet multiplicity, but b-tagged samples, where the W+HF samples are dominant, that the k factor of 1.36 is insufficient. The sample requires and addition k factor to be applied to compensate for this. For this analysis we use a value of 1.5 for each of the W+HF samples. This second k factor is a multiplicative factor so that we have for these samples a total k factor of 1.36×1.5.

There is a relatively large uncertainty of 20% on the k factor due to heavy flavor contribution [21], and this is the dominant uncertainty on the W+HF MC samples.

4.4 Calculating Event Yields of Monte Carlo Based Backgrounds

The rates of the backgrounds for our samples, as well as our signatures' acceptance, $t\bar{t}$, $t\bar{t}\gamma$ are calculated using an MC based approach. Several electroweak processes can contribute to the $t\bar{t}\gamma$, and $\ell\gamma\not\!\!E_T b$ samples including, WW, WZ, ZZ, as well as W$b\bar{b}\gamma$, W$c\bar{c}\gamma$, and Wcγ decays. For the $t\bar{t}$ sample we model with MC the backgrounds: W$b\bar{b}$, W$c\bar{c}$, and Wc decays, as well as diboson, and single top production.

The contribution to our sample is calculated:

$$N_{p\bar{p}\to X} = \sigma_{p\bar{p}\to X} \cdot A \times \epsilon \cdot \int dt \cdot \mathcal{L} \tag{4.1}$$

where $\sigma_{p\bar{p}\to X}$ is the theoretical cross section, $\int dt \cdot \mathcal{L}$ is the total integrated luminosity, and $A \times \epsilon$ is the acceptance of the signal times the selection efficiency. Many of the MC samples used were generated with 1 fb^{-1} statistics, so we must normalize these samples to our total integrated luminosity. The samples also have a scale factor ϵ which is based on object identification and trigger efficiencies which differ between data and MC. These efficiencies are calculated from available data periods, and averaged by luminosity in the data samples, and vary by lepton type.

Furthermore, for the W decay MC (W+HF, $W\gamma$+HF) in the $t\bar{t}$ sample there are two K-factors required to account for differences between generated MC and what is observed in the detector. A k-factor is an overall scale that must be applied to the samples to augment their rate (Sec 4.3.1).

DataSet	Common Name	Cross Section (pb)
$t\bar{t}$	tt0s75	6.7
W→eν+$b\bar{b}$+0p	bt0s0w	2.98
W→eν+$b\bar{b}$+1p	bt0s1w	0.888
W→eν+$b\bar{b}$+$\geq$2p	bt0s2w	0.287
W→ $\mu\nu$+$b\bar{b}$+0p	bt0s5w	2.98
W→ $\mu\nu$+$b\bar{b}$+1p	bt0s6w	0.888
W→ $\mu\nu$+$b\bar{b}$+$\geq$2p	bt0s7w	0.287
W→eν+$c\bar{c}$+0p	ct0s0w	5.00
W→eν+$c\bar{c}$+1p	ct0s1w	1.79
W→eν+$c\bar{c}$+$\geq$2p	ct0s2w	0.628
W→ $\mu\nu$+$c\bar{c}$+0p	ct0s5w	5.00
W→ $\mu\nu$+$c\bar{c}$+1p	ct0s6w	1.79
W→ $\mu\nu$+$c\bar{c}$+$\geq$2p	ct0s7w	0.628
W→eν+c+0p	st0sw0	17.1
W→eν+c+1p	st0sw1	3.39
W→eν+c+2p	st0sw2	0.507
W→eν+c+$\geq$3p	st0sw3	0.083
W→ $\mu\nu$+c+0p	bt0s0w	17.1
W→ $\mu\nu$+c+1p	bt0s1w	3.39
W→ $\mu\nu$+c+2p	bt0s2w	0.507
W→ $\mu\nu$+c+$\geq$3p	bt0s2w	0.083
Single Top (s-channel)	st0s00	0.88
Single Top (t-channel)	st0s01	1.98
WW	ihhs1a	12.4
WZ	jhhs1a	3.7
ZZ	khhs1a	1.4
Z→ $\tau\tau$ +0p	zt0st3	158
Z→ $\tau\tau$ +1p	zt0st4	21.5
Z→ $\tau\tau$ +$\geq$2p	zt0st2	4.14
Z→ ee+$b\bar{b}$ +0p	zt0sb0	0.511
Z→ ee+$b\bar{b}$ +1p	zt0sb1	0.134
Z→ ee+$b\bar{b}$ +$\geq$2p	zt0sb2	0.0385
Z→ $\mu\mu$+$b\bar{b}$ +0p	zt0sb5	0.511
Z→ $\mu\mu$+$b\bar{b}$ +1p	zt0sb6	0.134
Z→ $\mu\mu$+$b\bar{b}$ +$\geq$2p	zt0sb7	0.0385

Table 4.4: Monte Carlo samples used for $t\bar{t}$ sample.

5 Backgrounds: Fakes of the $\ell\gamma\not{E}_{T}b$, and $t\bar{t}\gamma$ Sample

In addition to the expectations from real SM processes that produce real $\ell\gamma\not{E}_{T}b$ and $t\bar{t}\gamma$ events described in Section 4.1 there are backgrounds due to misidentified leptons, photons and b-tags, and also incorrectly calculated $\not{E}_{T}$. We generically call these misidentifications 'fakes'. Each of the following backgrounds is calculated using a data- driven method.

5.1 Misidentified Photons

We consider three sources of fake photons: QCD jets in which a neutral hadron or photon from hadron decay mimics a direct photon, electron bremsstrahlung, in which an energetic photon is radiated off of an electron which is then much lower energy and curls away from the photon, and also photons from tau decays $\tau \rightarrow hadron + \gamma$.

5.1.1 Jets Faking Photon

High P_{T} photons are created from hadron decays in jets initiated by a scattered quark or gluon. In particular, mesons such as the π^{0} or η decay to photons which may satisfy the photon selection criteria. The numbers of lepton-plus-misidentified-jet events expected in the $\ell\gamma\not{E}_{T}b$ and $t\bar{t}\gamma$ samples are determined by measuring energy in the calorimeter nearby the photon candidate.

For each of the four samples, $e\gamma\not{E}_{T}b$, $\mu\gamma\not{E}_{T}b$, $t\bar{t}\gamma$ (e channel), and $t\bar{t}\gamma$ (μ channel), Figure 5.1 shows the distribution in the total (electromagnetic plus hadronic) calorimeter energy, E_{T}^{Iso}, in a cone of radius $R = 0.4$ in η-ϕ space around the photon candidate. This distribution is then fitted to the shape measured for electrons from $Z^{0} \rightarrow e^{+}e^{-}$ decays plus a linear background.

The systematic uncertainty for this misidentification is estimated using a sample of $W\gamma$. This decay is much less limited by statistics than any of our $\ell\gamma\not{E}_{T}$ or $t\bar{t}\gamma$ samples, and thus the uncertainty we find by varying our fit parameters gives us a better understanding of our systematic uncertainty. By repeating our fits with a quadratic function as a background shape instead of just a linear function, and by changing the range of the "photon" isolation energy over which the fit is made, we find there to be about a 20% uncertainty in this method.

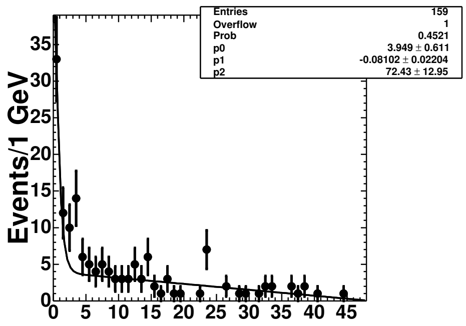

(a) Calorimeter Isolation of Photons Candidates ($e\gamma \not\!\!E_T b$)

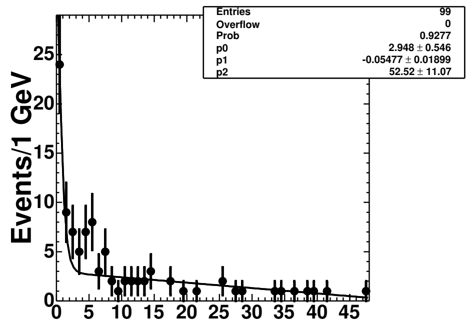

(b) Calorimeter Isolation of Photons Candidates ($\mu\gamma \not\!\!E_T b$)

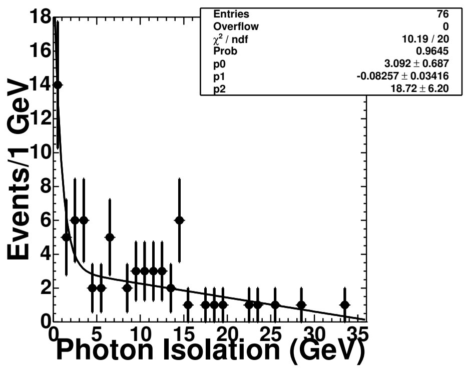

(c) Calorimeter Isolation of Photons Candidates ($t\bar{t}\gamma$ (e))

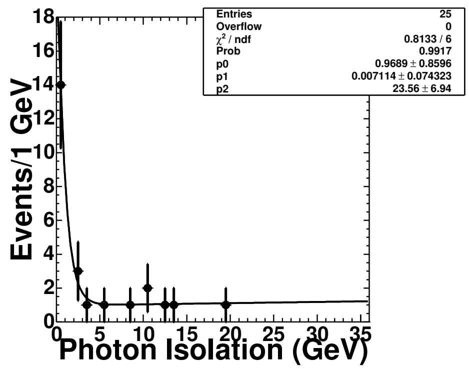

(d) Calorimeter Isolation of Photons Candidates ($t\bar{t}\gamma$ (μ))

Figure 5.1: The method and data used to estimate the number of background events from jets misidentified as photons. For each of the four samples, $e\gamma \not\!\!E_T b$ (left top), $t\bar{t}\gamma$ (e channel, right top), $\mu\gamma \not\!\!E_T b$ (left bottom), and $t\bar{t}\gamma$ (μ channel, right bottom), the number of events is plotted versus the total (electromagnetic plus hadronic) calorimeter energy, E_T^{Iso}, in a cone in η-ϕ space around the photon. This distribution is then fitted to the shape measured for electrons from $Z^0 \to e^+e^-$ decays plus a linear background.

To verify the linear behaviour of the background we create fake photon sample. To create the sample we require $\chi^2_{CES} > 20$ to reject real photons; we also omit calorimeter and track isolation requirements. The distribution in the total calorimeter energy, E_T^{Iso}, in a cone in η-ϕ space around the fake photon candidate, is shown in Figure 5.2.

The predicted number of events with jets misidentified as photons is 16.80±1.78

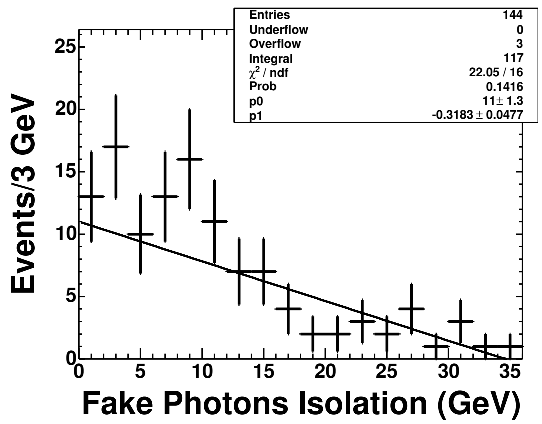

Figure 5.2: The distribution in the total calorimeter energy, E_T^{Iso}, in a cone in η-ϕ space around the fake photon candidate in lepton, $\not\!E_T$, and b-jet events. This distribution is then fitted with a linear function.

for the $\ell\gamma\not\!E_T b$ signature and 7.70 ± 2.61 for the $t\bar{t}\gamma$ events.

5.1.2 Electron Faking Photon

To determine the rate at which an electron fakes an isolated photon ($e \to \gamma$) in the central EM Calorimeter (CEM) we use Method-B described in [22]. The method provides a probability for an electron passing the standard tight electron cuts to fake a photon by extracting the ratio of the number of $Z^0 \to e\gamma$ events relative to $Z^0 \to ee$ events, the same method used for the 1.9 fb^{-1} analysis [18]. A $Z^0 \to e\gamma$ event occurs when a Z decays to two electrons and one of them radiates off a photon. The electron that radiated off the photon loses its energy and is not detected. The ratio of $Z^0 \to e\gamma$ events to $Z \to ee$ events gives a probability for an electron to fake a photon. Furthermore, the photon's E_T can be compared to similar E_T's of electrons, and our ratio can be parameterized as a function of E_T. We select events with a b-jet, substantial $\not\!E_T$, and a tight lepton, and further require a selection of electrons capable of faking photons. These list of electrons capable of faking photons includes all tight electrons with P_T greater than 10 GeV, as well as all loose electrons.

We then weight each event by the probability of the electron faking a photon divided by the number of possible combinations of electrons capable of faking photons in the event.

The predicted number of events with electrons misidentified as photons is 6.13 ± 0.57 for the $\ell\gamma\not\!\!E_{\mathrm{T}}b$ signature and 1.47 ± 0.25 for the $t\bar{t}\gamma$ events.

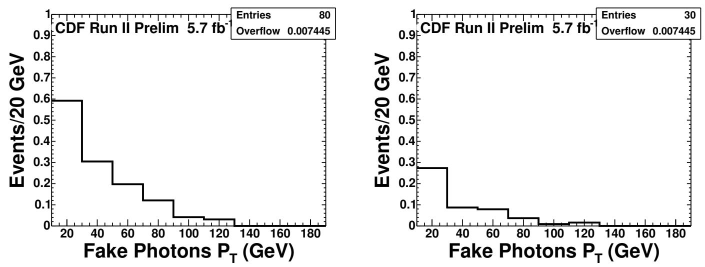

(a) $\mu\gamma\not\!\!E_{\mathrm{T}}b$ (b) $t\bar{t}\gamma$, muons

Figure 5.3: Spectrum of electrons faking photons used to calculate $e \rightarrow \gamma$ fake rate. We selected $\mu e\not\!\!E_{\mathrm{T}}b$ events, and then applied $e \rightarrow \gamma$ fake rate [22].

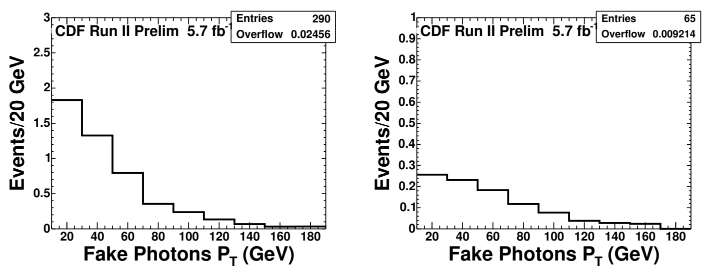

(a) $e\gamma\not\!\!E_{\mathrm{T}}b$ (b) $t\bar{t}\gamma$, electrons

Figure 5.4: Spectrum of electrons faking photons used to calculate $e \rightarrow \gamma$ fake rate. We selected $ee\not\!\!E_{\mathrm{T}}b$ events, and then applied $e \rightarrow \gamma$ fake rate [22].

5.1.3 $\tau \rightarrow \gamma$ Fake Rate

In addition to estimating number of $\ell\gamma\not\!\!E_{\mathrm{T}}b$ and $t\bar{t}\gamma$ events with jet faking photon ($j \rightarrow \gamma$), we also estimate number of events with tau faking photon ($\tau \rightarrow \gamma$).

The fake rate of $j \rightarrow \gamma$ is of order of 10^{-4} or smaller (Ref. [23]). The fake rate for taus is expected to be $\approx 10^{-2}$ which is two orders of magnitude larger. Due to the way jets fragment it is much harder for a jet to produce a single isolated (high $\mathrm{p_T}$) π^0 compared to a tau.

We evaluate $\tau \rightarrow \gamma$ fake rate from the $t\bar{t}$ Monte Carlo sample (ttopel sample). On the first step we select events on HEPG level with of the W's going to $\tau\nu$, $\tau \rightarrow hadron + \gamma$. Then we apply our analysis cuts to the stripped sample.

In total for $\ell\gamma\not{E}_{T}b$ category we observe 0.67± 0.29 $\tau \rightarrow \gamma$ events. For the $t\bar{t}\gamma$ category we observe 0.29 ± 0.08 $\tau \rightarrow \gamma$ events.

5.2 Misreconstructed b-jets

The perfomance of b-tagging algorithms is typcally characterized by the efficiency for identifying real b-jets and the rate at which jets are mistakenly tagged. Mistag rate is determined in a data-driven fashion, using a parametrized tag rate measured in generic jet events. We are looking for the rate at which a taggable light flavored jet is identifed as being a heavy flavored jet. A taggable jet has more than one SecVtx track coming from it, and appears to have a secondary vertex. Both of these conditions are common for jets occurring from B hadron decay. Positive and negative tags are accounted for separately, with the negative matrix being used to model the fake tag rate. Proper use of the mistag matrix requires a correction to the tag rate to account for heavy flavor tags in the generic sample. Negative rate are obtained by estimating negative tagging rates in data using method described in [24].

According to the procedure described in Ref. [24], in an event loop, first we cache all of the jets so a mistag matrix knows the event SumEt. We use raw (uncorrected), jet E_T for the mistag matrix. We cache all jets with $E_T > 10\ GeV$, $|\eta| < 2.4$. The mistag matrix identifies the parameters α and β. The former accounts for the amount of heavy flavor contribution in jets not identified as b-tagged, and the latter accounts for the amount of heavy jets in the sample compared to lighter flavor jets [25]. The rate of negative mistags, R^{-}_{mistag}, α, and β are defined below.

$$R^{-}_{mistag} = \frac{N^{-}_{light} + N^{-}_{heavy}}{N^{pre}_{light} + N^{pre}_{heavy}}$$

$$\alpha = \frac{N^{+}_{light}}{N^{-}_{light} + N^{-}_{heavy}}$$

$$\beta = \frac{N^{pre}_{light} + N^{pre}_{heavy}}{N^{pre}_{light}}$$

$$\alpha\beta R^{-}_{mistag} = \frac{N^{+}_{light}}{N^{pre}_{light}}$$

The positive and negative signs show whether a jet was tagged as a b-jet (+) or was not tagged as a b-jet (-). The pre superscript, dictates the amount of objects in the sample before the tagging value was applied. The subscript heavy denotes either b or c flavor jets. The parameters α, β, and R^{-}_{mistag} were determined using Monte Carlo and jet matching. The results are then compared to data for inclusive jets samples, and corrected with an overall scale factor.

After the mistag matrix is calculated we loop over the identified jets again and get the predicted tag rates and errors. We ask for R^{-}_{mistag} for the event and find the probability for a jet (heavy flavor or light flavor) to be incorrectly tagged (mistagged).

For a mistag file we are using :
BTagObjects/mistag_4100invpb/LooseSECVTXparam_4100invpb.root and tag type "loose".

Once we have the rate at which a jet is likely to be mistagged we define a sample of events that contain a tight lepton, a tight photon, and a taggable jet, and $\not\!\!E_{T}$ that passes our cuts (for $\ell\gamma\not\!\!E_{T}b$); and for $t\bar{t}\gamma$ events we further require three or more jets and H_{T} greater than 200 GeV. We then find the expected number of mistagged events to be our sample weighted by its respective mistag weight.

5.3 QCD (Jets Faking Lepton and $\not{E}_T$)

The QCD contribution to our signal occurs when we have events that look like our signature, however the leptons have come from neither a W or Z boson source. The "non-W/Z" leptons can possibly cause a mismeasurement of $\not{E}_T$; after leptons and jets have been identified, jet E_T values are corrected, and the $\not{E}_T$ is recalculated based on the new jet E_T values.

To estimate the contribution of our signal due to QCD processes faking leptons and $\not{E}_T$ we follow the lead of B. Cooper and A. Messina in CDF note 7760 ([26]). The method uses anti-electron objects (The full criteria of the selection of antielectrons can be seen in Table A.7) to mimic leptons occuring from the decay of jets.

Calculating the QCD background to the $\ell\gamma\not{E}_T b$ sample takes a couple of steps. First, we plot the spectrum of $\not{E}_T$ of events in data, from 0 GeV and up, in events that have an identified lepton, an identified photon, and a jet which has been b-tagged. Next we compare the spectrum of $\not{E}_T$ observed in data to what we observe from MC processes (normalized by cross sections and luminosity, etc.), again requiring an identified lepton, a b-tagged jet, and a photon. Then we compare the 0-20 GeV region of the $\not{E}_T$ distribution from data and the the sum of all of our MC processes. The difference between these distributions should be due to QCD contributions.

We expect the dominant contribution of QCD to be in the low-$\not{E}_T$ region, below 20 GeV of $\not{E}_T$. The difference between data and MC with $\not{E}_T$ below 20 GeV is fit using the anti-electron sample: a b-tagged jet, a photon, and an anti-electron. The anti-electron sample is scaled such that a chi-squared fit between the anti-electron sample and the difference between data and MC samples in the 0-20 GeV $\not{E}_T$ region is minimized. Once we have a fit in the low-$\not{E}_T$ region we assume the QCD signal can be inferred from this scaled anti-electron distribution. The anti-electron $\not{E}_T$ distribution is then integrated from 20-infinity. The distributions used to find this background are shown in Figure 5.5. The uncertainty on these measurements come from the statistical uncertainty on the number of events, as well as the systematic uncertainty due to the chi-squared fit. We use the same systematic uncertainty due to these fits as quoted by the authors of the method which is 8%.

To calculate the the amount of QCD due to any of our other signatures we would repeat this process in the same way but we require the samples to pass our selection criteria. So the $t\bar{t}\gamma$ samples would require $\mathrm{H_T} > 200$ GeV, and for there to be at least 3 jets. Using this prescription we find the total amount of QCD events in the $\ell\gamma\not\!\!E_{\mathrm{T}}b$ sample to be 16.16 ± 7.46; and in the $t\bar{t}\gamma$ sample we find the total to be 0.90 ± 0.88 events.

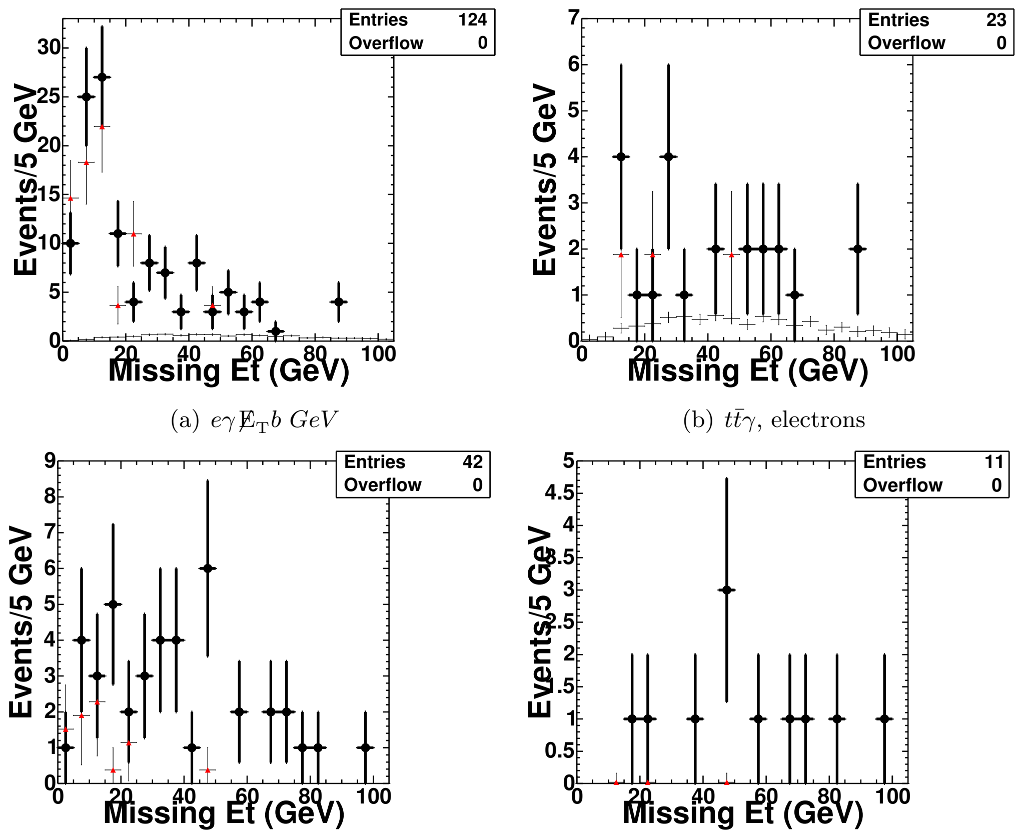

(a) $e\gamma\not\!\!E_{\mathrm{T}}b$ *GeV*

(b) $t\bar{t}\gamma$, electrons

(c) $\mu\gamma\not\!\!E_{\mathrm{T}}b$

(d) $t\bar{t}\gamma$, muons

Figure 5.5: Spectrum of anti-electrons used to calculate QCD fakes. We selected events with a bjet, a photon, and an anti-electron, and then scaled its $\not\!\!E_{\mathrm{T}}$ distribution below 20 GeV to those distributions of $\ell\gamma\not\!\!E_{\mathrm{T}}b$ without a $\not\!\!E_{\mathrm{T}}$ cut.

5.4 Double Counting of Fake Events

We describe an example procedure how we estimate and subtract double counting in our background estimates.

1. For instance, let's consider $e \rightarrow \gamma$ background. It is obtained by selecting $e\ell b\not{E}_{\mathrm{T}} + N_{jets}$ events, and each event is then multiplied by $f.r.(e \rightarrow \gamma)$. Therefore, we get expected number of events:

   $N1 = (e \rightarrow \gamma)\ell b\not{E}_{\mathrm{T}} + N_{jets}$

2. Now let's estimate a number of events with fake b, $j \rightarrow b$. We start from $\gamma\ell j\not{E}_{\mathrm{T}} + N_{jets}$, and each event is then multiplied by $f.r.(j \rightarrow b)$. Therefore, we get expected number of events

   $N2 = \gamma\ell(j \rightarrow b)\not{E}_{\mathrm{T}} + N_{jets}$

3. obviously, some of the events with fake photon ($e \rightarrow \gamma$) also have fake b ($j \rightarrow b$), so if we just take a total N1+N2, then we will overestimate our backgrounds. Therefore, we need to subtract the overlap between the two, which is

   $N1N2 = (e \rightarrow \gamma)\ell(j \rightarrow b)\not{E}_{\mathrm{T}} + N_{jets}$

   and therefore

   $N = N1 + N2 - N1N2$

4. To get this, we should apply step **2** to the events from which you obtain ($e \rightarrow \gamma$) background. Therefore, we take events with $e\ell j\not{E}_{\mathrm{T}} + N_{jets}$ and multiply each of them by $f.r.(e \rightarrow \gamma) \times f.r.(j \rightarrow b)$

5. If you apply "antielectrons" procedure, then you normally apply it to a sample of l+X (where "X = N_{jets}" is the case described in the antielectrons note). You can do the same with l+X, where X = $\gamma b + N_{jets}$, and to avoid double counting with $e \rightarrow \gamma$ you would apply the procedure to $\ell(e \rightarrow \gamma)b + N_{jets}$ i.e. you would start from $\ell eb + N_{jets}$ events, apply $f.r.(e \rightarrow \gamma)$ and at the same time repeat "antielectrons" procedure.

5.4.1 Double Counting of Jets Faking Photons, and Electrons Faking Photons

To measure the amount of jets faking photons and electrons faking photons requires substantial $\not{E}_T$, a b-tagged jet, and a tight lepton. The overlap comes from events which also have a photon candidate like the one described in section 5.1.1 (further requiring the photon's isolation be less than 2.0 GeV) as well as an electron capable of faking a photon as described in section 5.1.2.

We then weight the events by the probability of the electron to fake a photon divided by the number of electrons capable of faking a photon.

5.4.2 Double Counting of Jets Faking Photons, and Jets Mistagged as B-jets

To measure the amount of jets faking photons and jets misidentified as b-jets

requires substantial $\not{E}_T$, and a tight lepton. The overlap comes from events which also have a photon candidate like the one described in section 5.1.1 (further requiring the photon's isolation be less than 2.0 GeV) as well as a taggable jet capable of being tagged as a b-jet as described in section 5.2.

We then weight the events by the probability of the jets in the event to be mistagged as a b-jet.

5.4.3 Double Counting of Electrons Faking Photons, and Jets Mistagged as B-jets

To measure the amount of electrons faking photons and jets misidentified as b-jets

requires substantial $\not{E}_T$, and a tight lepton. The overlap comes from events which also have a photon candidate like the one described in section 5.1.2 as well as a taggable jet capable of being tagged as a b-jet as described in section 5.2.

The events are then weighted by the probability of the electrons in the event to be misidentified as photons divided by the number of electrons capable of faking photons. We then further weight these events by the probability of a jet to be misidentified as a b-jet.

5.4.4 Double Counting of QCD fakes, and Jets Mistagged as B-jets

To measure the amount of double counting due to jets mistagged a b-jets, and jets which fake leptons, we require a sample of an anti-electron, jets capable of being mistagged, substantial $\not{E}_T$, and a tight photon. In this case, the $\not{E}_T$ is correct by muons, and jets, and uncorrected by the anti-electron.

If the anti-electron were not designated as such, then it would have passed the selection criteria of a jet, and hence the $\not{E}_T$ would have been corrected by it.

These events are then weighted by the probability of a jet to be misidentified as a b-jet. The anti-electron must have a track isolation less than 4 GeV to enter our selection criteria for $\ell\gamma\not{E}_T b$. To enter the selection criteria for $t\bar{t}\gamma$ the event must further have $H_T > 200$ GeV and more than 2 jets (not including the anti-electron).

5.4.5 Double Counting of QCD fakes, and Jets Faking Photons

The procedure described in section 5.1.1 is repeated, with the new requirement that we have an anti-electron instead of a tight lepton. We still require a b-jet and substantial $\not{E}_T$ uncorrected due to the anti-electron. The reasoning is described in 5.4.4. We then look for events that have a photon candidate with Calorimeter Isolation less than 2 GeV, and require the anti-electron to have Track Isolation less than 4 GeV, to pass the $\ell\gamma\not{E}_T b$ selection criteria. We further require H_T greater than 200 GeV and 3 or more jets (not including the anti-electron) to enter into the $t\bar{t}\gamma$ selection criteria.

5.4.6 Double Counting of QCD fakes, and Electrons Faking Photons

The procedure described in section 5.1.2 is repeated, with the new requirement that we have an anti-electron instead of a tight lepton. We still require a b-jet, electrons capable of faking photons, and substantial $\not{E}_T$ uncorrected due to the anti-electron. The reasoning for this is described in 5.4.4. We require the anti-electron to have Track Isolation less than 4 GeV, to pass the $\ell\gamma\not{E}_T b$ selection criteria. We further require $\mathrm{H_T}$ greater than 200 GeV and 3 or more jets (not including the anti-electron) to enter into the $t\bar{t}\gamma$ selection criteria. These events are then weighted by the probabiliy of the electrons to fake a photon, divided by the number of electrons capable of faking a photon.

6 Fakes of the $t\bar{t}$ signature

When computing our yields for the $t\bar{t}$ signature, we have tried to keep the methods for calculating the fakes as close to the $t\bar{t}\gamma$ and $\ell\gamma\not{E}_{\mathrm{T}}b$ signatures as possible. However, there are some differences and we explain those in the sections that follow.

6.1 Mistag estimate

We follow the same prescription as in section 5.2 for caching jet information from our events. For the $t\bar{t}$ sample , we require a lepton, $\not{E}_{\mathrm{T}} > 20GeV$, $\mathrm{H_T} > 200GeV$ and 3 or more jets. The event is then weighted by the probability of being mistagged. A mistag estimate is then the summation of all such weighted events. This we will call the method1 estimate of mistagged b-jets.

We now correct the method1 estimate based on our understanding of events that pass our cuts. We isolate in data a pretagged sample of our events (one tight lepton, three tight jets, $\mathrm{H_T} > 200$ GeV, and $\not{E}_{\mathrm{T}} > 20$ GeV). Some events that will be mistagged, have a true b-jet involved in them, such as $t\bar{t}$ events, and W decays with associated heavy flavor quarks, such as $c\bar{c}$ or $b\bar{b}$. To better measure the amount of events likely to be mistagged, we subtract off the contribution to this pretagged sample the amount of events likely to be mistagged, but containing true heavy flavor contributions.

$$N^{W+LF}_{pretagged} = N^{data}_{pretagged} - N^{QCD}_{pretagged} - N^{t\bar{t}}_{pretagged} - N^{diboson}_{pretagged} - N^{singletop}_{pretagged} - N^{W+HF}_{pretagged} \tag{6.1}$$

We then scale the Method1 estimate of mistagged by the ratio of $\frac{N^{W}_{pretagged}}{N^{data}_{pretagged}}$. This fraction is the amount of mistagged events, that are due to events with a tight lepton, $\not\!\!E_{\mathrm{T}} > 20$ GeV, $\mathrm{H_T} > 200$ GeV, but have no true heavy flavor contribution. Hence these are events are truly mistagged, in the sense that the event is tagged as having a heavy flavor quark, when there is no such quark. The scaled Method1 result is the Method2 mistag estimate. The total prediction for the amount of misidentified b-tagged events in the $t\bar{t}$ sample is 527 ± 40.70 events.

6.2 QCD estimate

Our estimate for the QCD contribution to $t\bar{t}$ is calculated as outlined above in section 5.3, however we have dropped the requirement for a tight photon. We begin by taking the total yield of events from the electron stream, and the muon stream, with a tight electron or muon, a b-jet, $\mathrm{H_T} > 200 GeV$, and no $\not\!\!E_{\mathrm{T}}$ cut.

We look for electrons in the electron stream, and muon events in the muon stream. The events are plotted as a function of their $\not\!\!E_{\mathrm{T}}$ for the event. The anti-electron distribution comes solely from the electron stream, and also require a b-jet and $\mathrm{H_T} > 200 GeV$. Monte Carlo distributions are used for the estimate of events from $t\bar{t}$, diboson (WW, WZ, and ZZ), and W plus heavy flavor distributions. The mistag distribution is estimated using a Method 1 estimate for both the electron and muon signatures. The MC, and mistag contributions are summed, and the anti-electron distribution is scaled to fit the difference between data and the sum of the MC and mistag distributions. For the systematic uncertainty we use the same fraction as quoted by the authors of this method, which is 8%. We find the total amount of QCD background in the $t\bar{t}$ sample to be 221 ± 36.90 events.

6.3 Double Counting of QCD fakes, and Jet Mistagged as B-jets

In section 5.4.4, we described the procedure for measuring the amount of double counting we had between events that are likely due to QCD and events that are likely due to light jets being misidentified as heavy- flavour jets. However because

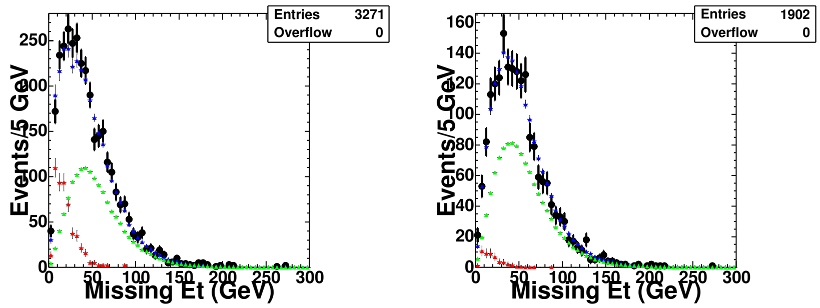

(a) $t\bar{t}(e)$ (b) $t\bar{t}(\mu)$

Figure 6.1: AntiElectron and data distribution for the $t\bar{t}$ signature. The red points are scaled antielectrons, green points are from the $t\bar{t}$ MC, and blue is all MC, as well as the distribution of mistags and the antielectrons summed together. We see good agreement in the 0-20 GeV region which determines the scale factor of the antielectrons, and the 20-∞ shows good agreement as well. The antielectrons' distributions show that the majority of the QCD signal is in the low $\not\!\!E_{\mathrm{T}}$ range.

of using the method 2 estimate there is no longer double counting to measure. Our mistagging estimate in 6.1 shows the removal of background due to mistagged QCD events. Furthermore, our QCD method uses as an input the $\not\!\!E_{\mathrm{T}}$ distribution, as a result we no longer have to worry about double counting of these two backgrounds.

7 Control Samples

Several control samples were used to validate our data-driven backgrounds and understanding of our signals, such as $Z\gamma$, $\ell\gamma\not\!\!E_{\mathrm{T}}$, and a pretagged $t\bar{t}$ sample. These samples were constructed to be very similar to signatures we are looking for involving many of the same objects. All of the samples are statistically rich which provides a nice workbench of both our understanding of the individual objects as well as the background methods that we use for our main analysis.

7.1 The $Z\gamma$ Control Sample

We began with constructing a $Z\gamma$ sample requiring two opposite-signed same-flavor leptons, and a photon with a three body mass between 86 and 96 GeV. Using this sample we are able to have a sample that is very nearly full of true photons. Furthermore, it allows us to measure the cross section of $Z\gamma$ in a sample rich environment. We find the cross section for $Z\gamma$ to be about 6.3 pb for our object selection. Here we are using merely standard lepton and photon selection cuts found in B.1, B.2, and B.4. We use that measured cross section for the $\ell\gamma \not{E}_T$ sample. Figure 7.1 shows the observed distributions summed of $ee\gamma$ and $\mu\mu\gamma$ events in a) the three-body mass of $\ell\ell\gamma$ system; b) the missing transverse energy, $\not{E}_T$; c) the E_T of the leptons of the event; and d) the E_T of the photon.

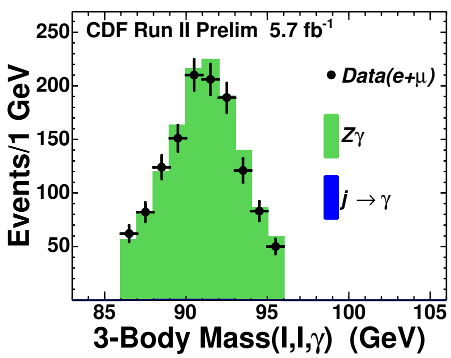

(a) Invariant mass of the two leptons and photon in $Z\gamma$ events

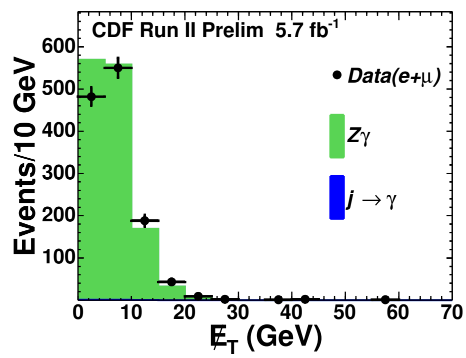

(b) $\not{E}_T$ from $Z\gamma$ events

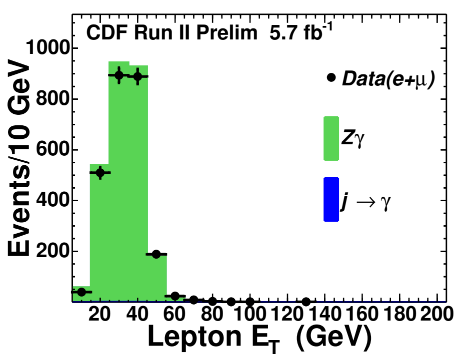

(c) E_T of electrons and P_T of muons from $Z\gamma$ events

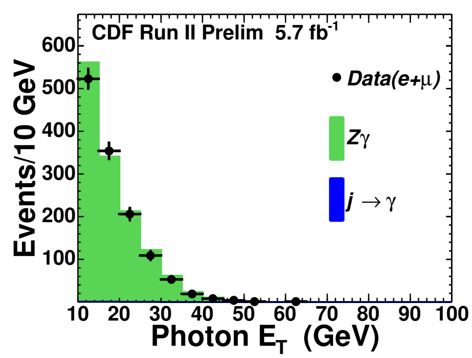

(d) E_T of photons from $Z\gamma$ events

Figure 7.1: Kinematic Distributions for $Z\gamma$ events showing a) the three-body mass of $\ell\ell\gamma$ system; b) the missing transverse energy, $\not{E}_T$; c) the E_T of the leptons of the event; and d) the E_T of the photon.

7.2 The $\ell\gamma \not{E}_T$ Control Sample

The $\ell\gamma \not{E}_T$ sample is constructed to better understand our jets faking photons, electrons faking photons, and non-W data-driven backgrounds, these are discussed in greater detail in Secs. 5.1.1, 5.1.2 , and 5.3 respectively. In the case of the $\ell\gamma\not{E}_T$ we have followed the background prescriptions of $\ell\gamma\not{E}_T b$ and $t\bar{t}\gamma$. The "fakes" backgrounds to the $\ell\gamma\not{E}_T$ sample included jets faking photons, electrons faking photons, and leptons and $\not{E}_T$ from QCD events. Double counting in these three categories is very small and was neglected from the calculations. We show kinematic distributions of this control sample in Fig. 7.2.

The $\ell\gamma\not{E}_T$ sample was chosen to be similar to the $\ell\gamma\not{E}_T b$ sample we looked for high-P_T electrons or muons, $\not{E}_T > 20$ GeV, and a photon with $E_T > 10$ GeV. This sample had 4248 $e\gamma\not{E}_T$ events, and 3647 $\mu\gamma\not{E}_T$ events. This signal is dominated by $W\gamma$ events, and events where jets fake photons. Unlike the $\ell\gamma\not{E}_T b$ and $t\bar{t}\gamma$ samples we are not statistics limited when we find the amount of jets faking photons in this sample, and this helps us to calculate the systematic uncertainty on the jets faking photons background measurement. Furthermore, while the electrons faking photons background is small, relative to $W\gamma$ and jets faking photons, in this sample, it is still an important part of our measurement in this sample and this allows a large-scale check of our method. The QCD background measurement is a large background in the $\ell\gamma\not{E}_T$ sample and is estimated as mentioned above, and allows us to check the systematic errors on the measurement. We present the total event yields and SM prediction for our $\ell\gamma\not{E}_T$ control sample in Table 7.1.

7.3 The Pretagged $t\bar{t}$ Control Sample

For a control sample to $t\bar{t}$ we constructed a pretagged sample of $t\bar{t}$, where we dropped our requirement for a tagged b-jet. The sample has only one data-driven background in this case, and that is leptons and $\not{E}_T$ from QCD events.

The pretagged $t\bar{t}$ sample is an ideal control sample for $t\bar{t}$ because the only non-MC background is the QCD sample. This provides a great cross-check on our QCD measurement techinique for $t\bar{t}$, and allows us to check on K-factors that W+HF MC samples require.

We find 10968 pretagged $t\bar{t}(e)$ events and 6969 pretagged $t\bar{t}(\mu)$ events. This sample is dominated by a W+LF background. The K-factors due to Heavy Flavor

CDF Run II Preliminary, $5.7pb^{-1}$			
$\ell\gamma\not\!\!E_T$, Isolated Lepton			
Standard Model Source	$e\gamma\ \not\!\!E_T$	$\mu\gamma\not\!\!E_T$	$(e+\mu)\gamma\not\!\!E_T$
$W\gamma$	2650 ± 350	2160 ± 280	4800 ± 630
$Z\gamma$	95 ± 12	390 ± 50	480 ± 63
QCD (j$\rightarrow l$ and $\not\!\!E_T$)	149 ± 22	2.6 ± 0.4	151 ± 23
$\ell j\not\!\!E_T (j\rightarrow\gamma)$	1560 ± 240	870 ± 130	2430 ± 370
$le\not\!\!E_T$ (e$\rightarrow\gamma$)	39 ± 5	17 ± 2	56 ± 7
Total SM Prediction	4490 ± 420	3430 ± 320	7920 ± 730
Observed in Data	4248	3647	7895

Table 7.1: A comparison of the numbers of events predicted by the standard model (SM) and the observations for the $\ell\gamma\not\!\!E_T$ search. The SM predictions for this search are dominated by the $W\gamma$, and $Z\gamma$ production, particularly when we miss a muon. Other contributions come from misidentified leptons, photons, or $\not\!\!E_T$. MC samples have been scaled to 5.7fb^{-1}. All other Data-driven numbers have been measured in the manner described in earlier sections.

content have a large uncertainty associated with them, and this drives the uncertainty on the histograms as shown in Fig. 7.7. The theoretical cross section of $t\bar{t}$ (6.7 pb) is used in the plots.

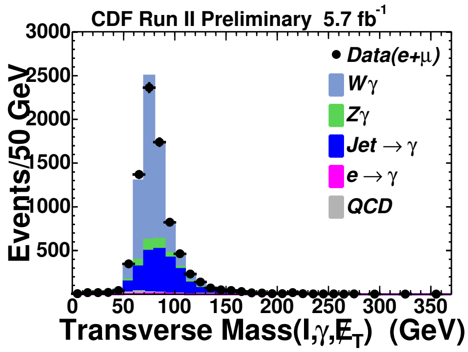

(a) Transverse Mass of the Lepton, Photon, and $\not\!\!E_{\mathrm{T}}$ object from $\ell\gamma\not\!\!E_{\mathrm{T}}$ events

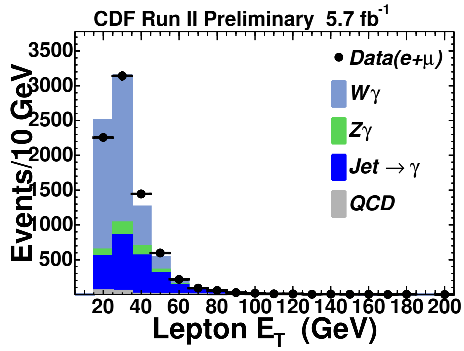

(b) The $\mathrm{E_T}$ of electrons and $\mathrm{P_T}$ of muons from $\ell\gamma\not\!\!E_{\mathrm{T}}$ events

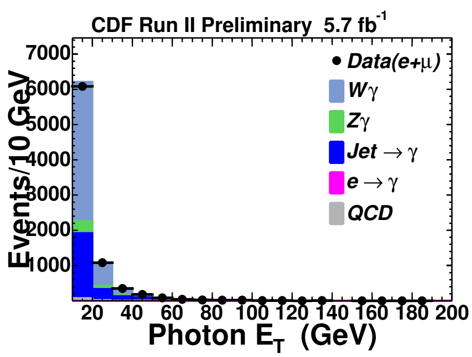

(c) $\mathrm{E_T}$ of the photons from $\ell\gamma\not\!\!E_{\mathrm{T}}$ events

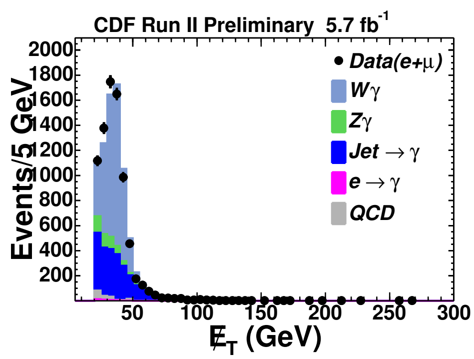

(d) $\not\!\!E_{\mathrm{T}}$ of events in the $\ell\gamma\not\!\!E_{\mathrm{T}}$ sample

Figure 7.2: Kinematic Distributions for $\ell\gamma\not\!\!E_{\mathrm{T}}$ events a) the three-body transverse mass of $\ell\gamma\not\!\!E_{\mathrm{T}}$ system; b) the $\mathrm{E_T}$of the leptons of the event; c) the $\mathrm{E_T}$ of the photon; and d) the missing transverse energy, $\not\!\!E_{\mathrm{T}}$.

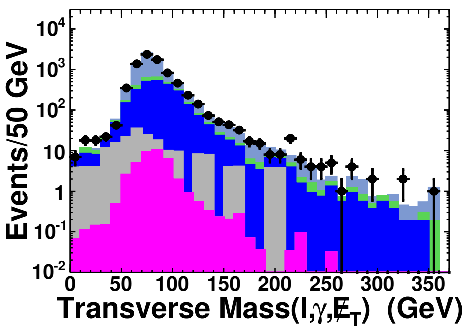

(a) $\ell\gamma\not{E}_T$

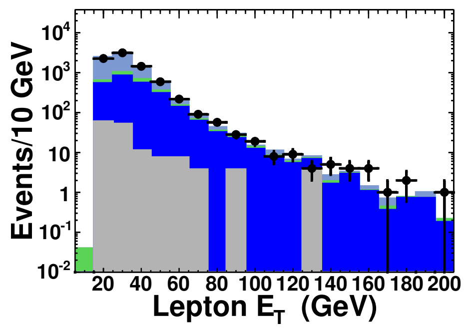

(b) $\ell\gamma\not{E}_T$

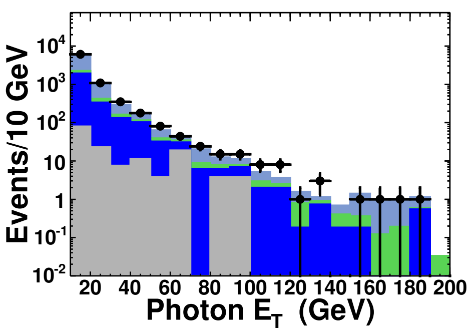

(c) $\ell\gamma\not{E}_T$

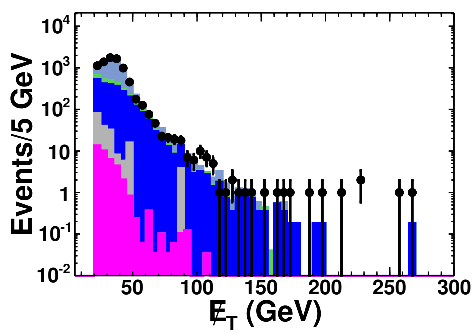

(d) $\ell\gamma\not{E}_T$

Figure 7.3: Kinematic Distributions for $\ell\gamma\not{E}_T$ events in logarithmic scale a) the three-body transverse mass of $\ell\gamma\not{E}_T$ system; b) the $E_T$of the leptons of the event; c) the E_T of the photon; and d) the missing transverse energy, $\not{E}_T$. These are the same plots as in Figure 7.2 but in logarithmic scale.

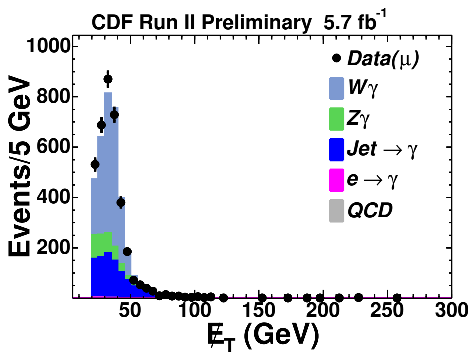

(a) $\mu\gamma\not{E}_{\mathrm{T}}$

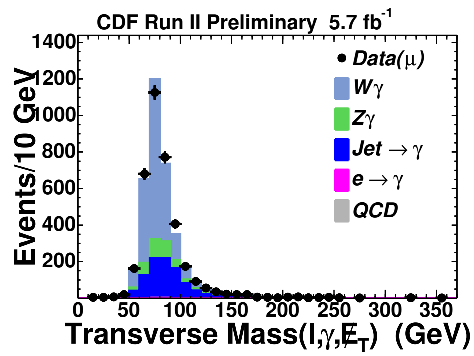

(b) $\mu\gamma\not{E}_{\mathrm{T}}$

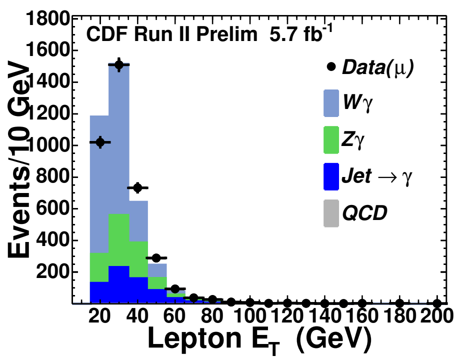

(c) $\mu\gamma\not{E}_{\mathrm{T}}$

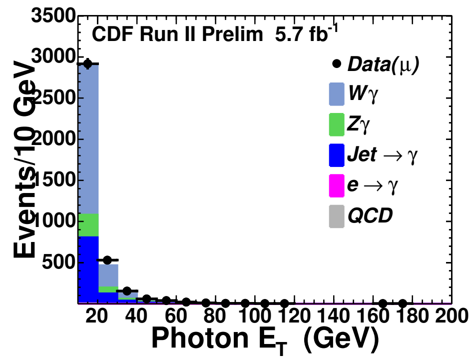

(d) $\mu\gamma\not{E}_{\mathrm{T}}$

Figure 7.4: Kinematic Distributions for $\mu\gamma\not{E}_{\mathrm{T}}$ events

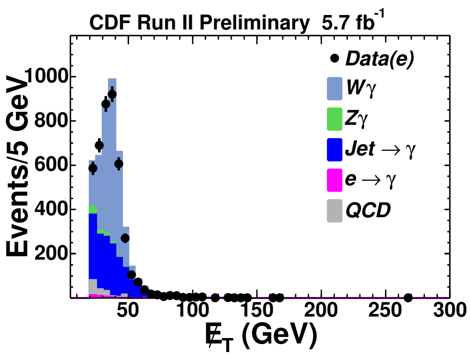

(a) $e\gamma\not{E}_T$

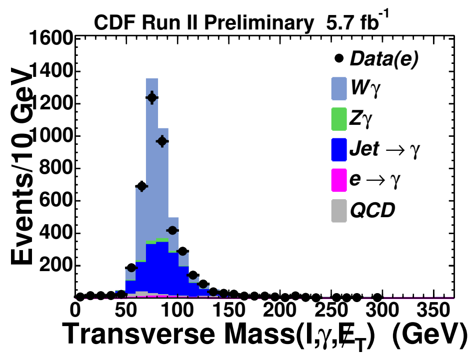

(b) $e\gamma\not{E}_T$

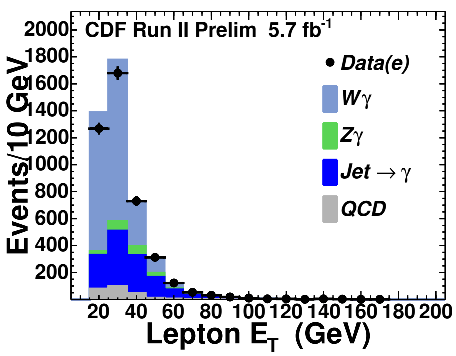

(c) $e\gamma\not{E}_T$

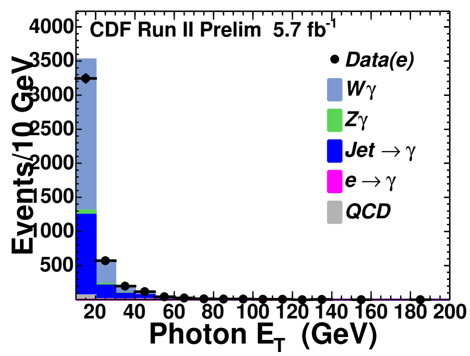

(d) $e\gamma\not{E}_T$

Figure 7.5: Kinematic Distributions for $e\gamma\not{E}_T$ events

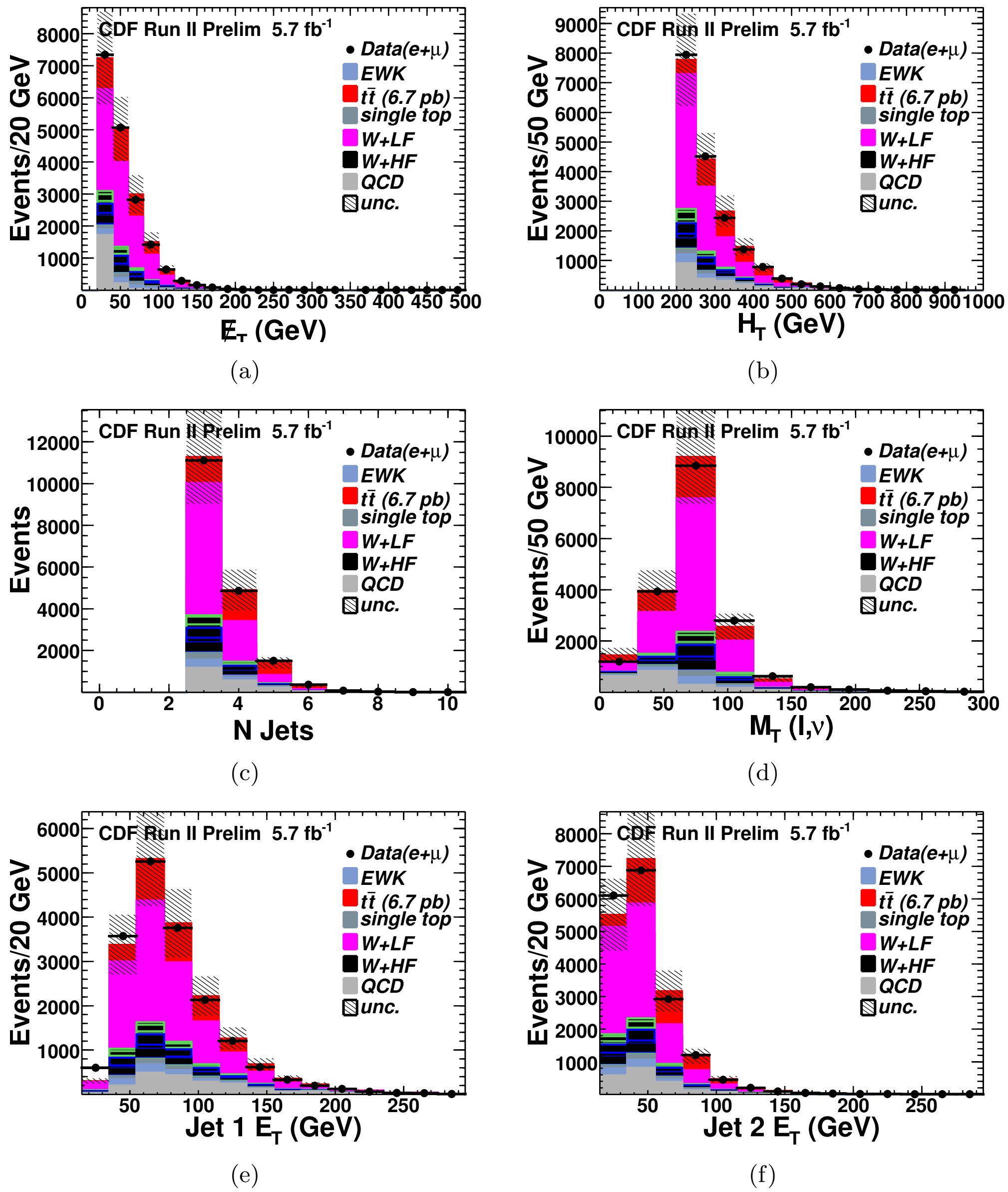

Figure 7.6: Spectrum of $\not{E}_T$ for pretagged $t\bar{t}$ events. We show a) the missing transverse energy ($\not{E}_T$); b) the total transverse energy (H_T); c) the total number of jets in the event; d) the transverse mass of the lepton and $\not{E}_T$; e) the p_T of the jet with the highest p_T f) the p_T of the jet with the second highest p_T The K-factors due to Heavy Flavor content have a large uncertainty associated with them, and this drives the uncertainty on the histograms. The theoretical cross section of $t\bar{t}$ (6.7 pb) is used in the plots.

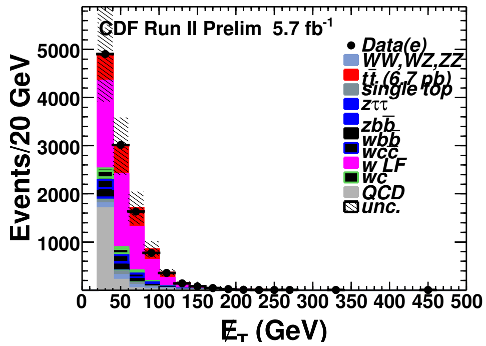

(a) Pretagged $t\bar{t}(e)$

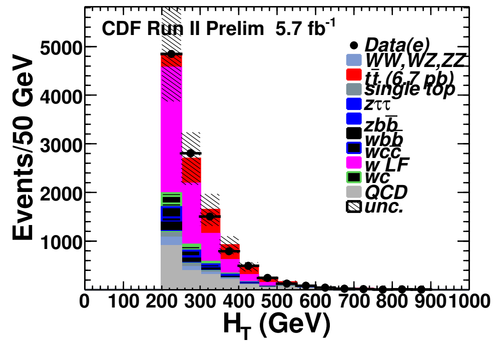

(b) Pretagged $t\bar{t}(e)$

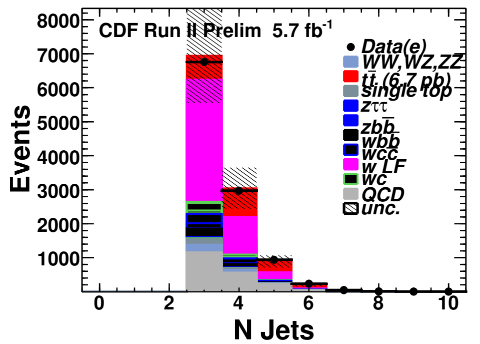

(c) Pretagged $t\bar{t}(e)$

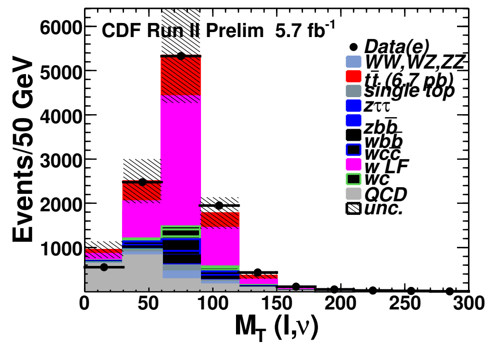

(d) Pretagged $t\bar{t}(e)$

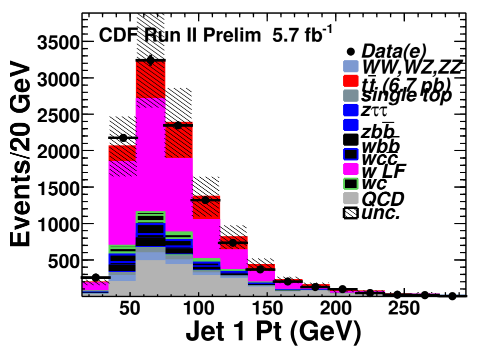

(e) $t\bar{t}(e)$

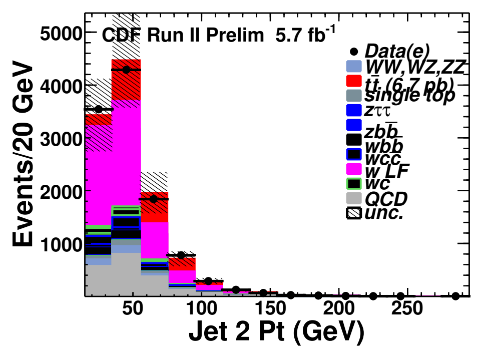

(f) $t\bar{t}(e)$

Figure 7.7: Kinematic spectra of pretagged $t\bar{t}$ events from the electron stream. We show a) the missing transverse energy ($\not\!\!E_{\rm T}$); b) the total transverse energy ($\rm H_T$); c) the total number of jets in the event; d) the transverse mass of the lepton and $\not\!\!E_{\rm T}$; e) the $\rm p_T$ of the jet with the highest $\rm p_T$ f) the $\rm p_T$ of the jet with the second highest $\rm p_T$ The K-factors due to Heavy Flavor content have a large uncertainty associated with them, and this drives the uncertainty on the histograms. The theoretical cross section of $t\bar{t}$ (6.7 pb) is used in the plots.

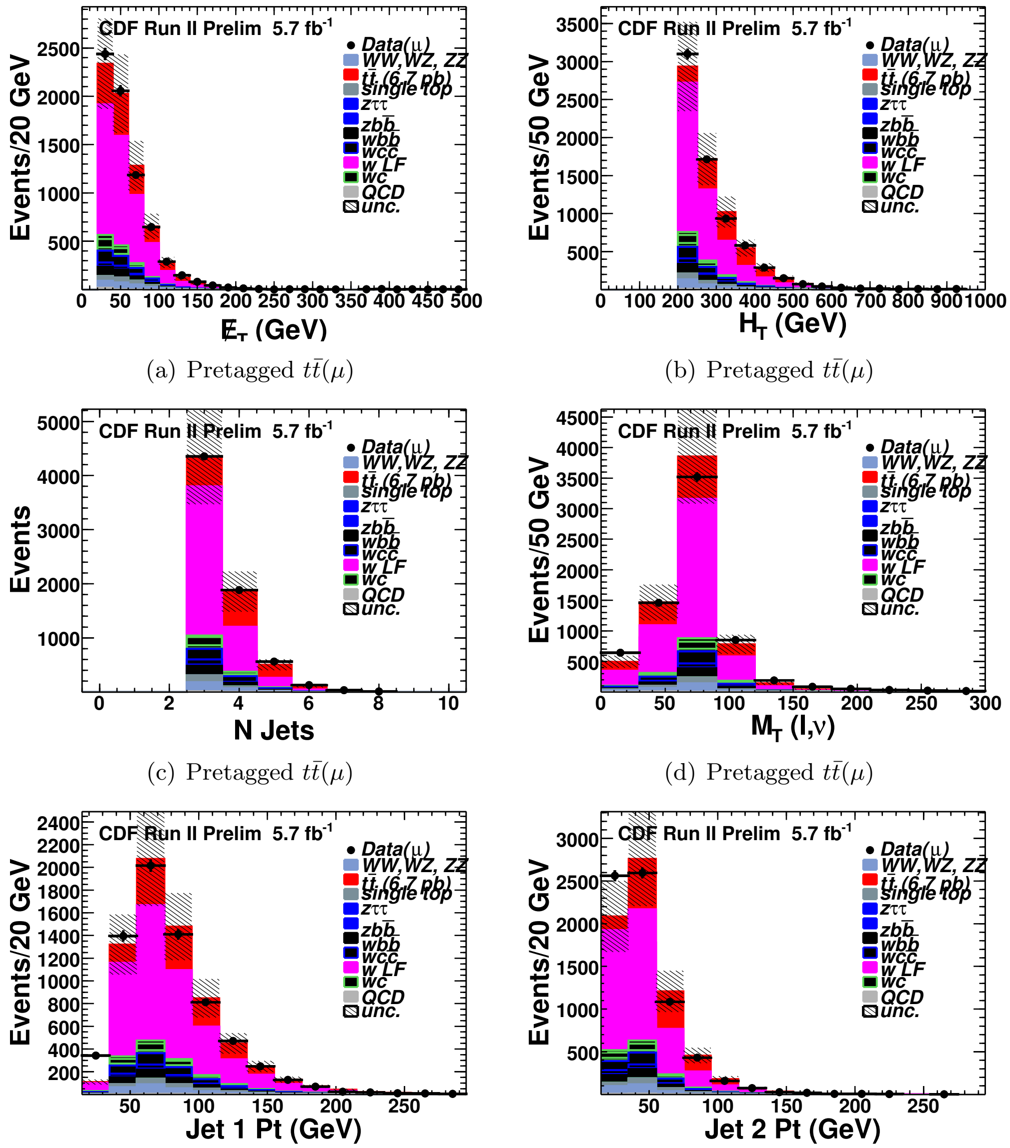

(a) Pretagged $t\bar{t}(\mu)$ (b) Pretagged $t\bar{t}(\mu)$

(c) Pretagged $t\bar{t}(\mu)$ (d) Pretagged $t\bar{t}(\mu)$

(e) $t\bar{t}(\mu)$ (f) $t\bar{t}(\mu)$

Figure 7.8: Kinematic spectra of for pretagged $t\bar{t}$ events from muon stream. We show a) the missing transverse energy ($\not\!E_T$); b) the total transverse energy (H_T); c) the total number of jets in the event; d) the transverse mass of the lepton and $\not\!E_T$; e) the p_T of the jet with the highest p_T f) the p_T of the jet with the second highest p_T The K-factors due to Heavy Flavor content have a large uncertainty associated with them, and this drives the uncertainty on the histograms. The theoretical cross section of $t\bar{t}$ (6.7 pb) is used in the plots.

8 Cutting on Chi Squared of Photon candidates

The chi-squared value of the shape of the photon's shower shape in the CES, is the average of chi-squared values along the strip and wires of the CES. It is a measure of how linear the position of hits along two dimensions are. Furthermore it is possible to distinguish one photon (from a charged lepton brehmstrahlung) from two collimated photons from a light jet decay such as a π^0.

While looking at Monte Carlo distributions of $t\bar{t}\gamma$ and its backgrounds, the plot of the photon's Chi-Squared distribution looked particularly promising for removing some of the largest background contribution, jets misidentified as photons. In order to find the most effective cut value for the photon candidates we chose to reproduce the Wγ distribution.

The Wγ distribution does contain all of the $t\bar{t}\gamma$ signal event, however there are considerably more data points in this distribution. When looking at the $t\bar{t}\gamma$ distributions for Monte Carlo, we are considerably limited statistically; the Wγ distribution, does not suffer from this limitation.

When looking at the Wγ MC distribution, we can see that the vast majority of these events are contained in the Chi-Squared less than 10 region.

We isolated a sample of pure photons by requiring events with two same flavor leptons, and a photon, that have a three-body invariant mass between 86 and 86 GeV; we call this sample Zγ. In this sample, however there was nearly no backgrounds due to fake photons. When comparing the Chi-Squared distribution between the Wγ distribution, and the Zγ distribution there are no obvious differences.

The control sample of Zγ is a sample of real photons, the Wγ sample is a mixture of both real photons and jets faking photons, and we also look at the jets faking photons distributions. We can use the Zγ sample to measure the efficiency of any of our potential cuts on photons, and the Wγ and Jets faking photons sample can be used to measure the purity of a sample of photons. We define the efficiency to be the amount of true photons from the Zγ distribution that pass a proposed cut, and the purity to be the fraction of good photons over total amount of photons accepted.

Photons come in two types in our studies, real and fake. The real photons radiate off from charged leptons, guage bosons, or quark; fake photons come from other sources such as π^0 decays. At low $\mathrm{E_T}$, the photon's χ^2 of the centroid in the CES is more likely to be smaller. Real photons should dominantly be arriving alone, but fake photons are more likely to come in a pair, and hence have a worse χ^2 value. In the event that a pair of photons are created via a hadronic decay, it is likely that the two photons will be collimated. This pair of photons might not be resolved, and it will look like one photon in our detector. The evidence that the one observed photon is actually a pair of collimated photons should be present in the χ^2 value. Since there will be two showers going through the CES it is likely that the path taken by the shower will look much more spread out than the shower due to a true photon. Unfortunately, we are unable to resolve this discrepancy is coming from two very energetic photons; but we are able to differentiate these types of photons when the $\mathrm{E_T}$ of the photon candidate is less than 25 GeV.

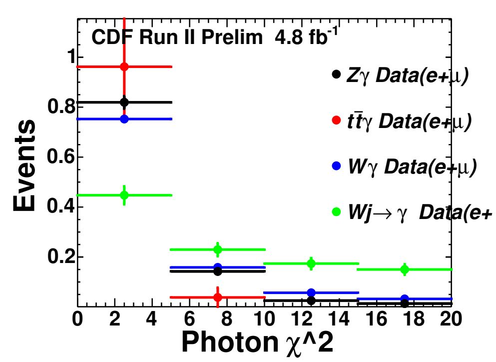

(a) Photon Distribution of Zγ, Wγ, Fake Photons, and $t\bar{t}\gamma$ Samples

Figure 8.1: Spectrum of the photon's Chi-Squared distributions normalized to unity, for different samples

Defining significance as:

$$Sig = \frac{S}{\sqrt{S+B}} \tag{8.1}$$

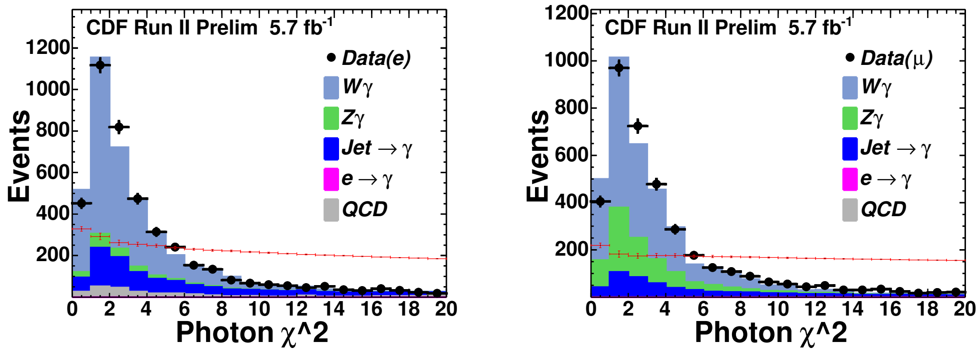

(a) $e\gamma\not\!\!E_{\rm T}$ (b) $\mu\gamma\not\!\!E_{\rm T}$

Figure 8.2: Spectrum of the photon's Chi-Squared distributions normalized by cross section and luminosity, for the $e\gamma\not\!\!E_{\rm T}$ (left) and $\mu\gamma\not\!\!E_{\rm T}$ (right) sample. The red crosses are proportional to the significance of the photon's χ^2; there is no peak in the curve for where to cut.

Where S is the signal of true Wγ events, as found by Monte Carlo, and B is backgrounds to the Wγ signal such as Jets Faking Photons, and Zγ events. We found that the significance, as a function of cutting on the photon's Chi-Squared distribution did not peak at a Chi-Squared between 0 and 20.

At this point we began a different tact: we used our smaples as described earlier but we split the groups based on the photon's $\rm E_T$. The lower energy scale had, $\rm E_T$ between 10 and 25 GeV, and the higher energy scale, $\rm E_T > 25$ GeV. We looked at the efficiency versus purity as a function of the chi-squared value for the lower energy photons. The efficiency was measured as the fraction of standard photons that survived a potential chi-squared cut, and the purity was the ratio of real photons to photon candidates that passed the chi-squared value.

The chi-squared value was changed in steps of 2 from 2 to the standard cut of 20. A step size of two was chosen to minimize statistical effects between the jets faking photons samples, and the photons from $Z\gamma$ decays. Figure 9.3(a) shows the efficiency versus the purity. The efficiency increases monotonically as the chi-squared value is raised, and the purity decreases monotonically. As we raise the accepted value for χ^2 for photon candidates, more photons from $Z\gamma$ decays are accepted as photons, so the efficiency rises. On the other hand as we raise the accepted value for

χ^2 more objects, both actual photons, and photons from hadronic decays, will be accepted as photons. So we would expect the purity to decrease since the amount of fake photons will increase. Using this information we chose to require the chi-square be less than 6, for photons with $E_T < 25$ GeV.

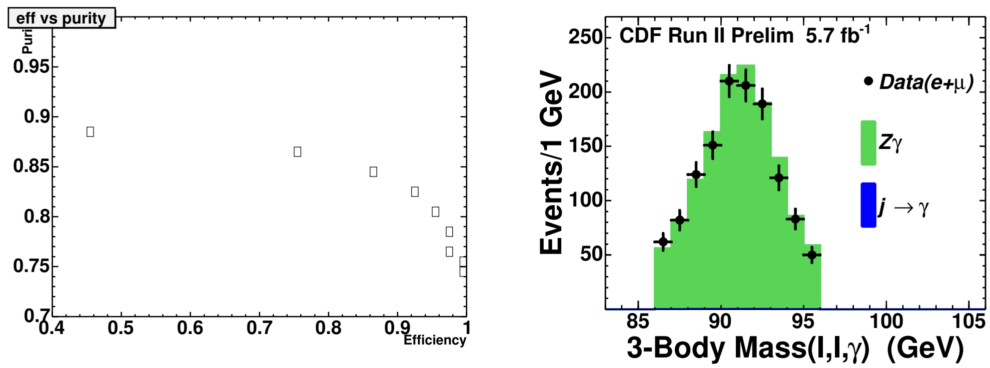

(a) $\ell\gamma\not{E}_T$

(b) $Z\gamma$

Figure 8.3: Distribution of efficiency versus purity of a proposed chi-squared cut for photons with $E_T < 25$ GeV. The proposed cut starts at 2 and increases in steps of 2 to the standard cut of 20. The efficiency increases monotonically with increasing the chi-squared cut; and purity decreases monotonically. We choose to require chi-squared be less than 6 for lower energy photons. True photons were collected from a $Z\gamma$ decays (3 body mass nearly the Z-mass), and fake photons had isolation > 2. For each proposed χ^2 cut, we found the fraction of true photons and fake photons contained in a $W\gamma$ decay. The χ^2 cut goes up in steps of two from left to right and top to bottom.

9 Systematic Uncertainties

Systematic uncertainties are calculated by varying a given parameter within its uncertainty and seeing the effect on a given MC or data-driven background, and summing in quadrature all such effects on the signal and backgrounds. We describe each of the systematics below.

9.1 Jet Energy Scale

The jet energy scale, in this analysis, is corrected for both the underlying event as well as for the possibiltiy of energy spilling out of the cone of 0.4 that we use for our jets. The parameterization we use for correcting the energy scale of the jets has uncertainties associated with each of them. Each of these uncertainties can be added together to give one total sytematic error as a standard deviation. To measure the effect of the jet energy uncertainties in the calorimeters we fluctuate the energy of each jet in our signal up and down one standard deviation and find the effect of this change on the total cross-section measurements and find it to be about 1%.

9.2 Tagging

The amount of SecVtx tags in Monte Carlo is not modeled properly and as a result we must scale the overall tagging rate by a factor with a 5% error.

9.3 Mistags

We use a systematic uncertainty of 8% on the total amount of predicted mistagged events as done in the previous $t\bar{t}\gamma$ analysis. To validate the results using current data, we have fluctuated the the systematic in the mistag matrix and found the difference between the old prediction, and the prediction after the systematic has been applied. We found that 8% was a reasonable uncertainty measurement.

9.4 QCD Contamination

The systematic uncertainty associated with our method of measuring the QCD contribution to our samples is quoted as 8% by the authors of the method. We are following the method's authors' recommendation of using that value for uncertainty.

9.5 Jets Faking Photons

In modeling a tighter cut on photon's χ^2 value we assembled a $\ell\gamma\not{E}_T$ sample. This sample has a very large jets faking photons contribution to the background, as a result we are not statiscally limited. We vary parameters in the fitting of the photon candidates' isolation shape, as well as the functional form that we believe the background should take and find the systematic error to be about 20%.

9.6 Electron Faking Photons

When modeling electrons faking photons, the electrons are weighted by a function that depends on the electron's E_T. These functions have an error associated with each parameter, and to calculate the uncertainty each of the parameters is allowed to fluctuate, and the resulting changes to the estimate are added in quadrature.

9.7 Photon Identification

The photon identification efficiency is 4% and this uncertainty is added in quadrature in the acceptance systematic uncertainty, as well as the uncertainty for MC samples with photons.

9.8 Trigger Efficiency

Detector specific corrections are applied to the MC to more correctly model the relative trigger efficiencies between CEM, CMUP, and CMX events. The uncertainty due to trigger efficiency is modeled using data-derived Z events and has a small uncertainty associated with them. There are two types of corrections trigger ID and trigger efficiencies. The resulting errors are added in quadrature to the total systematic uncertainty.

9.9 Heavy Flavor Corrections

There is a correction factor applied to the W+HF MC to account for a mismodelling of the amount of heavy flavor contribution found in the 1 and 2 jet bins where W+HF should dominate. This correction is applied in our signal region of 3 or more jets. The uncertainty on the correction factor is taken to be 20% on the W+HF MC.

9.10 Luminosity Uncertainties

The uncertainty in our luminosity is derived from detector accuracy and the theoretical cross section for the inelastic $p\bar{p}$ collisions. The uncertainty on the luminosity is 6%, and we leave this systematic uncertainty uncombined with other uncertainties until the very end. The 6% uncertainty comes from an 4.4% uncertainty from the acceptance and operation of the luminosity monitor, and 4.0% from the uncertainty on the calculation of the total $p\bar{p}$ cross section.

10 Event Display

We show in figure 10.1 a signature event for $t\bar{t}\gamma$. This event has a tight photon, has 2 b-tagged jets, substantial $\not{E}_T$, and the H_T of the event is large at 206.8 GeV, as well as tight lepton with track isolation less than 4 GeV. This is precisely the type of signature that we would expect from a $t\bar{t}\gamma$ type event.

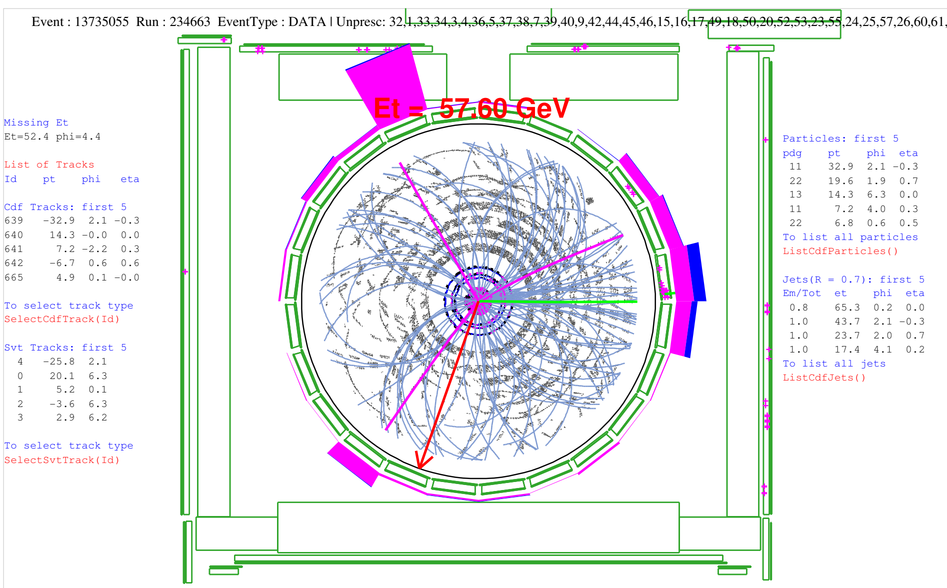

Figure 10.1: A hight pt electron event (run 234663 event 13735055) with 2 b-tagged jets, high ht, and electron track isolation less than 4 GeV. The H_T of the event is 206.8 GeV, and the $\not{E}_T$ is 56.8 GeV. There are 3 high p_T jets. The leading lepton p_T is 39.1 GeV, and the photon has a p_T of 18.7 GeV.

11 Full Comparison of Data to Signal and Background Composition

In this section we present our results for each of our selection criteria, our observed amount of data in 5.7fb^{-1}. We see excellent agreement across all three categories.

The contribution to double counting for each of the pairs of data-driven backgrounds can be found in Table A.9, A.10, and A.11.

11.1 Results from the signature based search for $\ell\gamma\not{E}_T b$

The predicted and observed totals for the $\ell\gamma\not{E}_T b$ search are shown in Table 11.1. We observe 84 $\ell\gamma\not{E}_T b$ events compared to the expectation of 86.4 ± 9.0 events.

There is no significant discrepancy in the $\ell\gamma\not{E}_T b$ signature. Figure 11.1 shows the observed distribution summed over the $e\gamma\not{E}_T b$ and $\mu\gamma\not{E}_T b$ events in a) the E_T of the lepton; b) the E_T of the photon; c) the number of jets distribution; d) the E_T of the b-jet e) the missing transverse energy ($\not{E}_T$); and f) the transverse energy (H_T) of the event.

The predicted and observed kinematic distributions for $\mu\gamma\not{E}_T b$ are compared in Figure 11.2. The distributions for the $e\gamma\not{E}_T b$ signature are compared in Figure 11.3.

CDF Run II Preliminary, 5.7fb^{-1}			
Lepton + Photon + $\not\!\!E_T$ + b Events, Isolated Leptons			
Standard Model Source	$e\gamma b\not\!\!E_T$	$\mu\gamma b\not\!\!E_T$	$(e+\mu)\gamma b\not\!\!E_T$
$t\bar{t}\gamma$semileptonic	6.42 ± 1.18	4.99 ± 0.92	11.41 ± 2.08
$t\bar{t}\gamma$ dileptonic	3.69 ± 0.67	2.91 ± 0.53	6.60 ± 1.19
$W^{\pm}c\gamma$	2.18 ± 0.43	2.04 ± 0.42	4.22 ± 0.67
$W^{\pm}cc\gamma$	0.24 ± 0.11	0.63 ± 0.19	0.87 ± 0.23
$W^{\pm}bb\gamma$	1.83 ± 0.31	1.25 ± 0.24	3.08 ± 0.45
WZ	0.22 ± 0.10	0.072 ± 0.059	0.29 ± 0.11
WW	0.28 ± 0.063	0.27 ± 0.063	0.55 ± 0.10
$\tau \rightarrow \gamma$ fake	0.35 ± 0.09	0.32 ± 0.09	0.67 ± 0.13
Jet faking γ ($ej\not\!\!E_T b, j\rightarrow\gamma$)	8.96 ± 2.52	5.54 ± 1.70	14.50 ± 3.84
MisTags	13.06 ± 1.30	9.05 ± 0.89	22.11 ± 2.08
QCD(Jets faking ℓ and $\not\!\!E_T$)	14.57 ± 7.41	1.52 ± 0.77	16.08 ± 7.46
$ee\not\!\!E_T b$, $e\rightarrow\gamma$	4.73 ± 0.69	–	4.73 ± 0.69
$\mu e\not\!\!E_T b$, $e\rightarrow\gamma$	–	1.25 ± 0.21	1.25 ± 0.21
Total SM Prediction	$56.5 \pm 8.1(tot)$	$29.8 \pm 2.4(tot)$	$86.4 \pm 9.0(tot)$
Observed in Data	51	33	84

Table 11.1: A comparison of the numbers of events predicted by the standard model (SM) and the observations for the $\ell\gamma\not\!\!E_T b$ search. The SM predictions for this search are dominated by the $t\bar{t}\gamma$, and $W\gamma$+Heavy Flavor production. Other contributions come from misidentified leptons, photons, b-jets, or $\not\!\!E_T$. MC samples have been scaled to 5.7fb^{-1}. Data-driven backgrounds have been found in the method described in previous sections.

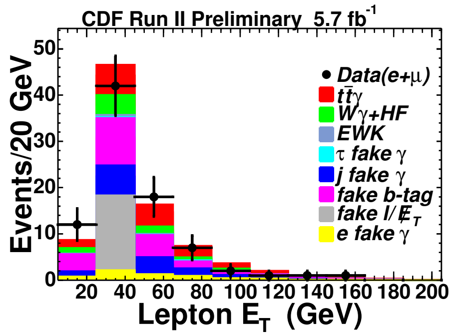

(a) $\mathrm{P_T}(l)$ in $\ell\gamma\not\!\!E_{\mathrm{T}}b$ events

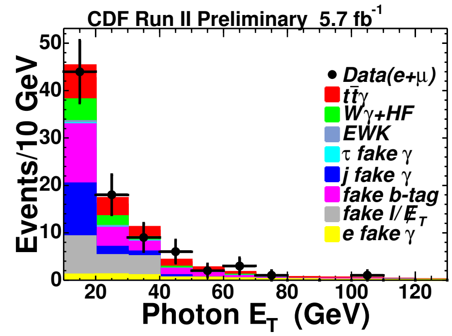

(b) $\mathrm{P_T}(\gamma)$ in $\ell\gamma\not\!\!E_{\mathrm{T}}b$ events

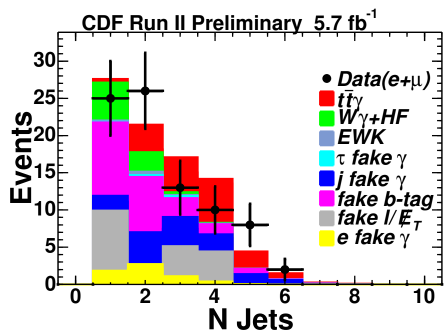

(c) N_{Jets} in $\ell\gamma\not\!\!E_{\mathrm{T}}b$ events

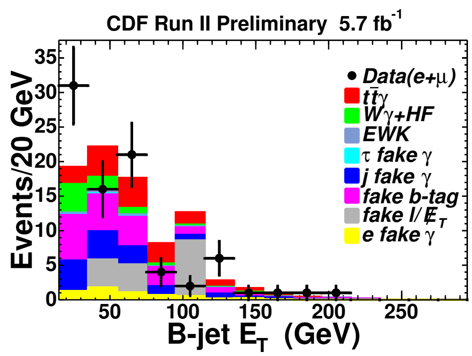

(d) $\mathrm{E_T}$ of b-tagged jet in $\ell\gamma\not\!\!E_{\mathrm{T}}b$ events

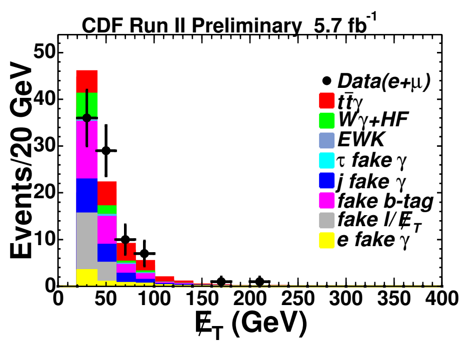

(e) $\not\!\!E_{\mathrm{T}}$ observed in $\ell\gamma\not\!\!E_{\mathrm{T}}b$ events

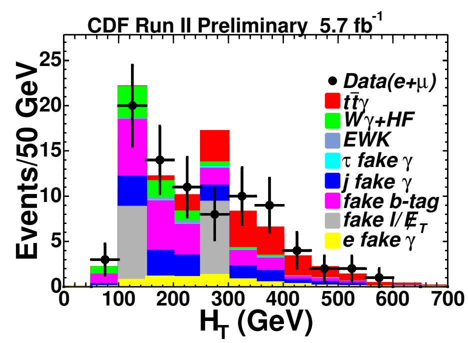

(f) $\mathrm{H_T}$ observed in $\ell\gamma\not\!\!E_{\mathrm{T}}b$ events

Figure 11.1: We show the following kinematic distributions for the $\ell\gamma\not\!\!E_{\mathrm{T}}b$ sample: a) the transverse energy (momentum) for electrons (muons); b) the transverse energy of the identified photon; c) the number of jets in the event; d) the transverse momentum of the identified b-jet; e) the missing transverse energy; f) the total transverse energy ($\mathrm{H_T}$). The black dots are data, and the histograms are MC and data-driven backrounds.

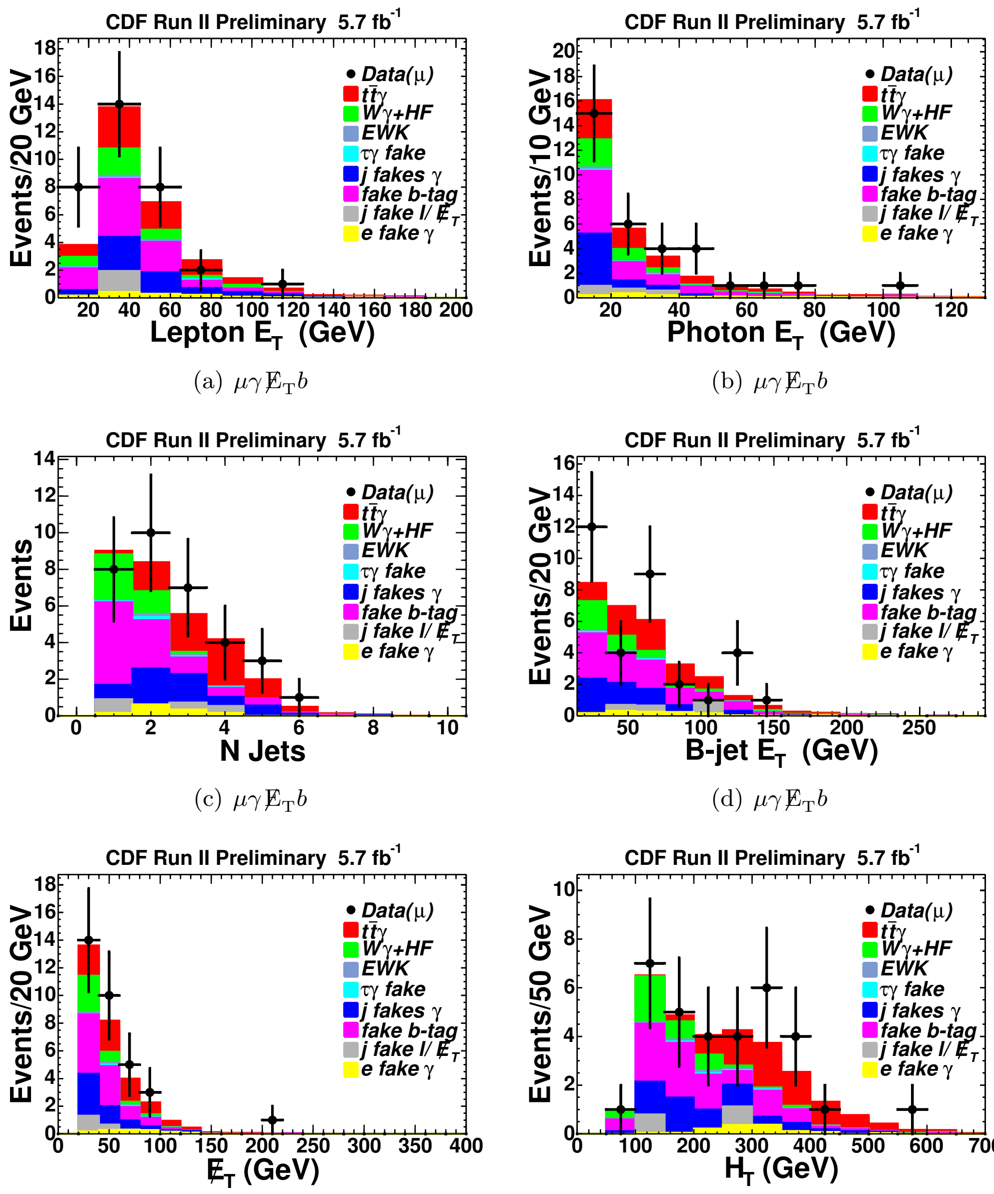

(a) $\mu\gamma\not\!\!E_T b$ (b) $\mu\gamma\not\!\!E_T b$

(c) $\mu\gamma\not\!\!E_T b$ (d) $\mu\gamma\not\!\!E_T b$

(e) $\mu\gamma\not\!\!E_T b$ (f) $\mu\gamma\not\!\!E_T b$

Figure 11.2: Spectrum of kinematic distributions for $\mu\gamma\not\!\!E_T b$ events

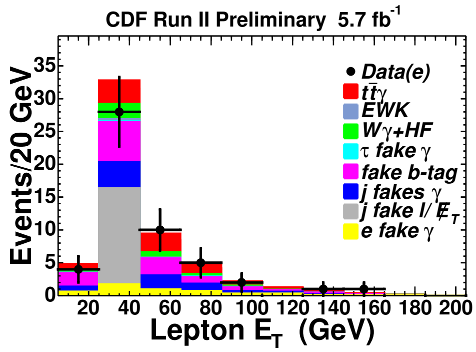

(a) $e\gamma\not{E}_{\mathrm{T}}b$

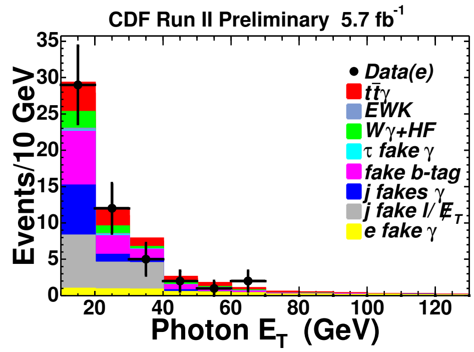

(b) $e\gamma\not{E}_{\mathrm{T}}b$

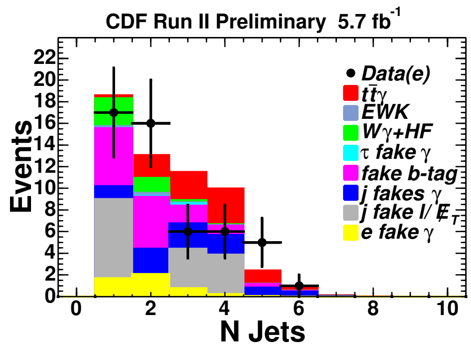

(c) $e\gamma\not{E}_{\mathrm{T}}b$

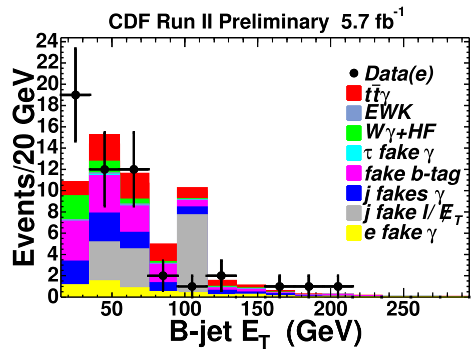

(d) $e\gamma\not{E}_{\mathrm{T}}b$

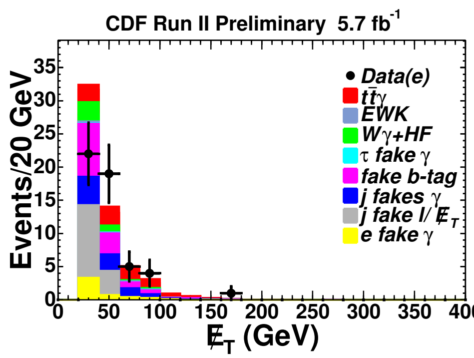

(e) $e\gamma\not{E}_{\mathrm{T}}b$

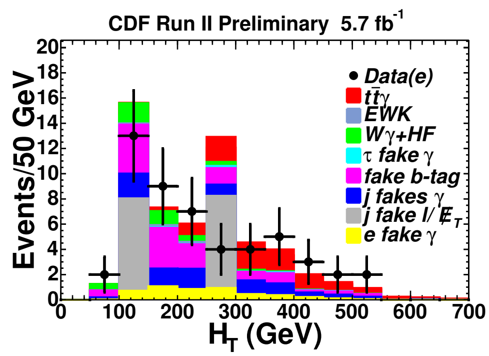

(f) $e\gamma\not{E}_{\mathrm{T}}b$

Figure 11.3: Spectrum of kinematic distributions for $e\gamma\not{E}_{\mathrm{T}}b$ events

11.2 Results for the $t\bar{t}\gamma$ Signature

The predicted and observed totals for the $t\bar{t}\gamma$ search are shown in Table 11.2. We observed 30 $t\bar{t}\gamma$ events compared to an expectation of 26.9 ± 3.4 events.

Figure 11.4 shows the observed distributions in a) the E_T of the lepton; b) the E_T of the photon; c) the number of jets distribution; d) the E_T of the b-jet e) the missing transverse energy ($\not\!\!E_T$); and f) the transverse energy (H_T) of the event.

The predicted and observed kinematic distributions for $t\bar{t}\gamma(\mu)$ events are compared in Figure 11.5. The distributions for the $t\bar{t}\gamma(e)$ events are comared in Figue 11.6.

CDF Run II Preliminary, 5.7fb^{-1}			
$t\bar{t}\gamma$, Isolated Leptons, Tight Chi2 on Photons			
Standard Model Source	$e\gamma b\not\!\!E_T$	$\mu\gamma b\not\!\!E_T$	$(e+\mu)\gamma b\not\!\!E_T$
$t\bar{t}\gamma(semileptonic)$	5.82 ± 1.07	4.59 ± 0.85	10.41 ± 1.90
$t\bar{t}\gamma(dileptonic)$	1.47 ± 0.27	1.17 ± 0.22	2.64 ± 0.48
$W^{\pm}c\gamma$	0 ± 0.064	0 ± 0.064	0 ± 0.09
$W^{\pm}cc\gamma$	0 ± 0.050	0.041 ± 0.045	0.04 ± 0.06
$W^{\pm}bb\gamma$	0.17 ± 0.08	0.054 ± 0.041	0.22 ± 0.08
WZ	0.044 ± 0.045	0.037 ± 0.041	0.08 ± 0.06
WW	0.056 ± 0.024	0.057 ± 0.025	0.11 ± 0.03
$\tau \rightarrow \gamma$ fake	0.17 ± 0.069	0.083 ± 0.047	0.25 ± 0.08
Jet faking γ ($ej\not\!\!E_T b, j \rightarrow \gamma$)	5.52 ± 1.70	1.91 ± 1.75	7.42 ± 2.61
MisTags	1.82 ± 0.38	1.60 ± 0.37	3.41 ± 0.57
QCD(Jets faking ℓ and $\not\!\!E_T$)	0.88 ± 0.88	0.02 ± 0.02	0.90 ± 0.88
$ee\not\!\!E_T b$, $e \rightarrow \gamma$	0.93 ± 0.19	–	0.93 ± 0.19
$\mu e\not\!\!E_T b$, $e \rightarrow \gamma$	–	0.49 ± 0.11	0.49 ± 0.11
Total SM Prediction	$16.9 \pm 2.1(tot)$	$10.0 \pm 2.0(tot)$	$26.9 \pm 3.4(tot)$
Observed in Data	17	13	30

Table 11.2: A comparison of the numbers of events predicted by the standard model (SM) and the observations for the $t\bar{t}\gamma$ search. The SM predictions for this search are dominated by the $t\bar{t}\gamma$ production. Other contributions come from misidentified leptons, photons, b-jets, or $\not\!\!E_T$. MC samples have been scaled to 5.7fb^{-1}. All other Data-driven numbers have been measured in the manner described in earlier sections.

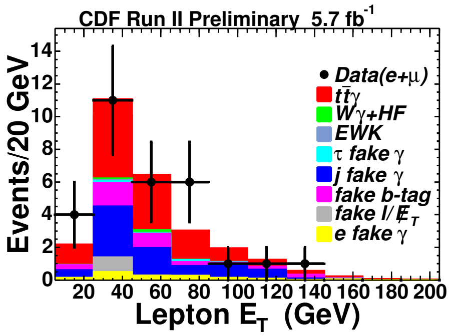

(a) $P_T(l)$ in $t\bar{t}\gamma$ event

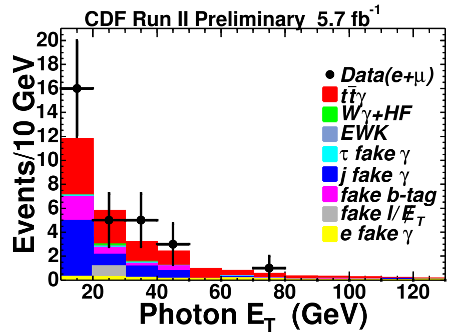

(b) $P_T(\gamma)$ in $t\bar{t}\gamma$ event

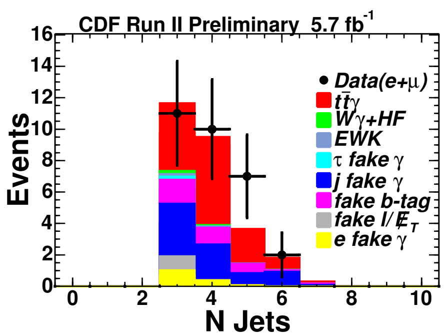

(c) N_{jets} in $t\bar{t}\gamma$ event

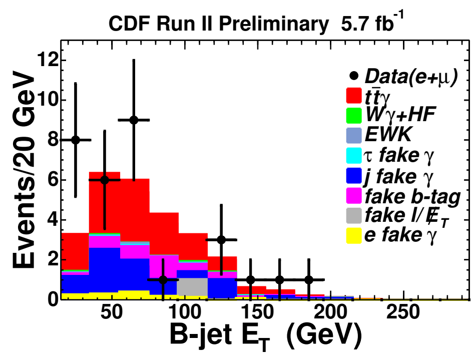

(d) E_T of the b-tagged jet

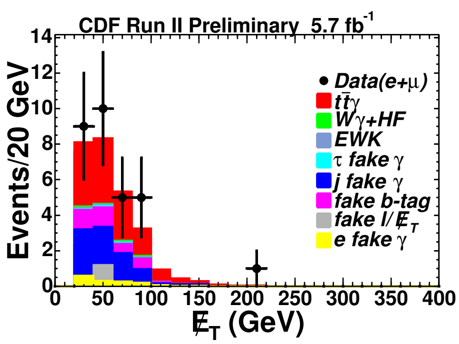

(e) $\not{E}_T$ in $t\bar{t}\gamma$ event

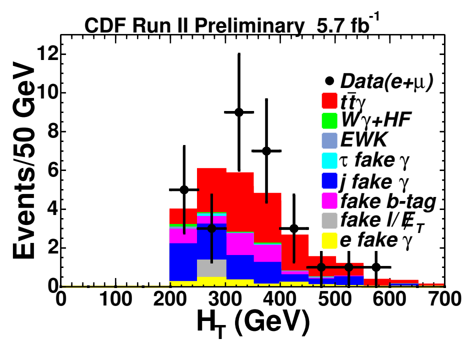

(f) H_T in $t\bar{t}\gamma$ events

Figure 11.4: We show the following kinematic distributions for the $t\bar{t}\gamma$ sample: a) the transverse energy (momentum) for electrons (muons); b) the transverse energy of the identified photon; c) the number of jets in the event; d) the transverse momentum of the identified b-jet; e) the missing transverse energy; f) the total transverse energy (H_T). The black dots are data, and the histograms are MC and data-driven backrounds.

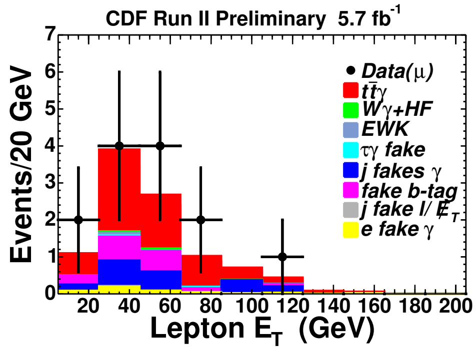

(a) $P_T(\mu)$ in $t\bar{t}\gamma(\mu)$ events

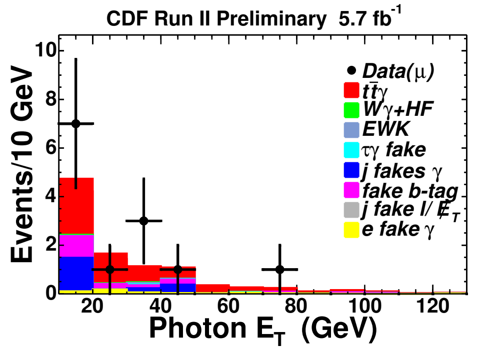

(b) $P_T(\gamma)$ in $t\bar{t}\gamma(\mu)$ events

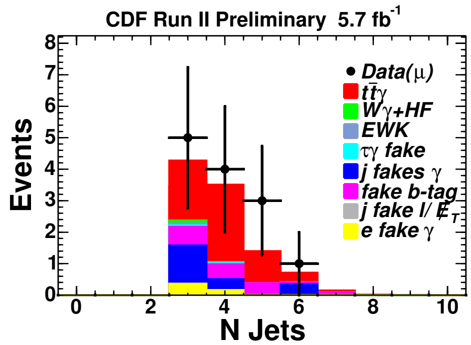

(c) N_{jets} observed in $t\bar{t}\gamma(\mu)$ events

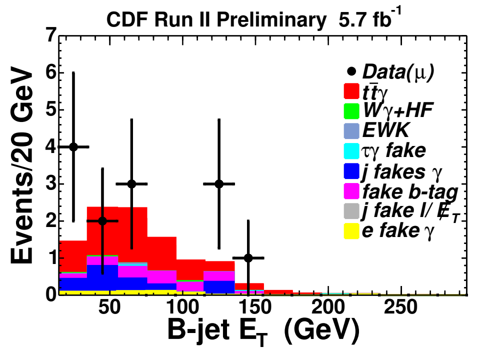

(d) E_T of b-tagged jet in $t\bar{t}\gamma(\mu)$ events

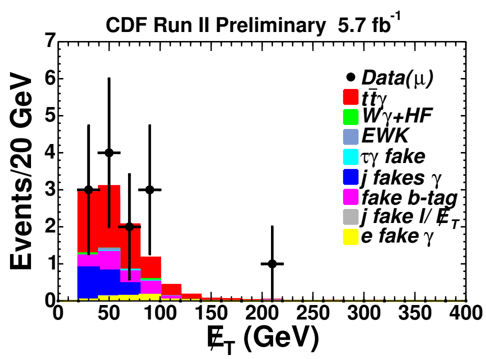

(e) $\not{E}_T$ observed in $t\bar{t}\gamma(\mu)$ events

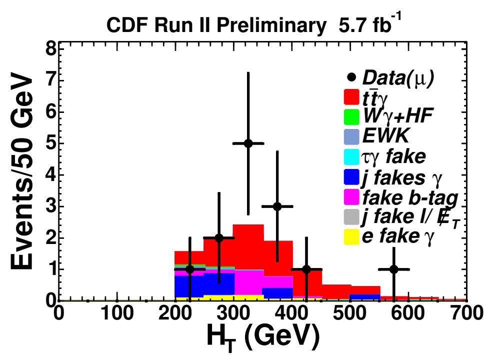

(f) H_T observed in $t\bar{t}\gamma(\mu)$ events

Figure 11.5: We show the following kinematic distributions for the $t\bar{t}\gamma$ (μ-channel) events: a) the transverse momentum; b) the transverse energy of the identified photon; c) the number of jets in the event; d) the transverse momentum of the identified b-jet; e) the missing transverse energy; f) the total transverse energy (H_T). The black dots are data, and the histograms are MC and data-driven backrounds.

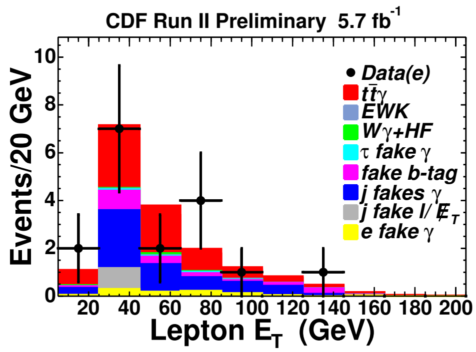

(a) $\mathrm{E_T}(e)$ in $t\bar{t}\gamma(e)$ events

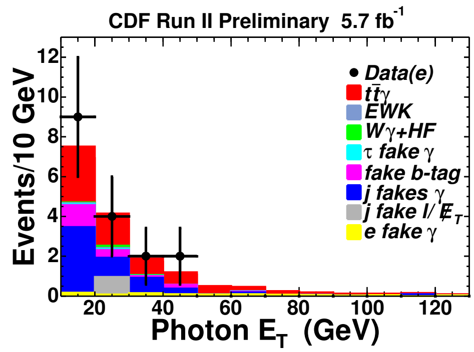

(b) $\mathrm{P_T}(\gamma)$ in $t\bar{t}\gamma(e)$ events

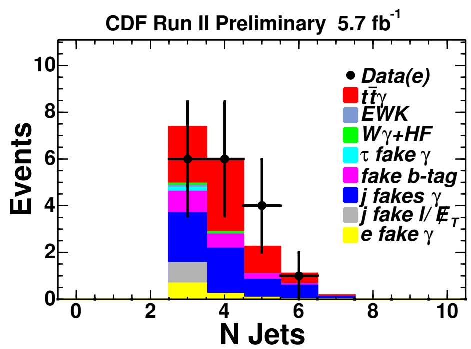

(c) N_{jets} in $t\bar{t}\gamma(e)$ events

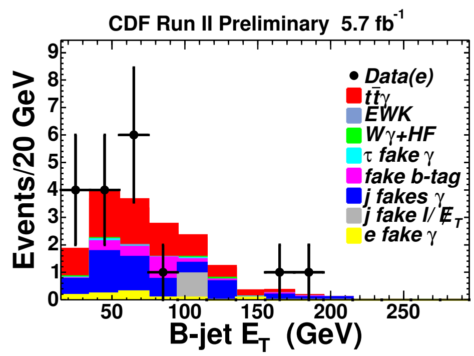

(d) $\mathrm{E_T}$ of b-tagged jet in $t\bar{t}\gamma(e)$

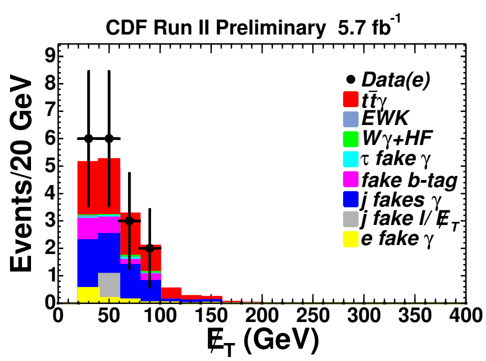

(e) $\not\!\!E_{\mathrm{T}}$ observed in $t\bar{t}\gamma(e)$ events

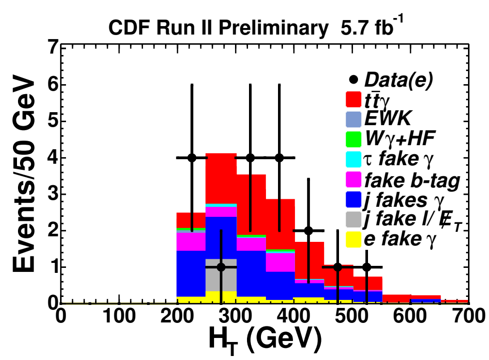

(f) $\mathrm{H_T}$ observed in $t\bar{t}\gamma(e)$ events

Figure 11.6: We show the following kinematic distributions for $t\bar{t}\gamma$ (e-channel) events: a) the transverse energy of the electron; b) the transverse energy of the identified photon; c) the number of jets in the event; d) the transverse momentum of the identified b-jet; e) the missing transverse energy; f) the total transverse energy ($\mathrm{H_T}$). The black dots are data, and the histograms are MC and data-driven backrounds.

11.3 Results from the search for $t\bar{t}$

CDF Run II, 5.7fb^{-1}			
$t\bar{t}$, Isolated Leptons, 3 or more jets, $H_T > 200$ GeV			
Standard Model Source	$eb\not{E}_T$	$\mu b\not{E}_T$	$(e+\mu)b\not{E}_T$
$t\bar{t}$	1360 ± 180	1040 ± 140	2400 ± 310
WW	28 ± 4	21 ± 3	49 ± 6
WZ	8 ± 1	6.2 ± 1	15 ± 2
ZZ	1.3 ± 0.2	0.9 ± 0.1	2.2 ± 0.3
$W^{\pm}bb$ (inclusive)	195 ± 33	140 ± 23	335 ± 56
$W^{\pm}cc$ (inclusive)	123 ± 22	90 ± 16	213 ± 39
$W^{\pm}c$ (inclusive)	82 ± 13	59 ± 9	141 ± 22
Single top (s-channel)	73 ± 10	56 ± 8	129 ± 17
Single top (t-channel)	64 ± 9	48 ± 7	111 ± 15
$Z \rightarrow llb\bar{b}$	30 ± 3	21 ± 2	51 ± 4
$Z \rightarrow \tau\tau$	5 ± 7	9 ± 7	14 ± 10
MisTags	343 ± 27	174 ± 15	527 ± 41
QCD (jets faking l and $\not{E}_T$)	201 ± 35	19.5 ± 3.4	221 ± 37
Total SM Prediction	2510 ± 187	1680 ± 140	4210 ± 327
Observed in Data	2581	1633	4214

Table 11.3: MC samples have been scaled to 5.7fb^{-1}. All other Data-driven numbers have been measured in the manner described in earlier sections.

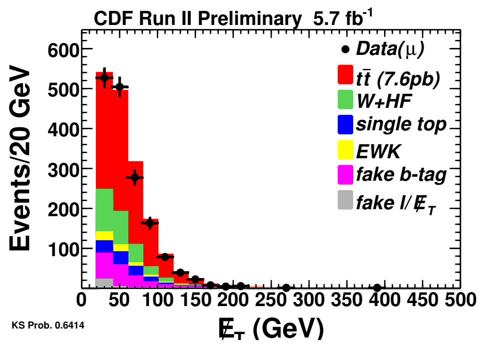

(a) $t\bar{t}(\mu)$

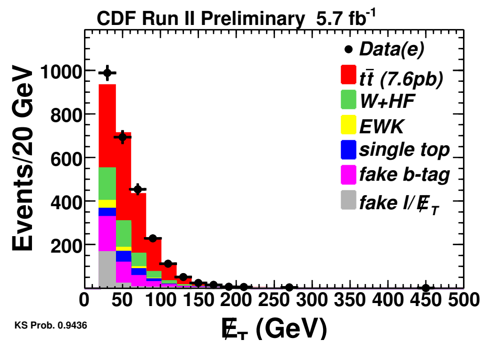

(b) $t\bar{t}(e)$

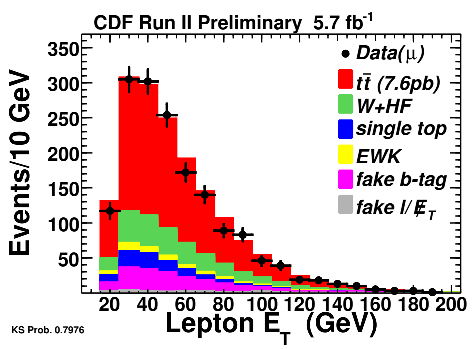

(c) $t\bar{t}(\mu)$

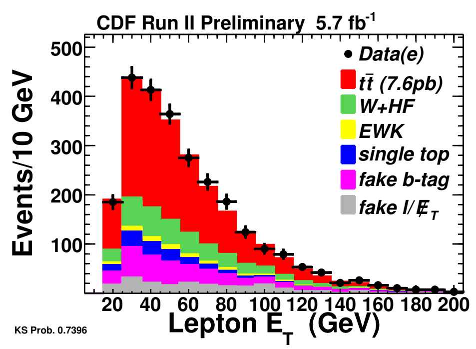

(d) $t\bar{t}(e)$

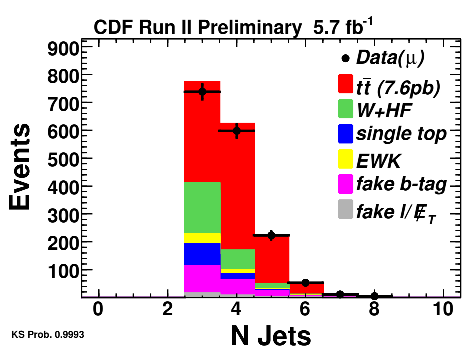

(e) $t\bar{t}(\mu)$

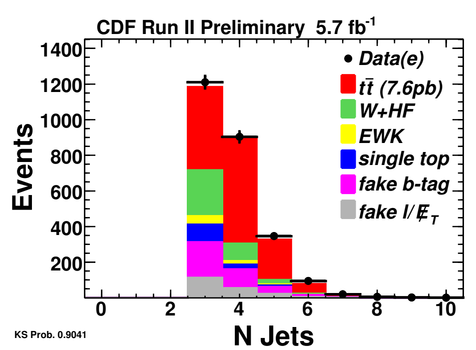

(f) $t\bar{t}(e)$

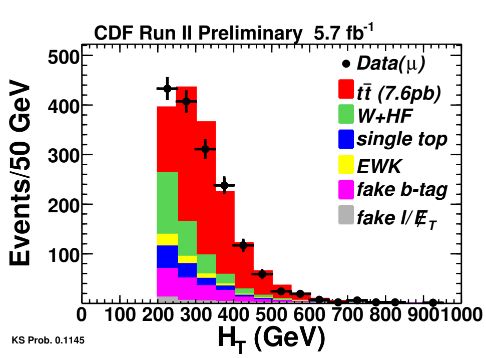

(g) $t\bar{t}(\mu)$

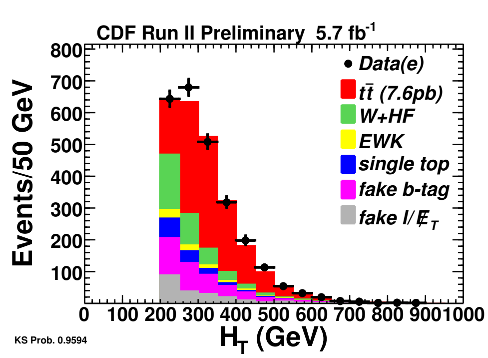

(h) $t\bar{t}(e)$

Figure 11.7: Kinematic Distributions for $t\bar{t}$ events

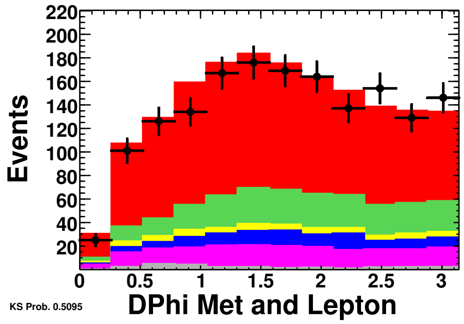

(a) $t\bar{t}(\mu)$

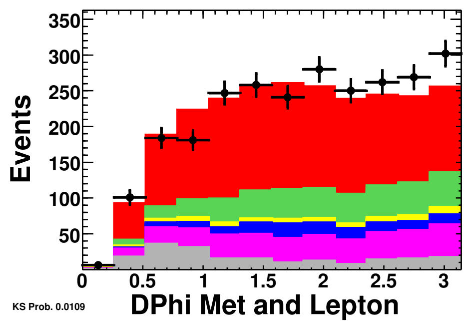

(b) $t\bar{t}(e)$

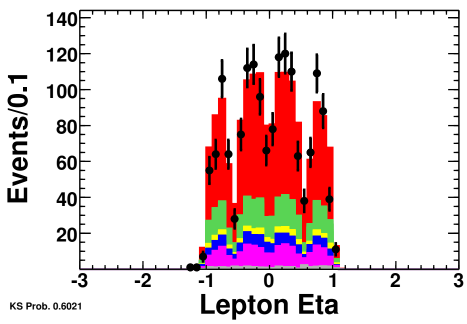

(c) $t\bar{t}(\mu)$

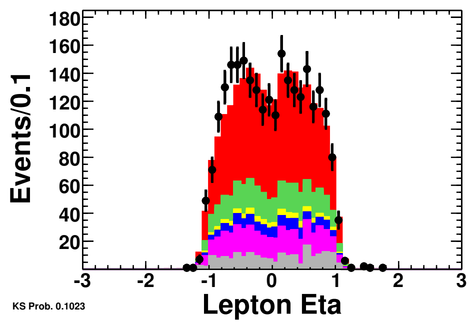

(d) $t\bar{t}(e)$

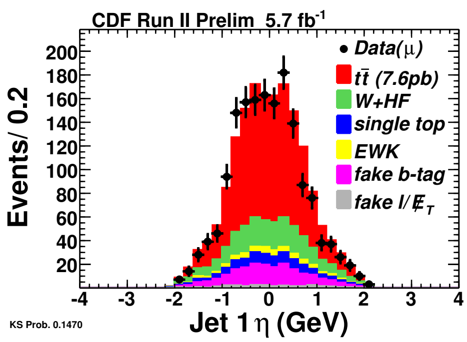

(e) $t\bar{t}(\mu)$

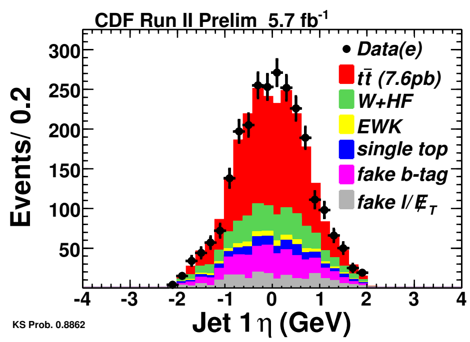

(f) $t\bar{t}(e)$

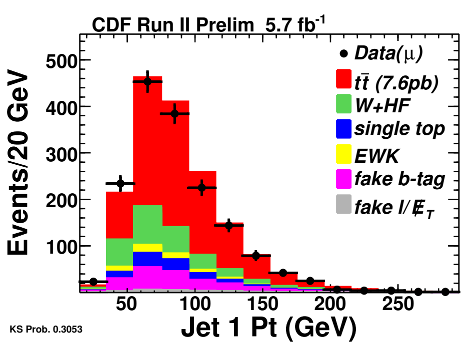

(g) $t\bar{t}(\mu)$

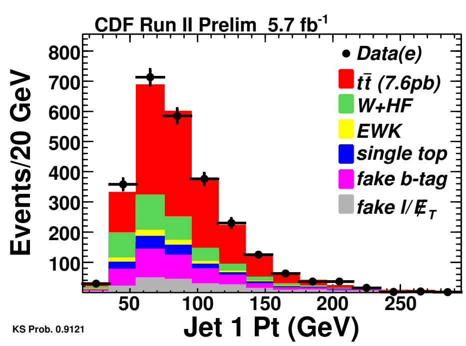

(h) $t\bar{t}(e)$

Figure 11.8: Kinematic Distributions for $t\bar{t}$ events

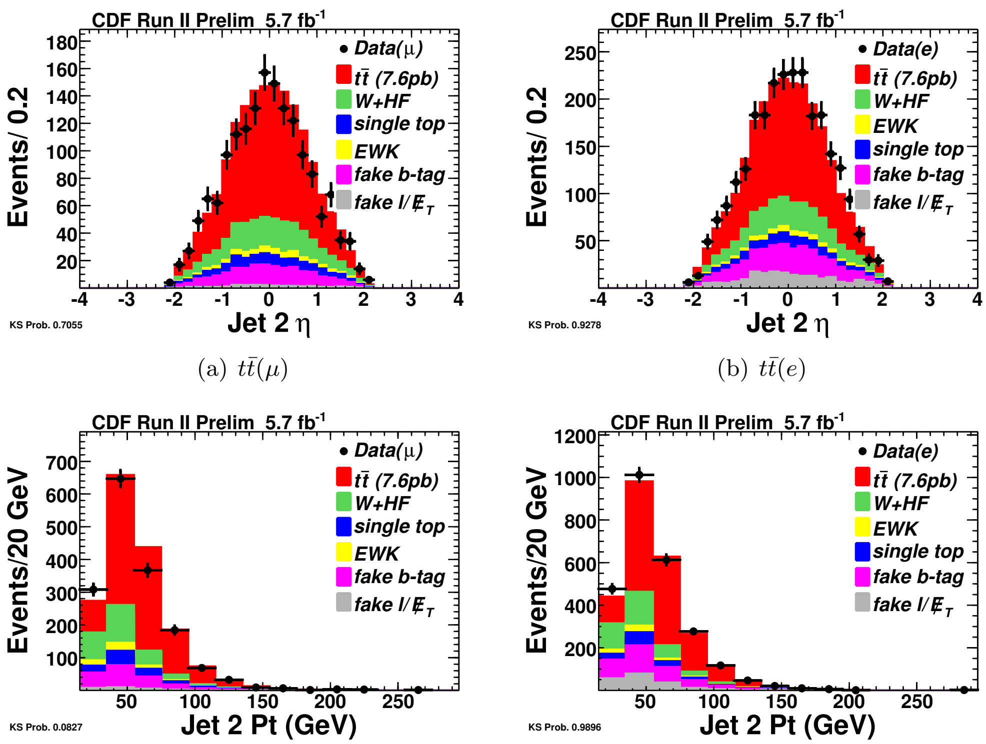

(a) $t\bar{t}(\mu)$ (b) $t\bar{t}(e)$

(c) $t\bar{t}(\mu)$ (d) $t\bar{t}(e)$

Figure 11.9: Kinematic Distributions for $t\bar{t}$ events

12 Conclusions

We presented a search for anomalous production of the signature $\ell+\gamma+b-quark+\not{E}_{\mathrm{T}}$ and a search for $t\bar{t}+\gamma$ events produced in $p\bar{p}$ collisions at $\sqrt{s} = 1.96$ TeV using data taken with the CDF detector in Run II at the Tevatron.

The theoretical production cross section of $t\bar{t}$ at the Tevatron is found to be $7.08^{+0.00+0.36}_{-0.32-0.27}$ [27]. A SM estimate for the production cross section of $t\bar{t}\gamma$ $\sigma_{semileptonic t\bar{t}\gamma} = 0.071$ pb using a LO generator (MadGraph) to be 0.073 pb, and is multiplied by a $k_{factor} = \sigma_{NLO}/\sigma_{LO} = 0.977$ [28]. Using the ratio of these theoretical cross sections we compute the ratio of $t\bar{t}\gamma$ to $t\bar{t}$ to be $0.010\ ^{+0.005}_{-0.006}$.

We measured $t\bar{t}\gamma$ cross-section

$$\sigma_{t\bar{t}\gamma} = \frac{(30\pm5.47)-(13.9\pm2.4)}{5.7\text{fb}^{-1}(0.0292\pm\text{x.xx})} = 0.10 \pm 0.04 \pm 0.02 pb$$

compared to $\sigma_{semileptonic\ t\bar{t}\gamma} = 0.080 \pm 0.012 pb$ obtained from MadGraph.

We measured the $t\bar{t}$ cross-section

$$\sigma_{t\bar{t}} = \frac{(4214\pm64.91)-(1806.61\pm27.33\pm89.75)}{5.7\text{fb}^{-1}(0.05497\pm\text{x.xx})} = 7.63 \pm .21 \pm .67 \pm .46 pb$$

Finally we compute the ratio between the production cross sections of $t\bar{t}\gamma$ and $t\bar{t}$ to be:

$$\Re = 0.013 \pm 0.005. \tag{12.1}$$

Our measurements agree well with theoretical predictions as well as previous similar measurements of similar signatures.

13 Acknowledgments

We thank Uli Baur for invaluable help with our analysis and help for generating MC processes, and help finding theoretical predictions of both the $t\bar{t}$ and the $t\bar{t}\gamma$ cross sections for the Tevatron. We thank Tim Steltzer, Steve Mrenna, and Fabio Maltoni for their support and development for MadGraph and Pythia and Soushi

Tsuno for help with our MC. Alexander Paramonov helped us to get started on the TTGNtuple. We thank Tom Schwarz for his valuable insights in helping us improve the $t\bar{t}$ sample. We also would like to thank our CDF collaborators Ray Culbertson, for their many contributions.

A Appendices

A.1 List Of Lepton-Photon-$\not\!\!E_{\mathrm{T}}$-B Events (1.9 fb^{-1})

run/event	$P_T(\ell)$	$\not\!\!E_{\mathrm{T}}$	M($\ell\not\!\!E_{\mathrm{T}}$)	$P_T(\gamma)$	M($W\gamma$)	H_T	$P_T(\ell\gamma)$	M($\ell\gamma$)	jets	b tags
196879/3659187	22.03	44.62	44.46	40.89	77.91	272.77	62.83	21.71	4	1
196892/77507	37.88	41.17	74.72	14.71	89.41	138.17	52.04	43.56	1	1
197321/1409712	27.36	57.74	51.78	20.42	62.56	323.96	46.91	18.62	5	1
193396/1050006	39.31	86.54	56.02	12.25	74.13	349.52	35.89	37.30	4	2
207488/2477561	73.01	89.01	6.43	13.62	23.96	413.75	84.99	17.48	4	2
209850/2864478	40.56	59.57	70.66	62.93	159.08	259.32	73.28	85.57	2	1
222835/7771229	66.94	21.69	41.06	35.33	109.30	243.99	40.11	94.72	3	1
223494/10133378	30.90	28.91	56.38	10.34	63.60	91.90	39.49	12.23	1	1
227377/11344663	53.97	29.02	78.48	10.23	86.21	116.46	63.48	24.03	1	1
231294/19688018	28.33	21.17	5.52	10.38	26.43	117.61	34.20	22.50	2	1
232226/1187677	37.45	23.52	59.19	32.60	86.34	134.06	55.72	68.69	1	1
233110/55577	88.95	29.68	96.10	10.04	105.16	187.45	90.74	39.83	1	1
233798/1492655	51.20	29.35	59.20	43.12	123.08	206.84	30.16	89.42	3	1
234663/13735055	39.13	56.83	81.25	18.65	100.18	206.77	57.63	29.17	3	2
236965/6459811	44.66	44.31	62.77	27.05	84.38	200.71	45.36	66.81	2	1
237478/34732412	28.46	28.07	7.68	27.26	28.46	219.67	53.49	20.93	3	1

Table A.1: List Of $e\gamma\not\!\!E_{\mathrm{T}}b$ Events

run/event	$P_T(\ell)$	$\not\!\!E_{\mathrm{T}}$	M($\ell\not\!\!E_{\mathrm{T}}$)	$P_T(\gamma)$	M($W\gamma$)	H_T	$P_T(\ell\gamma)$	M($\ell\gamma$)	jets	b tags
160591/847583	70.10	23.20	26.48	11.11	28.70	282.57	80.61	12.99	5	1
155996/1456579	27.42	31.06	51.75	21.88	74.81	107.33	46.60	26.19	1	1
197287/7739046	48.69	82.20	21.88	37.14	78.33	385.24	77.19	63.27	3	1
199620/711826	46.02	27.41	70.38	107.97	158.19	321.51	61.95	182.40	2	1
195343/9039070	27.59	53.02	68.64	45.81	97.28	213.05	67.14	37.49	3	1
206828/3127590	122.91	45.52	50.90	17.39	81.35	353.99	132.36	49.65	3	2
209532/76676	26.49	65.50	15.64	28.99	92.49	194.06	19.15	52.09	1	1
209819/2062462	46.11	72.74	7.19	16.51	17.70	342.24	61.45	15.28	3	1
209862/445276	37.65	47.25	55.31	13.75	84.58	332.52	31.44	47.38	3	1
218692/305924	22.25	32.01	49.37	46.57	94.67	162.16	34.96	59.28	3	1
221201/7636658	68.58	47.08	67.79	12.87	98.84	367.00	55.75	60.49	6	1
221723/9869061	22.44	98.04	19.44	13.77	67.72	351.00	27.08	32.02	5	3

Table A.2: List Of $\mu\gamma\not\!\!E_{\mathrm{T}}b$ Events

A.2 List of Lepton-Photon-$\not\!\!E_{\mathrm{T}}$-B events (5.7fb^{-1})

run/event	$P_T(\ell)$	$\not{E}_T$	M($\ell\not{E}_T$)	$P_T(\gamma)$	M($W\gamma$)	H_T	$P_T(\ell\gamma)$	M($\ell\gamma$)	jets	b tag
263189/1635317	39.74	38.57	75.97	10.49	83.78	110.43	42.65	27.82	1	1
185594/10091587	21.29	65.06	21.75	24.79	40.69	311.21	38.38	25.49	5	1
155996/1456579	27.42	31.08	51.74	21.85	74.79	107.69	46.57	26.22	1	1
160591/847583	70.10	23.20	26.47	11.11	28.70	281.76	80.61	12.99	5	1
195343/9039070	27.60	56.14	70.29	45.80	99.10	231.93	67.15	37.50	4	1
199620/711826	46.12	27.29	70.30	107.92	158.23	319.82	61.81	182.59	2	1
197287/7739046	48.57	82.11	21.80	37.12	78.21	383.10	77.06	63.27	3	1
209532/76676	26.52	65.53	15.62	29.06	92.65	193.33	19.19	52.18	1	1
209819/2062462	46.00	73.28	7.00	16.58	17.74	342.23	61.42	15.29	3	1
209862/445276	37.61	46.95	54.76	13.77	84.19	331.10	31.40	47.39	3	1
221723/9869061	22.46	97.88	19.48	13.77	67.71	349.34	27.10	32.03	5	3
218692/305924	22.30	31.96	49.43	46.57	94.65	161.31	34.94	59.35	3	1
221201/7636658	68.83	46.78	68.40	12.87	99.18	364.37	56.00	60.59	6	1
206828/3127590	122.94	45.41	51.14	17.39	81.53	351.44	132.39	49.65	3	2
239906/2521891	41.39	46.19	67.07	16.23	82.95	160.93	56.79	10.48	1	1
242648/1139872	45.10	46.95	80.16	69.34	140.79	238.57	109.91	32.37	1	1
244676/30558295	29.19	77.72	95.16	14.14	104.16	369.97	16.43	44.77	2	1
255090/1491384	20.29	42.65	41.39	11.35	50.82	137.75	17.06	26.65	2	1
255674/9652682	45.31	20.07	53.72	11.71	68.81	121.59	47.68	42.39	2	1
256581/55740	47.98	38.95	53.25	26.00	68.43	197.60	73.81	18.10	2	1
259189/993053	37.31	57.58	10.24	48.52	13.50	291.92	85.78	26.55	2	1
259673/16312239	47.70	37.26	81.68	12.39	95.23	323.45	53.18	43.62	4	1
265582/12252209	32.12	26.13	56.23	19.05	69.38	104.63	43.72	41.03	1	1
263877/861995	44.24	47.81	91.43	42.76	130.49	247.39	79.45	52.59	2	1
273941/7990271	21.17	70.39	77.07	52.12	131.18	284.96	59.52	48.85	2	1
274454/7114423	24.19	29.61	47.98	20.65	64.74	98.01	13.60	44.06	1	1
275267/4787467	39.85	31.02	56.11	15.51	63.64	147.91	54.00	12.26	3	1
283848/715117	20.17	32.65	50.75	30.64	76.43	109.73	46.81	32.76	1	1
289019/7952256	37.09	32.15	27.84	38.52	71.42	286.37	66.74	51.16	3	1
284145/12389851	31.64	37.53	63.29	13.64	79.60	179.06	19.87	42.52	2	1
286649/5942921	43.26	210.92	76.95	34.25	131.46	571.63	75.13	20.86	4	1
288288/8522938	22.08	44.30	35.14	20.17	51.00	206.80	42.16	16.75	2	1
287885/14307179	57.71	84.15	68.38	77.37	139.62	424.14	129.68	86.05	4	1

Table A.3: List Of $\mu\gamma\not{E}_T b$ Events 5.7 fb^{-1}

The stripped TTG ntuple begins with stripping the StNtuple to events which contain at least a loose lepton, or an anti-electron.

We then further strip the TTG ntuple requiring one of the following groups of objects must be in an event:

```
a tight lepton and a loose lepton

tight photon and loose lepton

loose lepton and met > 15

antielectron + a photon

antielectron + a bjet

met > 15 and bjet > 0

met > 15 and a tight photon

loose lepton and a bjet

bjet and a photon.
```

We used the following packages from the CDF software CVS repository:

```
BTagObjects, BTagMods, and JetUser
```

To compile the JetUser package we followed instructions that were written by Monica D'Onofrio, at the website:

```
cvsroot zoom

addpkg ZMutility

addpkg Exceptions

gmake ZMutility.all USESHLIBS=1

gmake Exceptions.all USESHLIBS=1

setup cdfsoft2 6.1.4 <--- setup cdfsoft AGAIN!

addpkg JetUser jetCorr12 (or whatever is the last JetCorr tag)

gmake JetUser.lib LINK_SHARED_ROOT=yes USESHLIBS=1

addpkg -h JESstudies

ln -s JESstudies/CalorGeometryLib .

gmake CalorGeometryLib.all USESHLIBS=1
```

and to install the BTagObjects and BTagMods packages we followed the instructions written by Thomas Junk:

```
setenv USESHLIBS 1
source ~cdfsoft/cdf2.cshrc
setup cdfsoft2 6.1.4
addpkg BTagMods btag_1invfb_v0
addpkg BTagObjects btag_4100invpb_v4
gmake BTagObjects.lib LINK_SHARED_ROOT=yes
```

A.3 TTGNtupler package

The TTGNtupler package is an ntupler built on top of the Stntuple framework using its classes and methods to access information about the data.

When first running the package over the Stntuples we produce TTGNtuples on the CDF CAF and saved them on the UChicago Clusters. We show the initial number of events in the Stntuple as well as the amount of events which have at least one loose lepton or one anti-electron.

We have made the following cross-checks against UCNtuple to verify the TTGNtupler code, for data periods bhel0h, bhmu0h, bhel0d, and bhmu0d:

- have compared number of dilepton events in both electron and muon data streams
- checked further across all six combinations of CMX, CMUP and stubless muons
- and for Z's decaying to both central electrons, or one central and one plug electron
- compared number of dilepton and photon events
- compared number of lepton, photon, and $\not\!\!E_{\mathrm{T}}$ events

For the first 1.78 fb^{-1} we further checked

- repeated comparisons mentioned above
- the run and event numbers of all $\ell\gamma\not\!\!E_{\mathrm{T}}b$ events

We have compared event yields obtained in the UCNtuple and in the TTGNtupler for the first 1.78 fb^{-1}, and results are shown in Tables A.8

A.4 Discussion on k-factor for $t\bar{t}\gamma$ MadGraph Samples

We have put here a feedback/discussion we have received from Uli Baur and Frank Petriello.

Uli Baur on k-factor:

"well, the NLO QCD corrections to ttbar-gamma still have not been calculated. However, those for ttbar-Z have recently been computed. Except for the mass of the Z, the two processes are very similar. So I would guess that the k-factors and the remaining scale uncertainty are similar.

I think the best procedure right now is to take the k-factor from ttbar-Z.

The people who calculated the NLO QCD corrections to ttbar-Z are Frank Petriello from Madison and collaborators. They have a couple of recent papers on the archive. One is for qqbar − > ttbar Z, the other also includes gluon fusion. Both papers are for the LHC, but maybe the authors can comment on the k-factor for the Tevatron."

Frank Petriello on k-factor:

"We have not yet completed the ttbar+photon calculation; we hope to have it done by the end of the summer. It is difficult to give an estimate. Since you're only interested in a 15% estimate I will give you one, but let me first give the caveats.

Besides the obvious (different phase space and pdfs), the matrix elements are quite different for ttbar+Z and ttbar+photon. ttZ has contributions from the axial couplings of the Z, which are enhanced by $(mt/mz)^2$. Furthermore, the ttH calculation of Dawson, Reina, Wackeroth showed a large difference when going from LHC − > Tevatron. The K-factor went from 1.2-1.4 (depending on scale choice) to 0.75-0.95. This was due to various phase space effects, pimarily Coulomb corrections. Because of this it is not clear that going from a massive Z to a massless photon is a minor change.

I would estimate the K-factor using the following argument. In the soft photon limit, the corrections will be the same as for ttbar production, and lead to a K-factor *of 1.3-1.4. For hard gluon emission, the negative Coulomb corrections would give a K-factor less than 1. The result should be some average of these two effects. Some effect like seen in ttH when going from LHC $->$ Tevatron should be present for ttZ and tt+photon (to a lesser extent).*

For lack of anything else right now, I would assign k=1.10+-0.15; larger than the ttH Tevatron result because of the phase-space, but not quite as large as just ttbar. This shouldn't be viewed as much more than a guess. It is important to note that this k-factor is using NLO α_s and pdfs for the NLO cross section and LO α_s and pdfs for LO, as ttH and ttbar are defined that way. I would definitely follow Uli's suggestion below to study the effect of various K-factors on your analysis."

So for k-factor we will take $k_{factor} = 1.10 \pm 0.15$

NLO cross-section from MadGraph with the k-factor applied is cross-section is $0.080 \pm 0.011 pb^{-1}$

For double-checking the cross-section we also contacted Uli Baur:

"ahhh! Now I know why you couldn't get agreement. Madgraph also includes contributions from single top production whereas we only include doubly resonant diagrams (ie. diagrams which have both a top and an antitop).

Uli Baur also advised us to use madgraph only:

"I think you should use the madgraph calculation as it appears to be more complete. And a k-factor.

run/event	$P_T(\ell)$	$\not\!\!E_{\mathrm{T}}$	M($\ell\not\!\!E_{\mathrm{T}}$)	$P_T(\gamma)$	M($W\gamma$)	H_T	$P_T(\ell\gamma)$	M($\ell\gamma$)	jets	b tag
193396/1050006	39.38	86.47	56.79	12.25	74.80	346.89	35.78	37.50	4	2
196879/3659187	22.04	44.71	44.11	40.90	77.80	274.41	62.81	21.91	4	1
196892/77507	37.90	41.19	74.61	14.71	89.34	137.60	52.02	43.70	1	1
197321/1409712	27.42	57.40	52.19	20.42	62.95	317.91	46.92	18.80	5	1
207488/2477561	72.99	88.74	6.03	13.62	23.77	407.81	85.00	17.43	4	2
209850/2864478	40.82	59.96	71.55	63.23	160.01	259.54	74.03	85.82	2	1
222835/7771229	67.22	21.63	41.27	35.33	109.62	244.20	40.14	95.00	3	1
223494/10133378	31.02	28.91	56.39	10.29	63.55	92.02	39.61	12.07	1	1
227377/11344663	54.19	28.99	78.55	10.19	86.25	116.81	63.64	24.09	1	1
231294/19688018	28.60	21.24	5.47	10.36	26.58	117.93	34.39	22.70	2	1
232226/1187677	37.98	23.49	59.55	32.92	87.14	135.11	56.10	69.77	1	1
233110/55577	90.28	28.85	92.70	10.08	101.89	215.32	92.05	40.28	2	1
233798/1492655	51.39	29.22	59.58	43.12	123.16	205.91	30.65	89.46	3	1
234663/13735055	39.28	56.87	81.10	18.65	100.08	207.33	57.75	29.31	3	2
236965/6459811	44.86	44.27	62.64	27.05	84.28	199.48	45.70	66.82	2	1
237478/34732412	28.62	27.99	7.77	27.25	27.93	217.81	53.78	20.57	3	1
238452/3001418	21.55	48.73	44.27	16.98	61.87	165.09	38.36	25.50	2	1
239853/6663393	60.92	46.39	69.29	21.24	89.48	368.03	60.51	58.17	2	1
243070/9866427	40.65	31.55	70.92	20.12	86.62	114.74	60.76	24.33	1	1
244485/6641451	23.71	69.29	51.48	27.54	67.42	307.21	50.43	17.69	3	1
255142/9581948	82.39	54.96	86.00	14.02	94.93	371.09	87.70	43.18	4	1
256076/323194	33.47	25.44	43.28	35.10	69.87	273.04	41.47	57.16	2	1
259929/17566118	29.34	27.90	49.42	11.32	65.89	527.85	21.03	40.07	5	1
263572/787882	40.23	46.51	86.51	19.58	105.22	125.87	56.99	25.17	1	1
263597/15412402	146.08	34.09	137.83	64.59	187.73	407.35	190.66	92.39	2	1
265865/2447364	57.02	85.64	139.50	21.21	158.91	241.44	63.60	50.25	2	1
266209/10796672	72.17	43.15	61.83	12.39	65.34	383.59	83.63	19.46	6	1
266618/2186795	91.69	50.40	132.51	13.75	151.17	401.23	78.46	73.94	3	1
267393/4100968	30.35	51.29	76.49	17.69	97.48	186.86	47.48	33.58	2	1
268356/2385623	35.51	63.74	71.46	23.53	107.44	178.61	52.33	27.68	1	1
268906/7480455	26.86	37.55	38.89	11.63	55.36	117.35	19.86	32.96	2	1
270000/10044710	31.03	53.26	67.28	14.86	92.22	153.25	34.37	31.81	2	1
270063/20707930	21.65	31.81	52.49	20.03	68.72	95.24	22.20	39.99	1	1
270140/651228	75.88	30.36	92.27	13.51	102.12	179.87	82.37	50.79	1	1
270434/8460797	60.57	61.68	114.47	25.16	146.26	320.34	61.08	60.77	4	1
273747/7624925	53.84	41.04	67.50	22.66	83.87	196.29	75.95	22.05	1	1
275728/4876317	64.15	41.17	76.86	30.98	129.09	177.44	51.82	90.94	1	1
275804/18282441	36.67	27.67	63.50	14.83	76.66	398.56	36.32	44.16	5	1
277505/3178590	32.92	64.37	54.22	12.73	58.62	210.24	40.01	32.67	2	1
284145/13516440	39.14	31.87	70.41	16.19	85.08	111.84	50.47	22.96	1	1
284548/13105874	136.03	30.76	19.61	12.88	36.16	388.59	146.01	29.66	4	1
285112/1499977	25.29	40.22	54.76	10.54	69.57	105.05	33.35	13.16	1	1
285220/11443424	25.62	39.89	60.48	18.87	81.55	297.76	43.84	9.22	2	1
285353/523667	32.77	34.52	56.43	11.29	70.42	116.21	41.11	16.48	1	1
285569/3068625	34.34	21.94	39.49	13.01	52.38	102.84	32.84	34.15	1	1
285851/8166809	26.19	61.52	79.48	34.65	122.32	470.84	59.61	40.83	5	2
286665/2186117	44.33	42.40	76.44	11.00	83.03	157.53	53.10	19.44	2	1
287396/3664026	31.43	53.51	81.97	18.71	95.25	132.23	15.04	47.87	1	1
288485/7268797	63.18	85.57	93.40	50.36	121.71	478.02	113.38	32.66	2	2
288886/8553454	45.46	38.82	75.89	20.84	103.50	125.71	44.74	56.01	1	1
289107/4996702	50.59	166.98	83.38	13.26	86.42	516.79	59.70	23.52	5	2

Table A.4: List Of $\not\!\!E_T b$ Events 5.7 fb^{-1}

Dataset	Stntuple	N Events	N Stripped	Begin Run	End Run	int.lumi (pb)
bhel0d	bhelbd	26,499,561	3,338,119	138425	186598	520
bhel0h	bhelbh	19,813,851	2,831,808	191208	203799	460
bhel0i	bhelbi	28,940,435	3,958,586	203819	228596	730
bhel0i, bhel0j	bhelbij	11,588,610	1,483,459	228664	233111	290
bhel0j	bhelbj	32,259,040	3,964,960	233133	246231	760
bhel0k	bhelbk	37,161,882	2,917,732	252836	261005	380
bhel0m	bhelbm	194,285,076	11,635,876	261119	289197	3430
bhmu0d	bhmubd	6,629,080	785,803	138425	186598	520
bhmu0h	bhmubh	5,740,083	629,063	191208	203799	460
bhmu0i	bhmubi	8,853,061	972,538	203819	228596	730
bhel0i, bhel0j	bhelbij	4,712,958	452,395	228664	233111	290
bhmu0j	bhmubj	12,578,391	1,216,406	233133	246231	760
bhmu0k	bhmubk	32,847,648	1,620,320	252836	261005	380
bhmu0m	bhmubm	127,623,660	6,150,455	261119	289197	3430

Table A.5: Results of isolating events with at least one loose lepton or anti-electron from raw Stntuples

Dataset	TTG Location (UC diskspace)	Stripped Location (Yale diskspace)
bhelbd	/cdf/s13/auerbach/cafTest/bhelbd/	/group/cdf/data/auerbach/benbhelbdNEW.11/
bhelbh	/cdf/s9/auerbach/cafTest/bhelbh/	/group/cdf/data/auerbach/benbhelbhNEW.11/
bhelbi	/cdf/s9/auerbach/cafTest/bhelbi/	/group/cdf/data/auerbach/benbhelbiNEW.11/
bhelbi, bhelbj	/cdf/s13/auerbach/cafTest/bhelij/	/group/cdf/data/auerbach/benbhelbij.11/
bhelbj	/cdf/s9/auerbach/cafTest/bhelbj/	/group/cdf/data/auerbach/benbhelbjNEW.11/
bhelbk	/cdf/s9/auerbach/cafTest/bhelbk/	/group/cdf/data/auerbach/benbhelbkNEW.11/
bhelbm	/cdf/s9/auerbach/cafTest/bhelbm/	/group/cdf/data/auerbach/benbhelbmh.11/ /group/cdf/data/auerbach/benbhelbmlow.11/
bhelbm	/cdf/s9/auerbach/cafTest/newbhelbm/	/group/cdf/data/auerbach/newelbm.11/
bhmubd	/cdf/s13/auerbach/cafTest/bhmubd/	/group/cdf/data/auerbach/benbhmubdNEW.13/
bhmubh	/cdf/s9/auerbach/cafTest/bhmubh/	/group/cdf/data/auerbach/benbhmubhNEW.13/
bhmubi	/cdf/s9/auerbach/cafTest/bhmubi/	/group/cdf/data/auerbach/benbhmubiNEW.13/
bhmubi, bhmubj	/cdf/s13/auerbach/cafTest/bhmuij/	/group/cdf/data/auerbach/benbhmubij.13/
bhmubj	/cdf/s9/auerbach/cafTest/bhmubj/	/group/cdf/data/auerbach/benbhmubjNEW.13/
bhmubk	/cdf/s9/auerbach/cafTest/bhmubk/	/group/cdf/data/auerbach/benbhmubkNEW.13/
bhmubm	/cdf/s9/auerbach/cafTest/bhmubm/	/group/cdf/data/auerbach/benbhmubmNEW.13/
bhmubm	/cdf/s9/auerbach/cafTest/newbhmubm/	/group/cdf/data/auerbach/newmubm.13/

Table A.6: Location of the TTGntuples processed on the CDF CAF, and then transferred to the University of Chicago machines.

Anti Electron Must Pass all of these	
Variable	AntiElectron
E_T	> 20 GeV
Track $\|z0\|$	< 60 cm
Fractional Calorimeter Isolation E_T	< 0.1
E/P	< 2.0
Anti Electron Must FAIL at least two of these	
Had/Em	$< 0.055 + 0.00045\times$E
Lshr	< 0.2
Chi2 Strips	< 10
ΔX	-3.0 cm $< Q_{trk} \times \Delta X <$ 1.5 cm or $\|\Delta X\| <$ 3.0 cm
$\|\Delta Z\|$	$<$ 3.0 cm or $<$ 5.0 cm
Track quality cuts	3 Ax, 2 St SL x 5 hits

Table A.7: Cuts required for Anti-Electrons.

Dataset	Number of Zs	Number of W's	Number of lg$\not\!\!E_{\mathrm{T}}$	Number of llg
TTG (μ)	31.43 ± 0.13	474.78 ± 0.52	0.72 ± 0.020	0.19 ± 0.010
UC (μ)	31.43 ± 0.13	474.95 ± 0.52	0.74 ± 0.020	0.19 ± 0.010
TTG (e)	31.91 ± 0.13	700.59 ± 0.63	0.83 ± 0.022	0.27 ± 0.012
UC (e)	31.86 ± 0.13	695.52 ± 0.63	0.83 ± 0.022	0.27 ± 0.012

Table A.8: TTG vs UC ntuple comparison for Muon events. The luminosity was found using the good run list v17 with em mu and silicon. We see decent agreement between TTG and UC ntuples with a disagreement of 2%. Using the good run list and the SAM lumi script we find the luminosity to be 1.78 pb^{-1}

CDF Run II Preliminary, 5.7fb^{-1}			
Lepton + Photon + $\not\!\!E_{\mathrm{T}}$ + b Events, Isolated Leptons			
Double Counting Source	$e\gamma b\not\!\!E_{\mathrm{T}}$	$\mu\gamma b\not\!\!E_{\mathrm{T}}$	$(e+\mu)\gamma b\not\!\!E_{\mathrm{T}}$
Jets Faking Photons and Electrons Faking Photons	0.0085	0	0.00850
Jets Faking Photons and Mistags	3.07	1.52	4.590
Jets Faking Photons and QCD	0	0	0
Electrons Faking Photons and QCD	0	0	0
Mistags and QCD	0.15	0.0027	0.152
Mistags and electrons faking photons	0.22	0.075	0.295
Total amount of Double Counting	3.45	1.60	5.050

Table A.9: This table shows the predicted amount of double counting between two data- driven backgrounds for the $\ell\gamma\not\!\!E_{\mathrm{T}}b$ signal

CDF Run II Preliminary, 5.7fb^{-1}			
$t\bar{t}\gamma$, Isolated Leptons			
Double Counting Source	$e\gamma b\not{E}_{\mathrm{T}}$	$\mu\gamma b\not{E}_{\mathrm{T}}$	$(e+\mu)\gamma b\not{E}_{\mathrm{T}}$
Jets Faking Photons and Electrons faking Photons	0.0085	0	0.00850
Jets Faking Photons and Mistags	0.90	0.54	1.440
Jets Faking Photons and QCD	0	0	0
Electrons Faking Photons and QCD	0	0	0
Mistags and QCD	0	0	0
Mistags and electrons faking photons	0.048	0.039	0.087
Total amount of Double Counting	0.96	0.58	1.540

Table A.10: This table shows the predicted amount of double counting between two data- driven backgrounds for the $t\bar{t}\gamma$ signal

CDF Run II Preliminary, 5.7fb^{-1}			
$t\bar{t}\gamma$, Isolated Leptons, Tighter Chi2 Cut on Photons			
Double Counting Source	$e\gamma b\not{E}_{\mathrm{T}}$	$\mu\gamma b\not{E}_{\mathrm{T}}$	$(e+\mu)\gamma b\not{E}_{\mathrm{T}}$
Jets Faking Photons and Electrons faking Photons	0.0085	0	0.00850
Jets Faking Photons and Mistags	0.36	0.19	0.550
Jets Faking Photons and QCD	0	0	0
Electrons Faking Photons and QCD	0	0	0
Mistags and QCD	0	0	0
Mistags and electrons faking photons	0.048	0.039	0.087
Total amount of Double Counting	0.42	0.23	0.650

Table A.11: This table shows the predicted amount of double counting between two data- driven backgrounds for the $t\bar{t}\gamma$ signal

B Selection Criteria

Some of the ID variables are different from those used in the UCNtuple. For instance, for the UCNtuple we've selected the primary event vertex as follows:

- **Step 1**:

  The vertex chosen is the class 12 vertex with the smallest pull under 5 sigma to the highest pt tight lepton.

- **Step 2**:

  If no vertices are close or there are no class 12 vertices, then the lepton z0 is used.

- **Step 3**:

  If there is no high pt tight lepton, it uses the highest sumpt class 12 vertex.

- **Step 4**:

  If there are no class 12 vertices, then the highest sumpt primary vertex is used.

- **Step 5**:

  If there are no vertices, then the origin is used.

For the Stntuple (and therefore, for the derived TTGNtuple, see Appendix A.3), we've selected the primary event vertex as follows:

- **Step 1**:

  The primary vertex is defined by the vertex which has the highest sum of objects' pt coming from it.

Choice of primary vertex affects E_T of photons and jets.

Other minor changes in object ID are described in the subsections below.

B.1 Lepton Selection: Muons

We require at least one 'tight central muon', photon, b-jet and $\not{E}_T$ in a event for it to be classified as a $\mu\gamma\not{E}_T b$ event. We also search for additional muons using a definition of 'loose central muon'. We describe these two sets of cuts below.

B.1.1 Muon Cuts

Variable	Tight	Loose	Stubless
Track P_t	$> 20\ GeV$	$> 12\ GeV$	$> 12\ GeV$
Track quality cuts	3x3SLx5 hits	3x2SLx5 hits	3x3SLx5 hits
Track $\|z0\|$	$< 60\ cm$	$< 60\ cm$	$< 60\ cm$
Calorimeter Energy (Em)	$<$ 2 + sliding	$<$ 2 + sliding	$<$ 2 + sliding
Calorimeter Energy (Had)	$<$ 6 + sliding	$<$ 6 + sliding	$<$ 6 + sliding
Fractional Calorimeter Isolation E_T	< 0.1	< 0.1	< 0.1
Cosmic	False	False	False
Chi2/(N of COT hits-5)	-	-	$<$ 3
Cal.Energy (EM+Had)	-	-	$>$ 0.1
CMUP muons cuts(*)	yes	yes	no
CMX muons cuts(**)	yes	yes	no

Table B.1: Muon Identification and Isolation Cuts for 533.

(*)CMUP muons cuts: $|\Delta X(CMU)| < 3\ cm$, $|\Delta X(CMP)| < 5\ cm$
No muons from CMP bluebeam section for run<154449
(**)CMX muons cuts: $|\Delta X(CMX)| < 6\ cm$, rho(COT) $>$ 140 cm (COT exit radius)
No muons from the CMX keystone or miniskirt before October 2004 shutdown (run 186598)

These cuts are identical to the standard cuts [29], [30]. with the exception that we have not applied the impact parameter cut and we don't use cuts on fiducial distance (x-fid, z-fid).

Classification of muons according to [29], [30] is as follows:

- **Tight** (CMUP or CMX)
- **Loose**
  - **Loose CMUP or CMX** (with looser COT cuts)
  - **Stubless** (without stub, or with either CMU or CMP, or BMU etc. stub only, i.e. not CMUP or CMX muons)

Tight central muons are identified by extrapolating tracks in the COT through the calorimeters, and the extrapolation is required to match to a stub either in both the CMU and CMP muon detectors (a ‘CMUP’ muon), or in the CMX system(a ’CMX’ muon). Tight central muons are required to have a track-stub matching distance less than 3 cm for CMU, less than 5 cm for CMP, and less than 6 cm for CMX.

“Region is OK” cut requires:

- for CMUP muons
  - No muons from CMP bluebeam section for run<154449
- for CMX muons
  - rho(COT) > 140 cm (COT exit radius)
  - No muons from the CMX keystone ot miniskirt before October 2004 shutdown (run 186598)

This is what we have for “Region is OK” column in event printouts:

```
BlueBeam : (fRegion   & 0x2) == true
MiniSkirt: (fRegion   & 0x1) == true
KeyStone : (fRegion   & 0x4) == true
All other:  fRegion = 0
```

We use both CMUP and CMX muons as tight muons.

To differentiate between CMU CMP, and CMX muons we check for stubs in the respective subdetectors. The stubs each have at least 3 hits in the detector.

The impact parameter calculation uses the default muon track rather than the parent COT track, and in the Top Group selection a tighter cut is applied if the track does in fact contain silicon hits.

The muon tracks used in the initial selection for this analysis are beam-constrained COT-only, as is done by the muon group in their efficiency studies [29]. For default muon tracks that contain silicon we link backwards to the COT-only parent track and use that track for all subsequent analysis. Muon tracks that have silicon hits and those that do not form two distinctly different samples, with different backgrounds [31], and different resolutions; this technique, while losing valuable information from the silicon at this stage, puts all prompt COT tracks on the same footing (however tracks with impact parameter, such as those from very high-momentum tau decay, would be much better treated using the silicon).

For tracks that are COT-only beam-constrained tracks, we also apply a curvature correction [32] for the track p_T in data before applying kinematic selection criteria and calculating additional kinematic variables. The form of the curvature correction is shown in Equation B.1 where Q is a charge of track(+1 for positive charge and -1 for tracks negative charge):

$$\begin{aligned}
&c = c + 0.00020 * sin(\phi + 3.4) \\
&c = c + 0.00022 * sin(3 * \phi + 0.9) \\
&c = c - (0.000026 + 0.000072 * cot(\theta) - 0.00024 * cot(\theta) * cot(\theta)) \\
&c = c - 0.0002 * cot(\theta) * sin(\phi - 0.9) - 0.0002 * cot(\theta) * cot(\theta) * sin(\phi - 4.1) \\
&p_T = Q/c
\end{aligned} \tag{B.1}$$

All central muons are required to have $|z_0| < 60\ cm$ so that the collision is well-contained within the CDF detector. In order to be well-measured, the muon track is required to have minimum of 3 axial and 3 stereo superlayers with at least 5 hits in each superlayer.

High energy muons are typically isolated 'minimum-ionizing' particles that have limited calorimeter energy. A muon traversing the central electromagnetic calorimeter(CEM) deposits an average energy of ~ 0.3 GeV. Therefore we require muon candidates to deposit less than 2 GeV total in the CEM towers (we take into account two towers in the CEM) the muon track intersects. Similarly, muons transversing the central hadronic calorimeter(CHA) deposit an average energy of ~ 2 GeV; we consequently require muon candidates to deposit a total energy less than ~ 6 GeV, also increasing with muon momentum, in the CHA towers intersected by the track extrapolation. To take into account the (slow) growth of energy loss with momentum, for very high energy muons ($p > 100\ GeV$) we require the measured CEM energy to be less than $2.0 + 0.0115 * (p - 100)\ GeV$ and CHA energy to be less than $6.0 + 0.028 * (p - 100)\ GeV$.

To suppress hadrons and decay muons created from hadrons in jets we require the total transverse energy deposited in the calorimeters in a cone of R=0.4 around the muon track direction(known as the fractional calorimeter isolation E_T) to be less than 0.1 of the muon track pt.

The COT cosmic finder by itself is essentially fully efficient. Therefore, to suppress cosmic rays we use the COT-based cosmic rejection from the CosmicFinderModule [33, 34] and reject events which it tagged as Cosmic Ray muons.

B.1.2 Loose Central CMUP and CMX Muons

While each $\mu\gamma\not{E}_{\mathrm{T}}b$ event has to contain at least one tight CMUP or CMX muon, both $\mu\gamma\not{E}_{\mathrm{T}}b$ and $e\gamma\not{E}_{\mathrm{T}}b$ events are searched for additional high-$\mathrm{P_T}$ muons that could come from the decays of heavy particles. There are two types of secondary muons we accept: 'Loose' CMUP and CMX muons, described here, and stubless muons (see Section B.1.3).

Loose muons are muon objects with either CMUP or CMX stubs, but with looser COT cuts than the tight CMUP or CMX muons (see Table B.1). We require 3 axial and 2 stereo COT super layers with at least 5 hits each for loose CMUP and CMX muons.

B.1.3 Loose Central Muons: Stubless

The cuts for the Stubless muons are looser than the tight cuts, and in particular do not require a stub in the muon chambers.

There are three types of 'Stubless' muons:

- CMU muons (muon track matches the CMU stub only);
- CMP muons (muon track matches a stub in the CMP only;
- CMIO muons (muon track doesn't match any stub).

We require at least some energy in the calorimeter towers that the muon extrapolates to, Calorimeter Energy (Em+Had) > 0.1 GeV, and a good fit to the COT track, χ^2/(N of COT hits-5)<3 [31, 29]. These two cuts are used to reject charged kaon decays in flight in which a low-momentum kaon ($\sim$ 5 GeV, typically) decays inside the COT with the kaon and decay-muon tracks forming a 'seagull' pattern which is reconstructed as a single high-momentum track.

The pattern-finding algorithm often removes a complete stereo layer in order to get a good fit, and so these tracks are badly mis-reconstructed in polar angle. Consequently they are often recorded leaving zero energy in the extrapolated traversed calorimeter towers [31].

B.2 Lepton Selection: Electrons

We require at least one 'tight central electron' in an event for it to be classified as an $e\gamma\not\!\!E_{\rm T}b$ event. We also search for additional 'loose' electrons in the CEM and PEM. We describe the tight central and loose central and plug cuts below.

B.2.1 Electron Selection Criteria

Variable	Tight	Tight100	Loose
E_T	> 20 GeV	> 100 GeV	> 12 GeV
Track P_T	> 10 GeV	> 25 GeV	> 10 GeV
Track $\|z0\|$	< 60 cm	< 60 cm	< 60 cm
Had/Em	< 0.055 + 0.00045×E	< 0.055 + 0.00045×E	< 0.055 + 0.00045×E
E/P	< 2.0	-	-
Lshr	< 0.2	-	-
Chi2 Strips	< 10	-	-
ΔX	-3.0 cm < $Q_{trk} \times \Delta X$ < 1.5 cm	$\|\Delta X\|$ < 3.0 cm	-
$\|\Delta Z\|$	< 3.0 cm	< 5.0 cm	-
Fractional Calorimeter Isolation E_T	< 0.1	< 0.1	< 0.1
Track quality cuts	3 Ax, 2 St SL x 5 hits	3 Ax, 2 St SL x 5 hits	3 Ax, 2 St SL x 5 hits

Table B.2: Central Electron Identification and Isolation Cuts for Offline Version 5.3.3.

The selection cuts are standard [35] with the exception that the fiducial requirement and the conversion cut are not applied (same as in Ref. [36]).

Variable	Tight	Phoenix Tight
E_T	> 15 GeV	> 15 GeV
Had/Em	< 0.05	< 0.05
Fractional Calorimeter Isolation E_T	< 0.1	< 0.1
Chi2 Strips	< 10	< 10
Delta R	< 3.0 cm	< 3.0 cm
PES 5by9 U and V	> 0.65	> 0.65
PEM $\|\eta\|$	$2.0 < \|\eta\| < 1.2$	$2.0 < \|\eta\| < 1.2$
PhxMatch	-	TRUE
Number of Silicon Hits	-	≥ 3
|Z(Phoenix)|	-	< 60 cm

Table B.3: Plug Electron Identification and Isolation Cuts for Offline Version 5.3.3. We are using the "Phoenix Tight" selection [1], [2].

B.2.2 Tight Central Electrons

The selection criteria for tight central electrons are described below.

Electrons are identified in the CEM by matching high momentum tracks to high-energy CEM clusters. The electron track is the highest momentum track which intersects one of two towers in the CEM cluster. The electron tracks that we use in this analysis are beam-constrained COT-only. We apply the same corrections to the electron tracks as we do to the muon tracks. The selection cuts are standard [35] with the exception that the fiducial requirement and the conversion cut are not applied.

An electron candidate is required to have tracking momentum (P) which exceeds half of its calorimeter energy (E). The electron track is required to have a minimum of 3 axial and 2 stereo SL segments containing at least 5 hits each. In order that the momentum resolution doesn't make for inefficiencies for very high-energy electrons, for $E_T > 100\ GeV$ the E/P cut is not applied (leaving only the the $\mathrm{P_T} > 25$ GeV cut as the requirement on the track). The electrons are required to have the track extrapolate to the beam line within $|Z_0| < 60\ cm$ so that CDF detector contains the collision well.

The position of the track extrapolated to the CES radius must satisfy the following requirements: it must fall within charge-signed CES shower position of the cluster in the r-phi view -3.0 cm $< Q_{trk} \times \Delta X <$ 1.5 cm and it must fall within 3 cm of the CES shower position in the Z-direction(ΔZ).

The CEM shower characteristics should be consistent with that of a single charged particle. We require the ratio of the total energy of the CHA towers located behind the CEM towers in the electron cluster to that of the electron itself to be less than than 0.055+0.00045×E GeV. A comparison of the lateral shower sharing with neighboring towers in the CEM cluster with test-beam data is parameterized by a dimensionless quantity, L_{shr}, which must have a value less than 0.2.

We require the χ^2 for the profile of energy deposited in the CES strips compared to that expected from test beam data to be less than 10. No χ^2 cut is made on the profile in the CES wires as bremsstrahlung will separate from the electron in the $r\phi$ view.

As an additional isolation requirement, the total transverse energy deposited in the calorimeter in a cone R=0.4 around the electron track, must be less than 0.1 of the E_T of the electron. The isolation is corrected via the standard algorithm [37], for leakage, but not the number of vertices.

We don't apply 'Conversion Flag' and 'Fiducial' cuts to select electrons.

The acceptance gain by removing the fiduciality requirement is approximately 14% [36].

B.2.3 Loose Central Electrons

While each $e\gamma \not{E}_{\mathrm{T}} b$ event has to contain at least one tight electron, both $e\gamma \not{E}_{\mathrm{T}} b$ and $\mu\gamma \not{E}_{\mathrm{T}} b$ events are searched for additional high-$\mathrm{P_T}$ electrons that could come from the decays of heavy particles. The cuts for these additional electrons are looser than the tight cuts, and in particular do not require any of the CES variables, i.e. no track-cluster match in ΔX or ΔZ and no cut on strip χ^2, and also no cut on Lshr.

B.2.4 Plug Electrons

Additional isolated electrons in the plug calorimeter with $E_T > 15$ GeV are identified for measured PEM rapidities of $1.2 < |\eta| < 2.0$. Each entry corresponds to a Cdf Plug Em Object. We require minimal leakage or activity in the hadron calorimeter, Had/Em < 0.05, a fractional isolation (isolation energy over the electron energy) less than 0.1, and the shower shape to satisfy the the PEM 3x3 χ^2 and PES 5by9 5-strip to 9 strip ratio cuts.

These cuts are similar to standard cuts [35] with the exception that we use PEM-based η instead of PES-based η (Pes2dEta).

We apply face corrections to the PEM energy of the plug electron candidate, add the PPR energy and scale resulting number by 1.0315, as shown in Equation B.2.

$$E_{plug\ electron} = (E_{pem}^{cor} + E_{ppr}) \times 1.0315 \qquad \text{(B.2)}$$

B.3 Photon Selection

The photon selection criteria are identical for photons in both the muon and electron samples; the photon cuts are described below.

B.3.1 Photon Selection Criteria

Variable	Cut
E_T^{corr}	> 10 GeV
Had/Em	< 0.125 or $< 0.055 + 0.00045 \times E^{corr}$
χ^2 (Strips+Wires)/2.0	< 20
N Tracks	≤ 1
Track P_T	$< 1 + 0.005 \times E_T^{corr}$ GeV
Cone 0.4 IsoE_T^{corr}	$< 2.0 + 0.02 \times (E_T^{corr} - 20)$ GeV
Cone 0.4 TrackIso	$< 2.0 + 0.005 \times E_T^{corr}$ GeV
2nd CES Cluster (Strip and Wire)	$< 2.4 + 0.01 \times E_T^{corr}$ GeV
Fiducial	Ces$|X| < 21$ cm, 9 cm $<$ Ces $|Z| < 230$ cm

Table B.4: Photon Identification and Isolation Cuts for Version 6.1.4 of the Offline Code.

A photon candidate is required to have corrected transverse energy greater than 10 GeV. For photons or electrons the CES shower position is determined by the energy-weighted centroid of the highest energy clusters of those strips and wires in the CES which correspond to the seed tower. The direction of the photon is determined by the line connecting the primary event vertex to the shower position in the CES.

To ensure that events are well-measured the shower position of the photon is required to fall within the fiducial region of the CES so that the shower is fully contained in the active region.

Photon candidates are required to have characteristics consistent with those of a neutral electromagnetically-interacting particle. No COT track with $\mathrm{P_T} > 1$ GeV may point at the photon cluster. One track with $\mathrm{P_T} < 1$ GeV may point at the cluster.

The variable 'IsoE_T^{corr}' is the Run I cone 0.4 isolation energy with the Run I correction to isolation energy due to phi-crack leakage [37]. The tracking isolation variable 'TrackIso' is the sum of the $\mathrm{P_T}$ of tracks in a cone 0.4 surrounding the photon, measured in GeV. Furthermore, for the $t\bar{t}\gamma$ signal, we require the χ^2 average between the wires and the strips to be less than 6. This is explained in detail in Section 8.

B.4 B-Tag Identification

The b-jet selection criteria are identical for b-jets in both the muon and electron samples and described below. We are using the b-tagging collection "PROD@SecVtxModule-JetClu-cone0.4-loose"

The jets used in this analysis are reconstructed from calorimeter tower using a cone algorithm with a radius R ≥ 0.4, for which E_T of each tower is calculated with respect to the z coordinate of the event. The calorimeter towers belonging to any electron candidate are not used by the jet clustering algorithm. The energy of the jet is corrected for the pseudo-rapidity dependence of the calorimeter response, the calorimeter time dependence, and extra E_T from any multiple interactions.

We require that the event contains at least one jet with Level 5 corrected

$E_T > 15 GeV$ and detector rapidity $|\eta| < 2$ is identified as a b quark candidate through the presence of displaced vertex within the jet arising from the decay of a long-lived bottom hadron (b-tag). We use loose SECVTX tagging method for b-tag identification.

For the $t\bar{t}\gamma$ category in addition to $\mathrm{H_T} > 200\ GeV$ we further require the total number of jets in the event to be > 2.

B.5 Calculating the Missing Transverse Energy and H_T

B.5.1 Calculating the $\not{E}_{\mathrm{T}}$

Missing E_T ($\not{E}_{\mathrm{T}}$) is the signature of neutrinos, or possible new non-interacting particles such as the gravitino or LSP. It also can come from mis-measurement of the true E_T of objects, or from backgrounds such as cosmic rays or beam halo.

Missing transverse energy $\not{E}_{\mathrm{T}}$ is calculated from the calorimeter tower energies in the region $|\eta| < 3.6$. Corrections are then made to the $\not{E}_{\mathrm{T}}$ for non-uniform calorimeter response [38] for jets with uncorrected $\mathrm{E_T} > 15\ GeV$ and $\eta < 2.0$, and for muons with $\mathrm{P_T} > 12\ GeV$:

- Muons: correct for $E_T - P_T$, where E_T is transverse energy deposited in electromagnetic and hadron calorimeters, and P_T is a transverse momentum of a muon track. We correct $\not{E}_{\mathrm{T}}$ for all muons with $\mathrm{E_T} > 20$ GeV.
- Jets: correct for $E_T - E_T^{corr}$, where E_T is a transverse energy of an uncorrected jet, and E_T^{corr} is a transverse energy of a jet, corrected for non-uniform calorimeter response. We correct for jets with $\mathrm{E_T^{corr}} > 15$ GeV.

When identifying jets we check that jet object does not have any of the objects identified in the current analysis close to it (within $\Delta R < 0.5$).

For the $\ell\gamma\not{E}_{\mathrm{T}}b$ and $t\bar{t}\gamma$ analysis we set the cut on $\not{E}_{\mathrm{T}}$ to be $\not{E}_{\mathrm{T}} > 20$ GeV.

B.5.2 Calculating the H_T

H_T is a sum of E_T's and P_T's of all objects in the event (leptons, photons, $\not{E}_{\mathrm{T}}$, jets). To calculate H_T we use Tight and Loose Central Electrons(Table B.2), Tight

Phoenix Electrons (Table B.3), Tight and Loose CMUP and CMX muons, Stubless muons(Table B.1), $\not\!\!E_{\mathrm{T}}$, and jets in the event with $|\eta| < 2$ and $E_T^{corr} > 15$.

For the $t\bar{t}\gamma$ analysis we set the cut on $\mathrm{H_T}$ to be $\mathrm{H_T} > 200$ GeV.

C Systematic Uncertainties

In this section we summarize preliminary estimates of the systematic uncertainties on the SM predicted rates. The errors are categorised as experimental(Section C.1, theoretical(Section C.2) and luminosity(Section C.3).

The contributing effects for the SM predictions we have considered are:

- Error is on the total theoretical prediction, including the NLO uncertainties (different for different samples, see Section C.2).
- Luminosity: 6%
- Trigger Efficiencies: 2% for muons and 1% for electrons for lepton triggers only.
- |z_vert| < 60: 1%
- Muon ID Efficiencies: 2%
- Electron ID Efficiencies: 1%
- Photons ID Efficiencies: 4%
- B-tagging ID Efficiencies: 5%

The systematic uncertainties on the backgrounds are included in the background estimates, discussed in Section 11 and Section 5.

The total systematic uncertainty for the SM predictions for the $t\bar{t}\gamma$ samples is 18%. The total systematic uncertainty is 13% for $W\gamma + HF$ and WW samples.

C.1 Experimental Systematic Uncertainties

The sources of experimental systematic errors [39, 40, 41] are summarized in Table C.1.

Source	%	Central	CMUP	CMX
Z_0 cut eff	1.0	x	x	x
photon cut eff	2.0	x	x	x
energy scale (γ)	3.0	x	x	x
conversion rate uncertainty	1.5	x	x	x
momentum scale (μ)	2.0		x	x
acceptance (e)	1.0	x		
acceptance (μ)	2.0		x	x
central e ID	1.0	x		
central e trigger	1.0	x		
energy scale (e)	1.0	x		
cosmic	0.01		x	x
Cot track reconstruction	0.4	x	x	x
B-tagging	5.0	x	x	x
CMUP ID	0.7		x	
CMUP reconstruction	0.6		x	
CMUP trigger	0.7		x	
CMX ID	0.8			x
CMX reconstruction	0.3			x
CMX trigger	0.6			x

Table C.1: Systematic error summary for $\ell\gamma$. 'x' means that channel needs to take into account its systematic uncertainty.

C.2 Theoretical Systematic Uncertainties

Limitations in the theoretical precision of the calculation, result in an uncertainty on the cross-section prediction. The effect of the errors on the cross-section for $W\gamma$ and $Z\gamma$ samples is studied in [39, 40, 41].

Based on these studies we estimate systematic error to be 10% for $W\gamma$+HF and WW samples. For the $t\bar{t}\gamma$ samples we also add k-factor (14% uncertainty, see Section A.4) systematic error in addition to the factorization scale error (2% as estimated for $W\gamma$ and $Z\gamma$ samples) and PDF uncertainty (6% as estimated for $W\gamma$ and $Z\gamma$ samples). The resulting theoretical systematic uncertainty for $t\bar{t}\gamma$ samples is 15%.

C.3 Luminosity Systematic Uncertainties

A total systematic uncertainty of 6% is quoted for all luminosity measurements. This includes a 4.4% contribution from the acceptance and operation of the luminosity monitor and 4.0% from the theoretical uncertainty on the calculation of the total $p\bar{p}$ cross-section [42].

References

[1] Tim Nelson, Rick Snider, David Stuart. Forward Electron Tracking with the PhoenixMods Package. CDF Note 6278, CDF, 2003.

[2] See http://www-cdf.fnal.gov/internal/physics/joint_physics/instructions/electron_cuts.html.

[3] U. Baur et al. Physics at future hadron colliders. *eConf*, C010630:E4001, 2001.

[4] U. Baur, A. Juste, L. H. Orr, and D. Rainwater. Probing electroweak top quark couplings at hadron colliders. *Phys. Rev.*, D71:054013, 2005.

[5] T. Aaltonen *et al.* Searching the $\ell\gamma\not{E}_T$ + b-quark for Radiative Top Quark Decay and Non-Standard-Model Processes. *Phys. Rev. D. 80, 011102 (2009)*, 2009.

[6] G.D. Kribs S.P. Martin S. Ambrosanio, G.L. Kane and S. Mrenna. *Phys. Rev. D*, **55**.

[7] Search for new physics in lepton + photon + x events with 305-pb**(-1) of p anti-p collisions at s**(1/2) = 1.96- tev. 2006.

[8] T. Affolder et al. *Nuc. Instrum. Meth.*, A526:249, 2004.

[9] S. Kuhlman et al. *Nucl.Instrum.Meth.*, A518:39–41, 2004.

[10] P. Melese G. Apillinari, K. Goulianos and M. Lindgren. *Nucl.Instrum.Meth.*

[11] S. Tokari V. Giakoumopoulouj N. Giokarisj I. Zaljubovskyh, I. Fedorkoi and A. Manousakis-Katsikakisj. Design and construction of new central and forward muon counters for cdf-ii. *Nucl.Instrum.Meth.*, A538:358–371, 2005.

[12] A. Ruiz et al. A time-of-flight detector in cdf-ii. *Nuc. Instrum. Meth.*, A518:605–608, 2004.

[13] et. al. D. Acosta. *Nucl. Instrum. Meth.*, A461:540–544, 2001.

[14] R. Downing et al. *Nucl.Instrum.Meth*, A570:36–50, 2007.

[15] A. Abulencia *et al.* Search for new physics in lepton+photon+X events with 929 pb^{-1} of $p\bar{p}$ collisions at $\sqrt{s} = 1.96$ TeV . *Phys. Rev. D. 75, 112001 (2007)*, 2007.

[16] P. Onyisi and the UC CDF Physics Group. The ucntuple is described on the web page:. http://hep.uchicago.edu/cdf/flatntuple, 2004.

[17] UC CDF Physics Group. The ucntuple sets are listed on the web page:. http://hep.uchicago.edu/cdf/datasets/, 2004.

[18] I.Shreyber, A.Loginov, H.Frisch. A search for anomalous production of the signature $\ell + \gamma + b - quark + \not{E}_T$ and a search for standard model $t\bar{t} + \gamma$ production in 929 pb^{-1}. CDF Note 9335, CDF, 2008.

[19] T. Stelzer and W. F. Long. Madgraph. *Comput.Phys.Commun.*, 357(81), 1994.

[20] S. Tsuno, A.S. Thompson. A CDF-interface module for Les Houches Accords. CDF Note 6333, CDF, 2003.

[21] T. Schwarz A. Ivanov and R.Erbacher. Cdf note.

[22] R.Culbertson, A.Pronko, Shin-Shan Eiko Yu. The Probability of an Electron faking an Isolated prompt photon in cem. CDF Note 8220, CDF, 2006.

[23] A.Goshaw B.Heinemann A.Nagano T.Phillips C.Lester, J.Deng. Measurement of the rate of jets faking central isolated photons using 1fb^{-1} of data. CDF Note 9033, CDF, 2007.

[24] See http://www-cdf.fnal.gov/internal/people/links/SarahBudd/mistag3.html.

[25] S.Grinstein, J.Guimaraes da Costa, D. Sherman. Secvtx mistag asymmetry for winter 2007. CDF Note 8626, CDF, 2007.

[26] B.Cooper, A. Messina. Estimation of the background to $\text{w}^{\pm} \rightarrow e^{\pm}\nu + n$ jet events. CDF Note 7760, CDF, 2005.

[27] N. Kidonakis. Top quark pair and single top production at tevatron and lhc energies. *arXiv*, hep-ph/1008.2460, 2010.

[28] Duan Peng-Fei et al. Qcd corrections to associated production of $t\bar{t}\gamma$ at hadron colliders. *arXiv*, hep-ph/0907.1324, 2009.

[29] Victoria Martin. High pt muons, recommended cuts and efficiencies for release 5.3.1. CDF Note 7031, CDF, 2005.

[30] Victoria Martin. High-pt muon id cuts and efficiencies for use with 5.3.1 data and 5.3.3 mc. CDF Note 7367, CDF, 2005.

[31] Lauren Beitler. Talk given to the W+Jets Meeting, Oct. 10, 2003.

[32] Larry Nodulman. Curvature corrections for 5.3.1. CDF Note 6971, CDF, 2004.

[33] Anyes Taffard. Run II cosmic ray tagger. CDF Note 6100, CDF, 2003.

[34] Anyes Taffard. Run II cosmic ray tagger perfomances. CDF Note 6255, CDF, 2003.

[35] C. Hill, J. Incandela, and C. Mills. Electron identification in offline release 5.3. CDF Note 7309, CDF, 2005.

[36] Henry Frisch Andrei Loginov. Search for lepton + photon + x. CDF Note 7550, CDF, 2005.

[37] P.J. Wilson. Calorimeter isolation and lateral shower leakage for photons and electrons. CDF Note 4170, CDF, 1997.

[38] A. Bhatti *et al.*, submitted to Nucl. Instrum. Methods, Oct. 2005; hep-ex/0510047.

[39] D. Acosta *et al.* Measurement of W gamma and Z gamma Production in p anti-p Collisions at s**(1/2) = 1.96 TeV. *Phys. Rev. Lett. 94, 041803 (2005)*, 2005.

[40] Helen Hayward. Measurement of $z^0\gamma$ production in $p\bar{p}$ collisions at $\sqrt{s}$=1.96 tev. Thesis.

[41] Michael Kirby. Measurement of W+gamma Production in Proton-Antiproton Collisions at root-s = 1.96 TeV. Thesis.

[42] S. Klimenko, J. Konigsberg, T.M. Liss. Averaging of the inelastic crosssections measured by the CDF and E811 experiments. *Fermilab-FN-0741*.